catalysts

MDPI

Review

Recent Advances in the Technologies and Catalytic Processes of Ethanol Production

Mohd Nor Latif [1,2], Wan Nor Roslam Wan Isahak [1,3,*], Alinda Samsuri [4,5], Siti Zubaidah Hasan [1], Wan Nabilah Manan [1] and Zahira Yaakob [1]

1 Department of Chemical and Process Engineering, Faculty of Engineering & Built Environment, Universiti Kebangsaan Malaysia, Bangi 43600, Selangor, Malaysia
2 GENIUS@Pintar National Gifted Center, Universiti Kebangsaan Malaysia, Bangi 43600, Selangor, Malaysia
3 Research Centre for Sustainable Process Technology (CESPRO), Faculty of Engineering and Built Environment, Universiti Kebangsaan Malaysia, Bangi 43600, Selangor, Malaysia
4 Centre for Tropicalization, National Defence University of Malaysia, Kem Sungai Besi, Kuala Lumpur 57000, Malaysia
5 Department of Chemistry and Biology, Center for Defence Foundation Studies, National Defence University of Malaysia, Kem Sungai Besi, Kuala Lumpur 57000, Malaysia
* Correspondence: wannorroslam@ukm.edu.my; Tel.: +60-3-8911-8339

Abstract: On the basis of its properties, ethanol has been identified as the most used biofuel because of its remarkable contribution in reducing emissions of carbon dioxide which are the source of greenhouse gas and prompt climate change or global warming worldwide. The use of ethanol as a new source of biofuel reduces the dependence on conventional gasoline, thus showing a decreasing pattern of production every year. This article contains an updated overview of recent developments in the new technologies and operations in ethanol production, such as the hydration of ethylene, biomass residue, lignocellulosic materials, fermentation, electrochemical reduction, dimethyl ether, reverse water gas shift, and catalytic hydrogenation reaction. An improvement in the catalytic hydrogenation of CO_2 into ethanol needs extensive research to address the properties that need modification, such as physical, catalytic, and chemical upgrading. Overall, this assessment provides basic suggestions for improving ethanol synthesis as a source of renewable energy in the future.

Keywords: carbon dioxide; catalytic hydrogenation; cascade reaction; ethanol production

check for updates

Citation: Latif, M.N.; Wan Isahak, W.N.R.; Samsuri, A.; Hasan, S.Z.; Manan, W.N.; Yaakob, Z. Recent Advances in the Technologies and Catalytic Processes of Ethanol Production. *Catalysts* **2023**, *13*, 1093. https://doi.org/10.3390/catal13071093

Academic Editors: Sagadevan Suresh and Is Fatimah

Received: 3 April 2023
Revised: 8 June 2023
Accepted: 10 June 2023
Published: 12 July 2023

Copyright: © 2023 by the authors. Licensee MDPI, Basel, Switzerland. This article is an open access article distributed under the terms and conditions of the Creative Commons Attribution (CC BY) license (https://creativecommons.org/licenses/by/4.0/).

1. Introduction

Nowadays, scientists, academics, policymakers, and environmental non-governmental organizations focused on global warming or climate change effect due to the impact of greenhouse gas emissions (GHG). Data show increment concentration patterns of methane (CH_4), carbon dioxide (CO_2), chlorofluorocarbons, and nitrous oxide in the environment every year, thus prohibiting the reradiation of solar heat and increasing the temperature of the surface of the earth. Global GHG emissions are from human activities, such as burning fuels for electricity generation systems [1–4], transportation [5,6], industry [7,8], and agriculture [9–11]. CO_2 is also known as the most important anthropogenic GHG for global warming or climate change that is associated with human activities [12–14]. The Global Carbon Budget 2021 reported that the global atmospheric CO_2 emissions growth is 5%. The global average amount of atmospheric CO_2 emissions in 2021 is 36 billion metric tons or equivalent to 415 ppm [15]. The increasing patterns of CO_2 concentration globally in the atmosphere are predicted to increase due to excessive industrialization, which leads to the development of heat retention since the introduction of the Fourth Industrial Revolution.

CO_2 is proven to be a recyclable, nonpoisonous, and inexpensive C_1 building block in the synthesis of high-value chemicals and fuels [16–19]. However, CO_2 is fully oxidized, chemically inert, and thermodynamically stable ($\Delta_f G_{298K} = -396$ kJ·mol^{-1}). Thus, its conversion into chemicals requires large energy and enormous H_2 resources [20–22]. Many CO_2 transformation approaches, e.g., hydration of ethylene, biomass residue, lignocellulosic materials, fermentation, electrochemical reduction, dimethyl ether (DME), reverse water gas shift (RWGS), catalytic hydrogenation, and other related processes, have been rapidly studied. Catalytic hydrogenation has been deemed a promising technology for generating a variety of products, such as hydrocarbons [23,24], alcohols [25,26], carboxylic acids [27,28], and aldehydes [29,30].

Ethanol is an ecological fuel that has an important advantage compared with conventional gasoline as a transportation fuel due to its properties of nontoxicity, accumulation of high oxygen content to promote improved combustion with reducing exhaust emissions, and high octane rating to give a high resistance to engine knock [31–34]. Hence, the establishment technology of fuel ethanol is needed in reducing environmental pollution problems [35,36]. Ethanol is produced from agricultural feedstock, such as corn (United States) and sugarcane (Brazil), and the European Union produces ethanol from wheat and sugar beet. The Renewable Fuels Association in 2021 reported that the main ethanol producer in the world is the United States, estimating ethanol production of more than 13,000 million gallons per year, which is more than half of the global ethanol production. Approximately 8000 million gallons per year of ethanol is produced in Brazil [37]. The use of agricultural feedstock especially corn in ethanol production is being criticized because of their importance as food. Food shortages and rising food prices will occur if agricultural feedstock is used as the raw material in ethanol production. Furthermore, the grain from corn will create environmental pollution problems, such as soil erosion, biodiversity loss, nitrogen oxide pollution, and emission of volatile organic compounds. The major constraint in commercial ethanol production is the disadvantage in energy balance and the area required for plantations [38,39]. Given these considerations, nations continue to look for new technologies and processes in reducing the cost of ethanol production without causing adverse effects on the environment.

2. Conventional Processes to Produce Ethanol

2.1. Ethanol Synthesis Based on the Hydration of Ethylene

In the petrochemical industry, the catalytic hydration of ethylene for ethanol production is a reversible exothermic reaction and is used commercially by Shell Oil Company in 1947 [40]. The process of reaction can be expressed by the following equation:

$$C_2H_4 + H_2O \rightleftharpoons C_2H_5OH. \quad (1)$$

The hydration of ethylene comprises three stages, i.e., reaction, recycling, and purification. Mohsenzadeh et al. [41] suggested that this process occurs in a fixed-bed catalytic reactor when ethylene is mixed with steam at a molar ratio of 0.6 at 250–300 °C, 70–80 bar, and the presence of a phosphoric acid catalyst (H_3PO_4/SiO_2) based on silica gel. The ethylene conversion is 4–25% with ethanol selectivity of 98.5 mol.%. A diagram of the hydration of ethylene is shown in Figure 1.

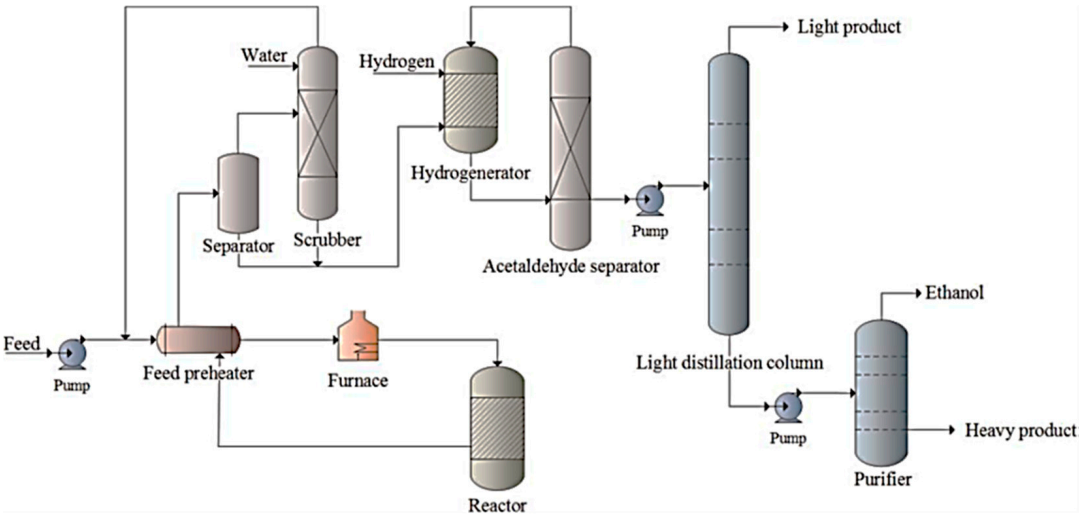

Figure 1. Hydration of ethylene [41].

A byproduct of this process, acetaldehyde, can be used directly in a cosmetic product or promoted to form ethanol through the hydrogenation process. The high-pressure separator is used to separate the unreacted reactants from the outlet stream mixture. Unreacted reactants are scrubbed with water to remove impurities before dissolution with ethanol. The molar ratio of ethylene to water is maintained at 1:0.6, and the mixture is combined with a recycle stream. When the bottom streams of the scrubber and the separator are fed to the hydrogenator, the nickel-packed catalyst promotes the formation of an ethanol mixture from acetaldehyde. The unreacted acetaldehyde in the separator column is removed and recycled in the hydrogenator. The ethanol concentration increases when the bottom stream is fed to light and heavy (purifier) columns [42].

The cost of a plant for the hydration of ethylene increases due to the formation of the ethanol-water mixture that will form an azeotrope mixture, which requires a special distillation process. The production of ethylene based on hydrocracking petroleum feedstocks, which are nonrenewable, is not economically feasible because of the market price of ethanol. The phosphoric acid catalyst that is used in this process is prone to leaching via vaporization, which causes the deactivation of catalysts and corrosion of the equipment. A solid acid catalyst, such as WO_3/ZrO_2 [43] and WO_3/TiO_2 [44], is introduced to overcome leaching issues; this route is still not favorable for the large-scale production of ethanol due to the price of ethylene and the rapid development of sugar fermentation during the hydration of ethylene.

The research on the gas-phase hydration of ethylene by using impregnated metal phosphates for catalytic activity at tin(IV) hydrogen phosphate ($Sn[HPO_4]\cdot 2H_2O$) showed that the weight-based rate is 0.94 $\mu mol\cdot min^{-1}\cdot gcat^{-1}$, which is approximately seven times higher than that at commercial H_3PO_4/SiO_2 catalyst [45]. The vapor-phase hydration of ethene has recorded a 93% selectivity for the tungsten trioxide (WO_3) monolayer loaded with titania. The co-presence of Brønsted and Lewis acid sites on the monolayer of WO_3 generated high selectivity for ethanol but the reaction process has issues from the environmental protection perspective [46]. The combination of vapor–liquid equilibria and the chemical stage equilibrium for the ethylene–water–ethanol ternary arrangement demonstrates that the crucial point of an azeotrope at 200 °C and 155 atm shows the active catalysis of H-pentasil zeolite for the maximum hydration of ethylene [47]. The ethanol production plant's simulated modeling was developed using the HYSYS software and the results of optimization over the catalytic hydration using zirconium-tungsten catalysts operating at 299 °C with column configuration for the extractive distillation which produced ethanol concentration of 99.7% and then linked to the Aspen Plus software [48].

The hydration process corresponds to petroleum-derived alkene over solid acid catalysts, which are limited by the low single-pass conversion (<5%), poor long-term stability,

and strong dependence on crude oil. The chemical equilibrium conversion of the hydration of ethylene decreases when using high temperatures to increase the rate of reaction. As a result, the temperature setting of the reactor is needed to accommodate between thermodynamics and kinetics [46]. A high amount of energy to heat gases generates high pressure and uses crude oil, a nonrenewable resource. The purification method uses benzene to separate the azeotropes of ethanol and water that produce hazardous ethanol.

2.2. Ethanol Synthesis Based on Biomass Residues

Biofuel is produced from biomass residues and wastes for energy purposes, such as transportation fuels, renewable electricity, and thermal energy [49–51]. The three types of biomass residual resources are primary, secondary, and tertiary (Figure 2). Corn stalks, husks, stems, roots, leaves, cob, bagasse, and straw make up the main residue, which is described as outcomes of the cultivation of certain food crops and agroforestry in the agriculture sector. Then, the secondary residue is obtained by the processing of crops into the final form of a product or the production of other biomass-based materials. Examples of agricultural and food processing wastes are sawdust, wood chips, nutshells, palm kernel cake, fruit bunches, coffee husks, rice hulls, bark, and scrap wood. The tertiary residue consists of sewage sludge or wastewater derived after the consumption of biomass-based products, such as municipal solid waste. Human, animal, and industrial wastes have been identified as the main source of municipal solid waste [52–54].

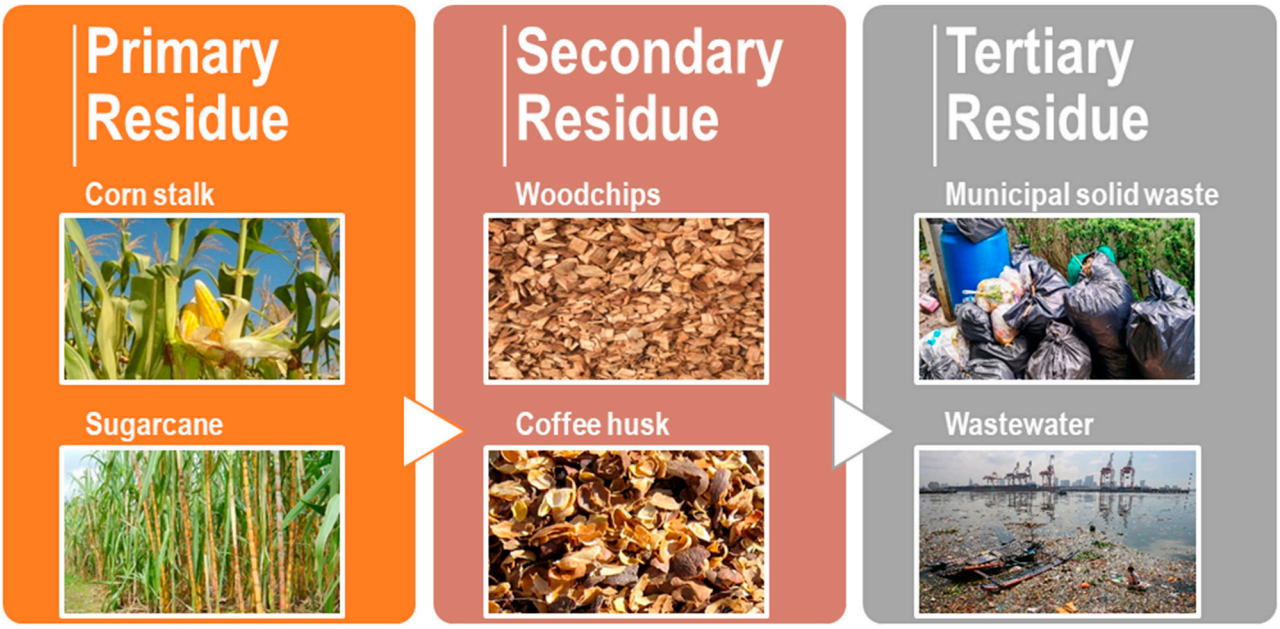

Figure 2. Categories of biomass residues.

A study showed that wood processing residues, such as discarded logs, sawdust, and wood chips produced from sawmill and lumber processing, can be utilized as steamer fuels and feedstock for ethanol synthesis [53,55]. Tropical countries have been shown to apply the concept of economic utilization by using sugarcane residues, such as sugarcane bagasse and leaf residue, for ethanol production and value-added commercial product [56–58]. According to the research on delignified coconuts waste and cacti, an ethanol yield of 89.15% is recorded by utilizing the semisimultaneous saccharification and fermentation configuration, and this yield is higher compared with that obtained by simultaneous saccharification and fermentation (SSF) configuration [59]. The pretreatment mixture of 0.06 $g \cdot g^{-1}$ hydrogen peroxide to green liquor and furfural residues pretreated to cassava residue saccharification liquid with a ratio of 1:1 recorded an advantageous pretreatment method by producing a 93.6% yield of ethanol. This study shows that the increment of a high

ethanol yield and lower byproduct concentrations occur when the proportion of lignocellulosic substrates was enhanced in the SSF of the substrate mixture of cassava residue and furfural residues [60]. The investigation of the carnauba straw residue by the SSF configuration process in a single reactor in the presence of *Kluyveromyces marxianus* ATCC-36907 and observed that cultivation at 45 °C results in the maximum ethanol concentration of 7.53 $g \cdot L^{-1}$ [61]. The mangosteen pericarp waste that has undergone popping pretreatment and enzymatic hydrolysis in the separate hydrolysis and fermentation (SHF) configuration method can achieve 75% ethanol [62]. The ethanol produced from the combination of *Salacca zalacca* and coconut sewage shows that the energy required for coordination obtained at 85 °C is 346.32 W, and the resulting ethanol is obtained at 40% and mass flow rate of 0.0655 $kg \cdot s^{-1}$ [63]. Rahman et al. [64] developed a green biorefinery concept to produce ethanol by integrating the pretreatment of fermentation and ethanol-assisted liquefaction in the presence of *Nannochloropsis* sp. The process increases the lipid content of fermented microalgae by 40%, whereas 10% of the required ethanol is produced through liquefaction. The utilization of wet algae increases the crude biodiesel yield threefold compared with the liquefaction of microalgae. The fermentation of over-ripened Indian blueberry at 33 °C, pH 5.2, and specific gravity of 0.875 obtain 6.5% ethanol [65].

However, biomass residue requires an energy-intensive process from large and specific machinery due to different types of biomass, thus increasing the cost of operation because of expensive machinery and the fuel needed for operation. The low density of biomass also influences the cost of operation by occupying increased volume and needing increased transportation for space. The other challenge is developing effective pretreatment technologies that cover physical, chemical, and biological pretreatments. The ideal pretreatment increases the rate of enzyme hydrolysis and decreases the amount of enzyme needed to convert the biomass into sugars in the presence of the microorganism. Issues regarding environmental pollution also need to be addressed because the conversion of biomass residue into ethanol produces a huge amount of CO_2.

2.3. Ethanol Synthesis Based on Lignocellulosic Materials

Lignocellulosic materials, which comprise nonedible feedstock from various agricultural and forestry residues, are abundantly available without geographical limitation and have a low cost. Extensive research showed the production of ethanol and value-added chemical by using different types of lignocellulosic sources, including waste paper [66,67], orange peel [68,69], sugarcane straw [70,71], corn stover [72,73], sugarcane bagasse [74,75], rice straw [76,77], wheat straw [78,79], sweet sorghum [80,81], oil palm empty fruit [82,83], and banana waste [84,85]. Figure 3 shows the composition of lignocellulosic materials that consist of three major fragments of cellulose (40–50%), hemicellulose (25–35%), and lignin (15–20%), which always exist beside other extracts and mineral traces [86–89]. However, the composition differs on the basis of the type of biomass, cultivation, and atmospheric conditions. The complex and rigid structure of lignocellulosic materials is made by noncovalent interactions with covalent cross-linkages [90].

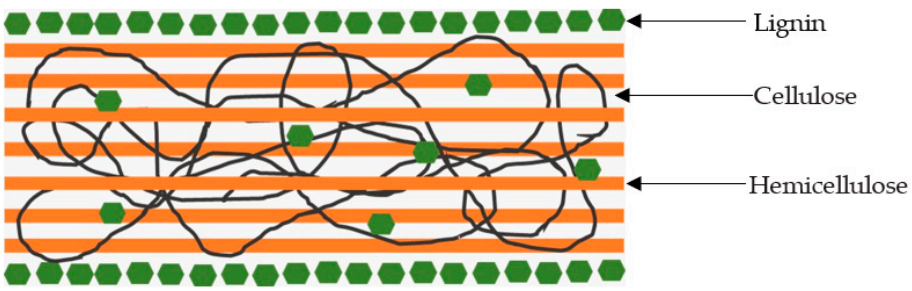

Figure 3. Composition of lignocellulosic materials (an adaptation from [91]).

The conversion of lignocellulosic materials into ethanol involves pretreatment, enzymatic hydrolysis, fermentation, and distillation [92–95]. During the pretreatment process,

various cutting-edge technologies are utilized to open the structure of lignocellulosic materials by physical, chemical, physicochemical, and biological techniques and separate complex interlinked structures among hemicellulose and lignin from the matrix [87,96–98]. Chemical pretreatment uses a variety of chemicals such as acid and alkaline chemicals to break down the structures present in the lignocellulosic biomass at a constant ambient temperature which subsequently enhances the biomass surface availability to enzymatic hydrolysis, permitting the cellulose and hemicellulose for further conversion of fermentable sugars into biofuels [99–101]. The research on the bioconversion of lignocellulosic by-product corn stover into the value-added fermentative product L-lactic acid using the furfural tolerant *Enterococcus mundtii* WX1 and *Lactobacillus rhamnosus* SCJ9 showed that corn stover pretreated with 1% (v/v) sulfuric acid was selected for L-LA fermentation and shows the highest efficacy of fermentable sugar with the optimal conditions achieved for the release of glucose and xylose at 24.5 g/L and 11.2 g/L, respectively, from 100 g/L pretreated corn stover at 121 °C for 30 min [102]. A similar result was presented by other researchers reported in the study of tobacco stem waste [103], palm kernel shell [104], sugarcane bagasse [105], and oil palm frond bagasse [106] that the dilute acid for chemical pretreatment is effective to attain high reactivity and generates protons that have a quick diffusion which substantially enhances the hydrolysis of amorphous cellulose chains and the solubilization of hemicellulose.

Dilute acid pretreatment has received wide attention due to its cost-effective, non-toxicity, lower degradation products, corrosive, and hazardous processes that do not require as much corrosion-resistant equipment, making it easier to scale-up the operation process [107–109]. Alkaline pretreatment leads to the delignification of agricultural biomass by cleaving the intermolecular ester linkages between hemicelluloses and lignin fragments, increases the amorphous surface area of the cellulose as well as the porosity of the biomass, reduces the degree and crystallinity of the polymerization rate at low temperature and pressure, resulting in an enhanced hydrolysis and fermentation yield and a high amount of sugars [110–112]. In a comparison of various alkaline pretreatment techniques, alkaline hydrogen peroxide (AHP) pretreatment is the most effective as it increases the fermentation yield at mild conditions effectively by solubilizing lignin from the complex recalcitrant structure of the macromolecules because H_2O_2 could degrade to oxygen and H_2O without any residues left and increases the enzyme digestibility and fermentation efficiency of the feedstock required for subsequent processing [99,113–115]. The primary advantages of AHP pretreatment are environmentally friendly chemicals and reagent reusability, high effectiveness for various biomass concentrations providing high efficiency of enzymatic hydrolysis, high lignin, and hemicellulose solubilization values for the liquid fraction without a loss of carbohydrates retention, low energy consumption, less formation of toxic byproducts, no need for special reactors, compatibility with high solid loadings, and sterility conditions provided by alkaline H_2O_2 without a need to use antibiotics [116–118].

Organosolv pretreatment with aliphatic organic solvents is among the most promising pretreatments compared to acidic or alkaline pretreatment by producing a very distinctive separation of high-purity cellulose content from the remaining lignocellulosic constituents, such as lignin and hemicellulose at relatively low temperatures (below 180 °C), while preserving the integrity of the hemicellulose structure from thermal degradation kinetics [119–121]. Organosolv pretreatment using ethanol has also some advantages over other methods such as low toxicity and environmentally friendly nature, high delignification rates, high reaction stability, good solubility of lignin, miscibility with water, complete restoration of ethanol solvent due to its low boiling point and potentially provides substantial economic benefits [122–125].

The hydrolysis process breaks down the hemicellulose and cellulose components in the presence of cellulolytic enzymes or acids to form monosaccharides [126–128]. The conversion of sugars into ethanol by using a variety of potential microorganisms occurs during the fermentation process. *Saccharomyces cerevisiae*, a microorganism that is commonly used as baker's yeast on a large scale at the industrial level, has been identified to have

a tolerance for ethanol production, robust ethanol dehydrogenase, and potential good resistance against inhibitors generated during the process. The use of this strain results in high ethanol productivity and efficient conversion of most of the sugars into ethanol rather than other byproducts [129,130]. The last step is distillation where the purification of the fermentation broth occurs. Distillation is an effective and favorable separation technique as the preferred choice for industrial application due to high alcohol recovery of 99.5% *v*/*v* purity, sufficient energy efficiency at moderate feed concentrations, and the ability to simulate the process using process simulation software which makes the integration of mass and energy in other processes easier to accomplish [131–133]. All formed byproducts and other impurities are removed during this process, and only imprints remain. Most energy-intensive units have remarkable effects on the gross energy demand that takes place during the distillation process. The cost of plant operation also increases due to the formation of an ethanol–water mixture that produces an azeotrope mixture where the simple distillation method cannot be used to change its composition [134,135].

The SHF process has been studied for ethanol production from waste paper. The pretreatment process of waste paper is applied using 0.5% (*v*/*v*) hydrogen peroxide at 121 °C for 30 min. The office paper that has been pretreated by hydrolytic enzymes produces 24.5 $g \cdot L^{-1}$ sugar equivalent to 91.8% hydrolysis efficiency. Then, the fermentation process that uses *S. cerevisiae* through hydrolysate obtains 11.15 $g \cdot L^{-1}$ ethanol with ethanol productivity of 0.32 $g \cdot L^{-1} \cdot h^{-1}$ [67]. Oil palm trunk chips are introduced into a two-stage pretreatment, i.e., steam explosion and alkaline extraction. The steam explosion pretreatment shows that the reduction and isolation of hemicellulose occur in biomass recalcitrance. The alpha-cellulose content has been improved from 40.83% to 87.14% with alkaline extraction pretreatment at the conditions of 15% (*w*/*v*) NaOH at 90 °C for 60 min. By using *S. cerevisiae*, the ethanol concentration at SSF (44.25 $g \cdot L^{-1}$) is prominent compared with that at prehydrolysis SSF (31.22 $g \cdot L^{-1}$) [136].

The SHF process of the pretreatment of rice straw using *Saccharomyces tanninophilus* produces 9.45 $g \cdot L^{-1}$ ethanol with 83.5% yield. The saccharification of pretreated rice straw with *A. fumigatus* by using 1.0% NaOH in 200 $FPU \cdot mL^{-1}$ crude enzyme for 20 h of reaction obtains 22.15 $g \cdot L^{-1}$ limiting sugars, demonstrating high lignin-degrading manganese peroxidase activity and the activity of laccase enzymes [76]. The effectiveness of SHF and SSF techniques for the synthesis of ethanol originating from oil palm empty fruit bunch (OPEFB) with the conditions of 10% (*w*/*v*) loading of the substrate, pH 5, 1% (*v*/*v*) *K. marxianus* at 37.50 °C for 48 h of reaction is compared. SHF and SSF obtained 25.80 and 28.10 $g \cdot L^{-1}$ ethanol, respectively. The acid–alkali pretreatment of OPEFB is conducted by the loading of the substrate at 12.50% *w*/*v* with 0.2 M concentration of H_2SO_4 at 121 °C for 53 min followed by 5% (*w*/*v*) NaOH at 121 °C for 20 min. This result demonstrates that the acid–alkali pretreatment increases the cellulose yield to 72.10 wt.% and this process is a feasible method for eliminating hemicellulose and lignin from lignocellulosic biomass [82].

The cellulosic ethanol production by using *Issatchenkia orientalis* KJ27-7 in 90% wheat straw hydrolysate media for 24 h has obtained 10.3 $g \cdot L^{-1}$ ethanol corresponding to 0.50 $g \cdot g^{-1}$ glucose (97% of efficiency relative to the theoretical yield). The correlation of ethanol production with wheat straw hydrolysate concentrations is observed [78]. Studies on the effect of varying lignocellulosic feedstocks on technical performance for ethanol production that use the dilute acid pretreatment show that the switchgrass produces 46.2% energy efficiency of feedstock LHV, which is the highest carbohydrate content with the lowest forest residues compared to the *Eucalyptus globulus*., *Birch* sp. residues, *Spruce* sp. residues, *Miscanthus*, corn stover, and wheat straw [137]. Cunha et al. [138] reported that the direct production of ethanol by using non-detoxified hemicellulose liquor by *S. cerevisiae* using hydrothermally pretreated corn cob without external hydrolytic catalysts results in 11.1 $g \cdot L^{-1}$ ethanol titer correlated with the ethanol yield of 0.328 $g \cdot g^{-1}$ potential sugar. The consolidated bioprocessing (CBP) of pretreated corn cob with the addition of commercial hemicellulases is more efficient than SSF in hemicellulosic ethanol production.

Diverse sources and seasonal lignocellulosic biomass affect the chemical characteristics of ethanol produced due to different harvesting times, resulting in the inconsistent composition of lignocellulosic biomass components. Pentose sugars are not fermented by the brewer's yeast, i.e., *S. cerevisiae*, during the hydrolysis of hemicellulose, thus compromising the ethanol production from total sugars in lignocellulosic materials. Hence, the energy consumption during the distillation process for ethanol recovery and treatment of a large amount of stillage increases due to the subsequent reduction of discharge. The pretreatment process produces lignin from inhibitors that act as limiting agents for high biomass loading and do not react productively with lignocellulosic materials. As a result, the ethanol production from cellulose is lower compared with that from grains. Other limitations of ethanol production from lignocellulosic materials, such as high capital, operational expenditure, dwindling price of gasoline, process uncertainty, low growth, and product yield, have also been identified.

2.4. Ethanol Synthesis Based on Fermentation

The major steps in ethanol production via the fermentation process are the treatment of a solution containing fermentable sugars, the formation of ethanol from sugars through fermentation, and distillation for the separation and purification of ethanol [134,139,140]. The main metabolic route involved in ethanol production by fermentation is glycolysis, which converts glucose into pyruvate that is further reduced to produce ethanol and CO_2 under anaerobic conditions [65,141]. Based on the stoichiometric equivalence, 1 mol glucose creates 2 mol CO_2, which is then expelled from the reactor as a weight loss and is proportional to ethanol yield.

$$C_6H_{12}O_6 \rightarrow 2C_2H_5OH + 2CO_2. \quad (2)$$

The fermentation process can be produced in different systems, such as a batch, fed-batch, or continuous bioreactor. The batch bioreactor fermentation is a simple method with a closed culture system where both biomass and substrates are added to the fermenter in a single step of the procedure in which nothing is added or removed during the process and the products are only removed at the end of the process [142,143]. The system operation produces high cell densities, of which almost 99.5% is recycled in subsequent fermentation. The closed-loop design system that uses a high concentration of sugars generates a high concentration of ethanol [143]. In the conventional batch fermentation process at an ideal temperature and under anaerobic conditions, *S. cerevisiae* is used to convert glucose into ethanol. However, this process only occurs in hexose sugars but not in pentose sugars [97,129]. Although equipped with multiple vessels, the batch fermentation system is considered the simplest operation system due to its ability to complete the sterilization process, resulting in a low risk of contamination, low operation costs due to no labor required, easy control of feedstock processes, and flexibility for various product specifications. The disadvantage of this process is solvent inhibition, time consumption, difficulty in maintaining the sterilization of bioreactors, major downtime, long lag phase, and low productivity.

The fed-batch bioreactor process is a semicontinuous or partly open system that allows the addition of fermentation medium gradually or consistently during the process after the initial substrate has been used, overcoming the difficulties of substrate constraint in the batch bioreactor process. This process enables the overall proportion of substrate uptake to increase and sustain a low concentration of substrate within the fermentation vessel, thus decreasing the negative influence of osmotic pressure or rheology-related limitation linked with highly viscous substrates [143,144]. Knudsen and Rønnow [145] reported the highest ethanol production from wheat straw by using *S. cerevisiae* in the co-fermentation stage at the C5/C6 fermenting yeast, where glucose and xylose are fermented simultaneously. With the addition of urea and a primary yeast pitch of 0.2 $g \cdot L^{-1}$ completed broth in at least five fermenter volumes, the fed-batch fermentation process is stable, yielding an ethanol yield >90% during the experiment. The fed-batch fermentation process by using the mixture

of sugarcane and molasses based on the Central Composite Design evaluates the effect of temperature at 27 °C, the concentration of sugar at 300 $g \cdot L^{-1}$, and the concentration of cells at 15% (v/v) in the presence of *S. cerevisiae* for 30 h of reaction. This process has obtained ethanol concentration, productivity, and yield of 135 $g \cdot L^{-1}$, 4.42 $g \cdot L^{-1} \cdot h^{-1}$, and 90%, respectively [146]. The fed-batch process is a cost-effective operation with an efficient cultivation strategy, short fermentation time, high dissolved oxygen concentration in the medium, and low toxic efficacy of medium constituents. However, the ethanol production in fed-batch fermentation is minimal; the concentration of cell mass and feed rate of the reaction thus provided a point of ingress for contamination and allowed the buildup of inhibitory agents and toxins. The outcome of high cell density numbers and product yields are difficult to deal with downstream, creating bottlenecks in the whole process.

The continuous fermentation process is carried out by continuously feeding substrates, new media, and nutrients into a bioreactor containing active microbes. This process concurrently harvests the used medium and cells, removes toxic metabolites, and replaces the consumed nutrients from the culture. As a result of the equivalency process of addition and removal, the culture volume in this process remains constant. Then, the maximum working volume of the vessel does not limit the amount of fresh medium or feed solution which can be added to the culture in the course of the process. However, the long cultivation period increases the risk of contamination and genetic changes in the cultures. This process also difficult to keep a constant population density over prolonged periods and the products of a continuous process cannot be neatly separated into batches for traceability. The production of high residual sugar and ethanol in this process is caused by the continuous exposure of yeast cells that may affect cell growth until biomass washout [147]. Margono et al. [148] developed the uncontrolled continuous fermentation process equipped with an integrated aerobic–anaerobic baffled reactor (IAABR) to study molasses in the presence of *S. cerevisiae* and generated 92.55 $g \cdot L^{-1}$ ethanol with a productivity of 4.63 $g \cdot L^{-1} \cdot h^{-1}$ for a residence time of 19.2 h. The ethanol productivity with IAABR is 3.4% higher compared with that through the industrial batch process, and the maximum operation reaches 14 days of fermentation without contamination.

The cassava supernatant subjected to continuous ethanol production with a high cell density strategy at the dilution rate of 0.092 h^{-1} generated 104.65 $g \cdot L^{-1}$ ethanol and ethanol productivity of 9.57 $g \cdot L^{-1} \cdot h^{-1}$. The ethanol yield of this system is 96.96%, which is approximately 4.2% higher compared with that obtained by traditional fermentation with free cells. This research shows that cells sustain optimum condition activity by switching the flow direction in the in-series bioreactors and extend the long-term stability of continuous fermentation without any possibility of a contamination effect [149]. The continuous fermentation with a high cell density recycle operation demonstrates a better result compared with typical molasses-based batch fermentation by obtaining 0.44 $g \cdot g^{-1}$ ethanol from xylose and glucose and ethanol productivity of 3.4 $g \cdot L^{-1} \cdot h^{-1}$ [150]. The continuous fermentation method yields an improved output in minor bioreactor volumes, has low operational costs by lowering production times, is cost-effective, allows for growth control via nutrient supply management, and is scale-up friendly. Some limitations of the continuous fermentation process, such as low product concentration, complicated downstream processes, difficulty in maintaining sterilization conditions, high risk of contamination with the extended culture time, limited yeasts' capacity to create ethanol and periodic handling, which may also increase the costs of operation, are observed.

Syngas fermentation is a biological carbon fixation process that uses a gaseous feedstock, primarily composed of a mixture of CO, CO_2, and H_2 which is obtained from biomass, coal, animal or municipal solid waste, and industrial CO-rich waste gases, that is a promising approach converted into valuable chemicals and fuels by microorganisms through a hybrid thermo/biochemical process [151,152]. Several Clostridium species are known to produce different bioproducts, but only a few of them use syngas as the sole carbon and energy source [153,154]. *Clostridium carboxidivorans* are acetogenic bacteria that are known to grow autotrophically with syngas and chemoorganotrophically with

a wide range variety of sugars [155–157]. It is able to ferment these carbon sources to produce volatile fatty acids and alcohols that can be employed as platform chemicals or as feedstock for liquid fuel production qualifying it as an interesting microorganism for industrial production [152,158,159]. However, the issues that must be addressed in order to incorporate the syngas fermentation into an industrial-scale process include the gas-liquid mass transfer limitation brought to the low aqueous solubilities of the gaseous substrates that occur when cells have the capacity to process more gas than the bioreactor can supply. The resistance of gaseous substrate diffusion at the gas-liquid interface has been identified as the limiting step in syngas fermentation [160–163]. The other challenge identified as low carbon fixation yield, high production cost, and the effects of gaseous impurities such as NH_3, H_2S, and NO_x even at low concentrations by limiting microbial growth, enzyme activities or by changing physiochemical conditions led to the unintended accumulation of organic acids and decreased alcohol formation [152–154,159,164,165].

The SSF method combines enzymatic hydrolysis and fermentation in a single phase to produce value-added products. This method involves hydrolyzing cellulose and extracting sugars by using an enzymatic complex. These sugars are then used by microbes and transformed into value-added compounds [166]. The combination of the semicontinuous fermentation of sugarcane bagasse and SSF system produces 9.07% (v/v) ethanol with <1% residual glucose at the optimum conditions of 1% (w/v) NaOH, 160 °C, and 20 min of reaction. This study shows no remarkable variation throughout the whole process and that the system achieves a constant state [167]. Compared with SHF, SSF has several advantages. These advantages include the use of an individual vessel for fermentation and saccharification, which reduces the residence period and capital expenditure, and the reduction of the inhibitory composite from enzymatic hydrolysis, which enhances inclusive operational achievement. SSF has been intensively studied for the manufacture of ethanol from lignocellulosic and starchy raw materials because of these benefits. The optimal temperature for enzymatic hydrolysis is often higher than the fermentation temperature, and the SSF reaction is limited by the pH and temperature of the operation.

Meanwhile, in the pre-hydrolysis simultaneous saccharification and fermentation (PSSF) configuration, the pretreated material is pre-hydrolyzed at the optimum temperature of the cellulolytic enzyme, and the temperature is then lowered for further inoculation with no other additional step [168,169]. The main advantage of PSSF is significantly reduced overall fermentation time, environmentally friendly, increased initial velocity (V_0) of enzymes, and provided the optimum conditions for both the enzyme and yeast to utilize the substrate sufficiently that also reduces the production cost and favors the distillation process for high ethanol yields [170,171]. The banana peel with 25% (w/v) of high solid loading using commercial S. cerevisiae at 64 h of fermentation has been demonstrated as the promising feedstock for ethanol production by PSSF by achieving a maximum ethanol concentration of 32.6 g/L [172]. The bioconversion of barley straw to bioethanol was carried out by PSSF where the kinetic model was used as guidance in the choice of pre-hydrolysis time step. The highest ethanol concentration reached in the present study was 46.62 g/L at a high solid loading of 20% (w/v) of barley straw by applying 16 h of pre-hydrolysis. The mass balance of PSSF showed that the reduction in ethanol yield when solid loading increases could be attributed to the decrease in cellulose enzymatic conversion [173]. Under the PSSF strategy in the development of a process using *Sargassum* biomass at high pretreated solid loading 13% (w/v) was subjected to high-pressure technology for biomass fractionation recorded the maximum ethanol concentration of 18.14 g/L after 12 h of fermentation [174]. The ethanol production from potato peel waste subjected to the PSSF process allowed for reaching a maximum ethanol concentration of 104.1 g/L at high productivity with 54 h of fermentation [175].

The simultaneous saccharification and co-fermentation (SSCF) method breaks down cellulose into sugars called hexoses by using an enzyme complex. Specialized microorganisms with the capacity to ingest substrates consume these sweeteners generated in situ along with pentoses following a pretreatment to acquire a product of significance. The

research on the corn stover subjected to temperature-profiled SSCF at 12% of glucan loading eliminated sugar accumulation and alleviated ethanol repression by process optimization, 59.8 g·L^{-1} ethanol. It suggested that the high-temperature resistant strain helped the xylose-utilizing strain maintain cell viability in SSCF at high temperatures (42 °C) which are higher compared with the threshold concentration for the economic distillation process [176]. Xylose utilization in the study of sugarcane bagasse by using SSCF with a thermotolerant *S. cerevisiae* at 40 °C demonstrated 99% xylose in the hydrolysate during the co-fermentation process, generating 36.0 g·L^{-1} ethanol [177]. The differences in pH, temperature, and other parameters required for the enzymatic hydrolysis and co-fermentation process have been recognized as limiting factors in the SSCF.

The enzymes that hydrolyze cellulose in the production of ethanol require high-temperature conditions, i.e., thermotolerant yeast and bacteria, to produce high enzyme contents. The thermotolerant microorganisms are beneficial in terms of efficiency improvement of processes by obtaining higher yields in saccharification, reducing costs associated with a cooling system while reducing the risk of bacterial contamination [178–181]. Many studies have examined various thermotolerant yeasts with their optimized temperature for ethanol production. The isolate *Pichia kudriavzevii* at 28 °C achieved the optimal ethanol concentration of 10.10 g/L and a productivity of 0.21 g/L/h in monoculture fermentation [182]. The optimal conditions of *Meyerozyma guilliermondii* at 45 °C using sugarcane bagasse as a substrate achieved the maximum ethanol concentration of 11.12 g/L and a productivity of 0.23 g/L/h [183]. The optimum fermentation conditions for ethanol production from sweet sorghum juice with the thermotolerant yeast *S. cerevisiae* at 37 °C revealed a maximum ethanol concentration of 99.75 g/L and a productivity of 2.77 g/L/h was achieved [184]. *K. marxianus* at 42 °C also effectively utilized biopretreated elephant grass hydrolysate and produced the maximum ethanol concentration of 14.65 g/L and a productivity of 0.62 g/L/h [185]. Fermentation or hydrolysis can be achieved under ideal specifications, and the microorganism must be specialized for both substrates and only applicable at high-temperature conditions. The process requirements also point to the necessity for the creation of specialized microorganisms. With the use of genetic engineering, the SSCF process offers several advantages, including the utilization of minimal equipment, short processing times, reduced contamination risk, and high ethanol production efficiency.

The development of consolidated bioprocess (CBP) of lignocellulosic biomass is the most integrated process for the bioconversion approach, where the process of hydrolysis, fermentation, and enzyme production occurs in a single reactor. The conversion of pretreated lignocellulose employs genetically modified single microorganisms or a microbial consortium capable of hydrolyzing biomass with enzymes produced on its own and fermenting monosugars into value-added products could provide the environmentally friendly, economically competitive by reducing costs for infrastructure, raw materials, and enzyme production [117,186,187]. The effective fermentation of monosugars obtained from lignocellulosic biomass is the next bottleneck in bioethanol production reaching an industrial scale. Several factors might affect its low conversion efficiency, including low enzyme concentrations at the start of the fermentation, temperature, time, pH, inoculum size, solid-to-liquid ratio, agitation rate, oxygen content, and rotation speed [188–190]. The isolated bacterium of *Hangateiclostridium thermocellum* in the study of pre-treated *Nannochloropsis gaditana* biomass converted into ethanol through CBP was investigated. In this study, the hemicellulose removal of dilute H_2SO_4 treatment was found to be best for the pretreatment of biomass at the concentration of 2.5% under 100 °C for 60 min, effectively disrupting a complex matrix of the holocellulose sample and removing the hemicellulose. The optimized conditions of the medium components and process parameters yielded a maximum ethanol concentration of 12.90 g/L [191]. The investigation on the potential of the fungus *Trichoderma asperellum* to produce ethanol and the physicochemical parameters required for paddy straw waste conversion via CBP using the numerical optimization was statistically validated by comparing the volume of ethanol produced, to the volume analyzed via Response Surface Methodology (RSM). The investigation proved that the

fungus is a potential organism for on-site enzyme production with a maximum ethanol concentration of 0.94 g/L [192]. The maximal ethanol production capability of *Fusarium moniliforme* integrated biodelignification and CBP of Napier grass at solid-state conditions is 10.5 g/L by feeding the fungus with a surplus of glucose for fermentation. These results demonstrated the characteristics of a fungus for potential ethanol production from cellulose, mixed sugars, and lignocellulosic materials [193]. The study of the bioconversion of *Sargassum wightii* via CBP using the bacterial isolate, *Lachnoclostridium phytofermentans* shows excellent growing ability in the optimized production medium conditions with the maximum ethanol concentration of 13.75 g/L [194].

The pretreatment of feedstocks minimizes their size and makes following the procedures easy. Cellulose and hemicellulose are hydrolyzed into sugars that may be fermented. These carbohydrates are fermented into ethanol by using yeasts. *S. cerevisiae* is widely utilized as a yeast strain for the ethanol fermentation of lignocellulosic hydrolysates due to fast growth, high tolerance, efficient glucose anaerobic metabolism, high selectivity, cost-effective process for high ethanol yield, high rate of fermentation, low accumulation of byproducts, and use of a broad scale of disaccharides (e.g., sucrose and maltose) and hexoses (e.g., glucose, mannose, and galactose) [195,196]. Table 1 shows ethanol production by *S. cerevisiae* from a different type of feedstock at varying treatments.

Table 1. Ethanol production by *S. cerevisiae* from different types of feedstock at varying treatments.

Feedstock	Parameters			Ethanol Concentration (g/L)	Ref.
	Temperature (°C)	Agitation Speed (rpm)	Incubation Time (h)		
Galactose	30	200	28	96.90	[197]
Rice husk	43	150	96	15.63	[198]
Oil palm frond	30	152	15	4.79	[199]
Cellulose and sucrose/xylose	30	200	96	4.30	[200]
Papaya peels	30	200	48	0.51	[201]
Pineapple leaf	30	150	72	9.75	[202]
Pomegranate peel	30	100	24	5.58	[203]
Sweet sorghum	30	150	18	97.54	[204]
Sugarcane distillery waste	30	150	48	49.77	[205]
Corn starch	30	300	192	98.13	[206]
Rice straw	30	150	72	18.07	[207]
Sugarcane molasses	30	200	56	114.71	[208]
Corn stover	34	150	48	21.47	[209]
Oil palm trunk	30	150	18	44.25	[171]
Microalgae biomass	30	150	48	52.10	[210]
Sugar beet molasses	30	140	112	79.60	[211]
Cassava starch	30	200	72	81.86	[212]
Suweg starch	37	80	78	99.52	[213]
Frond Waste	50	150	96	33.15	[214]

Industrial ethanol production is efficiently produced from lignocellulosic hydrolysates by yeast strains with high hexose and pentose fermentation. This result is due to the high xylose and glucose contents in lignocellulosic biomass [215,216]. The modest acid stress caused by lignocellulosic materials also inhibits yeast fermentation. The presence of weak acids in deficient concentrations can boost ethanol synthesis through cellular division. In *S. cerevisiae*, weak acids are shown to increase glucose consumption, ethanol synthesis, and tolerance to 5-hydroxymethylfurfural and furfural [217,218]. Despite the fermentation route having been commercially realized, the cost is expensive due to the energy-intensive distillation steps and low yield to meet the market demand. Other remarkable obstacles to ethanol generation, such as excessive temperatures, prominent ethanol concentrations, and capacity to ferment pentose sugars remain in yeast fermentation. The main disadvantage

is that yeasts grown in anaerobic states for an extended period lose the capacity to manufacture ethanol. Furthermore, at high dilution rates, which allow for high productivity, the substrate is not entirely utilized, resulting in low yield. The rate of development and metabolism of yeasts increases as the temperature rises until the optimal level is reached. The inhibition of microorganism expansion and viability can occur when ethanol concentrations rise during fermentation. The difficulty of *S. cerevisiae* growing on a medium with a high concentration of alcohol causes ethanol production to be inhibited. The limitation of *S. cerevisiae* is the inefficient fermentation of glucose and xylose. As a result, yeast strains that can ferment glucose and xylose or utilizing two separate yeast strains that can utilize these sugars individually should be found.

3. Future Directions of CO_2 Conversion into Ethanol

3.1. Ethanol Synthesis Based on Electrochemical Reduction

A carbon-neutral energy cycle is through the transformation of sunlight towards energy-dense fuels via electrolytic CO_2 reduction to fuels [17,219,220]. Based on the Nernst equation, electrochemical reduction potentials are translated into the reversible hydrogen electrode (RHE) range:

$$E_{RHE} = E_{Ag/AgCl} + 0.059 \times pH + E^0{}_{Ag/AgCl}, \quad (3)$$

where the potential, E_{RHE} vs. RHE, $E^0{}_{Ag/AgCl} = 0.198$ V at 25 °C, and the potential measured, $E_{Ag/AgCl}$ vs. the reference electrode, Ag/AgCl.

The conversion of electrochemical CO_2 into ethanol involves a set voltage flow with steady or unnoticeable current conditions. This process determines the best voltage to convert CO_2 into ethanol via electrochemical synthesis easily. The conversion of CO_2 into ethanol is a nonspontaneous reaction (E^0 = negative) that requires an external voltage source from the power supply. A predetermined voltage flow with stable or imperceptible current states is used to convert electrochemical CO_2 into ethanol. This process makes identifying the appropriate voltage for the conversion of electrochemical CO_2 into ethanol easy. The conversion of CO_2 into ethanol is a nonspontaneous reaction (E^0 = negative) that needs a power supply voltage source. Splitting the process into two separate electrochemical stages is used to pursue ethanol synthesis. The intermediate product in the assembly cascade technique should be a stable species that can be easily isolated from the initial electrolyte. CO is chosen as the stable intermediate product from the start, as evidenced by CO_2 electroreduction at excessive faradaic efficiencies:

$$CO_2 + H_2O + 2e^- \rightarrow CO + 2OH^- \qquad E^0 = -0.10 \text{ V vs. RHE} \quad (4)$$

The poor solubility of CO causes the easy separation of intermediate products for transfer to the second-stage electrolyzer, leading to excessive current density due to the difficulty of the CO reduction process. Han et al. [221] concluded a feasible approach to solve the restricted CO coverage and deficiency in CO solubility in the catalytic position is to develop a cocatalyst for the formation of CO and reduction of CO_2 in the electrocatalytic reaction. Thus, the catalyst system can be prepared by coupling two sites, where one site efficiently reduces CO_2 to CO, which further distributes to the construction of C–C coupling in the formation of long carbon chain species that occur on the other sites of coupling. Yuan et al. [222], Kou et al. [223], and Ramírez-Valencia [224] reported that the CO-producing site's pyridinic N-doped carbon species components show excellent performance selectivity and high catalytic accomplishment for the reduction of CO_2 to CO. The development of N-doped porous carbon components influences the electronic order and size of the Cu catalyst and further improves the gas transport for enhanced availability to pyridinic N during the process of adsorption of CO_2 and reduction of CO. The electrocatalyst reaction for the direct transformation of CO_2 into ethanol demonstrates competitive faradaic efficiencies but prefers high current densities, low overpotentials, and poor selectivity with the long-term stability of the operation [225–227].

The overall cathode half-reaction for ethanol formation is as follows:

$$2CO_2 + 9H_2O + 12e^- \rightarrow C_2H_5OH + 12OH^- \qquad E^0 = 0.09 \text{ V vs. RHE} \tag{5}$$

The advantage of the electrochemical synthesis of ethanol from CO_2 is the product selectivity generated on each electrode terminal. Then, the equipment and substance used are basic and have a low cost. The process is controllable and flexible with a safe and mild operating background and empowers the nonfossil energy from renewable energy sources with environmentally friendly coupling [224]. The kind of metal utilized on the electrode affects the electrochemical synthesis efficacy of converting CO_2 into ethanol. The electrocatalytic characteristics of metals employed as electrodes affect the transformation percentage of CO_2 and the distribution in overall compounds. The category of catalyst, reaction potential, properties of electrolyte solution, cell design, pH value, and reaction circumstances, such as temperature and pressure, influence the outcomes of electrochemical synthesis [228–230]. The variety of alkaline electrolytes ranging in pH from neutral to alkaline has shown the potential to improve C_2 products [231–233]. Some studies in the electrochemical synthesis operation for converting CO_2 into other chemicals revealed that the category of electrode used and the sensor preparation have a remarkable effect on the results produced [234,235].

In the electrochemical synthesis process, where the water oxidation reaction occurs, carbon is an inert electrode attribute that does not react when utilized as an anode. Carbon is not affected during electrochemical production because of its inert characteristics. Water is oxidized and becomes a source of protons and electrons because carbon is an inert compound, and the bicarbonate anion (HCO_3^-) does not oxidize in water. The mechanism of the reaction of ethanol synthesis at the cathode involves 12 protons and electron transfer, which aid the process of ethanol formation at the cathode [17,232,236–238]. In the electrolytic CO_2 reduction, normal metallic electrocatalysts only generate the C_1 building block but copper (Cu) elements have been identified to catalyze the manufacturing of low hydrocarbons at reasonable excessive faradaic efficiency (FE). The transformation of CO_2 into multicarbon alcohols via multiple electron transfer reactions facilitates C–C coupling reactions to produce C_2 products, resulting in decreased system's energetic competency and poor selectivity [221,239,240]. Various factors of the selectivity and activity, such as catalyst size, catalyst surface structure, catalyst oxidation state, structural morphology, crystallographic orientation, composition, type of electrolyte ions, pH, pressure, temperature, design of the electrochemical cell, and the existence and number of deficiencies (i.e., point fault, contamination, unorganized location, grain limits), enhance the catalytic performance of CO_2 electroreduction towards multicarbon products [230,239,241,242]. Nanocatalyst morphologies, supporting materials, nanograin boundaries, and catalyst surface changes can all have an impact on contrary reaction pathways.

Zhu et al. [243], Zhou and Yeo [244], and Chen et al. [245] believed that Cu-based catalyst arrays' structure elevates local pH, which favors CO generation and C–C coupling to generate C_2 products. Zhang et al. [246] agreed that on the Cu surface, the conversion of CO_2 to form C–H is difficult because it requires several electron reductions, protonation, and C–C coupling reactions. The restructuring of Cu facet coordination has stabilized facets on metal surfaces under electrolysis conditions, promoting the production of hydrogen. Compared with a traditional H-cell, a gas-fed flow cell improves FE toward CO_2 reduction products [239,247]. Jung et al. [248] also highlighted the importance to generate C_2 products selectively, which is critical to regulate and maintain the morphology of amorphous Cu nanoparticles. Density functional theory (DFT) calculation has shown that Cu is the preferable electrocatalyst for the formation of C_2 products [249–251]. CO_2 activation and CO dimerization to form C_2 products are remarkably improved by the linkage between the functional surfaces of Cu. The outcome also reveals that using the Cu complex as a precursor is critical for excellent performance because the Cu catalyst generated via direct electrodeposition has substantially low efficiency. The combination of copper with other metals produces higher catalytic activity for converting CO_2 into ethanol than pure copper

metal. This finding is proven by the combination of Pd–Cu nanoparticles [252], copper-modified boron-doped diamond [253], copper–cuprous oxide [249], copper surface with a family of porphyrin-based metallic complexes [254], copper–silver composites [255], and cuprous oxide nanocubes with silver (Ag) nanoparticles [256]. Table 2 shows a summary of the experimental procedure applying copper-based catalysts in the transformation of CO_2 into ethanol.

Table 2. Summary of the experimental procedures applying copper-based catalysts in the transformation of CO_2 into ethanol.

Catalyst	Electrolyte	Cell Configuration	Current Density (h)	Overpotential	Faradaic Efficiency (%)	Total Current Density (mA cm^{-2})	Reference
Cu	1.0 M KOH 0.5 M $KHCO_3$	Electrochemical flow cell	4	−0.58 V vs. RHE	46	200	[257]
Cu	0.1 M KBr	H-type glass cell	3	−1.10 V vs. RHE	23	170	[258]
Cu	1.0 M KOH	Two compartment electrochemical H-cell	16	−0.95 V vs. RHE	32	126	[259]
Cu/Ag	1.0 M KOH	Electrochemical flow cell	not available	−0.70 V vs. RHE	25	300	[260]
$Ce(OH)_x$-doped-Cu	0.1 M KCl	Three-electrode electrochemical cell	6	−0.70 V vs. RHE	43	128	[261]
Cu	0.1 M $KHCO_3$	Flow cell reactor	6	−0.60 V vs. RHE	40	200	[262]
Cu/Ag	1.0 M KOH 1.0 M $KHCO_3$	Flow cell reactor	2	−0.67 V vs. RHE	41	250	[263]
Cu	1.0 M $KHCO_3$	MicroFlow® cell	20	−0.97 V vs. RHE	89	300	[264]
Cu	1.0 M KOH	Electrochemical flow cell	65	−0.71 V vs. RHE	90	520	[265]
FeTPP[Cl]/Cu	1.0 M $KHCO_3$	Electrochemical flow cell	12	−0.82 V vs. RHE	41	124	[254]
N-C/Cu	1.0 M KOH	Flow cell reactor	15	−0.68 V vs. RHE	52	156	[266]
zCu/Ni-N-C	1.0 M KOH	Electrochemical flow cell	103	−0.70 V vs. RHE	62	415	[267]
Cu_2O	1.0 M $KHCO_3$	Gas diffusion electrode flow cell	10	−0.85 V vs. RHE	76	300	[268]
np-Cu/VO_2	1.0 M KOH	Electrochemical flow cell	12	−0.80 V vs. RHE	38	102	[269]
ZnO/4Cu_2O	1.0 M KOH	Electrochemical flow cell	not available	−1.0 V vs. RHE	50	140	[270]
Cu_{50}/$PTFE_{15}$	1.0 M KOH	Gas diffusion electrode flow cell	2	−1.85 V vs. RHE	47	200	[271]
Cu_2O/Ag	1.0 M KOH	Gas diffusion electrode flow cell	not available	−1.18 V vs. RHE	73	243	[256]
Cu/C/PTFE	1.0 M KOH	Gas diffusion electrode flow cell	2	−1.0 V vs. RHE	76	250	[272]

Despite advancements in the electrochemical CO_2 reduction process, creating highly operative and selective nanocatalysts for the electrochemical CO_2 reduction reaction remains a major issue. The Cu-based catalyst of the nanostructure is chemically unstable, which demonstrates various catalytic performances via different procedures of operations due to the uncontrolled facet of oxidation and is related to the alternate in facet chemistry. The local reaction environment is further altered by electron reduction and protonation, making it challenging to stabilize the nanocatalyst. Facet coatings are a common way to improve the strength of nanocatalysts but affect the Cu's facet chemistry and its capability to convert CO_2 to form C–H hydrocarbon. MOFs are favorable support materials in stabilizing and improving the catalysts due to their electrical conduction. MOFs require pressured reactant supply and an outcome separation mechanism due to their porous nature. More experimental research should be conducted to stabilize Cu nanocatalysts for the discovery of their catalytically functional area and improved activity/selectivity. Other challenges

include the effect of the poor transfer current densities causing the ineffective electron exchange rate of kinetics, the deactivation of electrodes, enormous overpotential (or low energy performance), restricting practical use, deficient selectivity of the product, which necessitates expensive separation processes, and technological commercialization.

3.2. Ethanol Synthesis from DME

The thermochemical approach to the production of ethanol from CO_2 via DME has two phases of reaction. The initial step is to make DME from CO_2 and H_2. Methanol synthesis and dehydration are the two phases in the traditional commercial DME synthesis from syngas, which includes CO and CO_2. However, a one-step experimental procedure on multifunctional catalysts is favorable due to its thermodynamic stability and operational cost-effectiveness [273,274]. DME is a cheap and bulk chemical with environmental acceptability, has high quality, and is an excellent replacement fuel for use in diesel engines [275–277]. DME is also used as a critical intermediary to bulk chemicals in the industrial sector by producing acetic acid, olefins, and hydrocarbons [278–280]. The commercialized process reaction of the DME synthesis reactor is based on the equation below.

CO Hydrogenation:

$$CO + 2H_2 \rightleftharpoons CH_3OH \qquad \Delta H^0{}_{298} = -90.8\ \mathrm{kJ{\cdot}mol^{-1}} \tag{6}$$

CO_2 Hydrogenation:

$$CO_2 + 3H_2 \rightleftharpoons CH_3OH + H_2O \qquad \Delta H^0{}_{298} = -49.5\ \mathrm{kJ{\cdot}mol^{-1}} \tag{7}$$

RWGS:

$$CO_2 + H_2 \rightleftharpoons CO + H_2O \qquad \Delta H^0{}_{298} = +41.2\ \mathrm{kJ{\cdot}mol^{-1}} \tag{8}$$

Methanol dehydration:

$$2CH_3OH \rightleftharpoons CH_3OCH_3 + H_2O \qquad \Delta H^0{}_{298} = -23.4\ \mathrm{kJ{\cdot}mol^{-1}} \tag{9}$$

Methanol catalysts, e.g., $Cu/ZnO/Al_2O_3$ (CZA), catalyze the reactions at Equations (6)–(8), whereas catalysts with acidic properties such as HZSM-5, zeolites or γ-alumina catalyze reactions at Equation (9) [281–284]. CZA is a dominant conventional catalyst in the DME reaction due to its capability to improve the catalytic performance and selectivity toward methanol production. Studies on the CZA catalyst for CO_2 hydrogenation to methanol for 720 h time-on-stream of the reaction demonstrated that the space–time output of methanol is reduced to 34.5% during long-term testing [285]. The addition of Zr in the CZA catalyst, which forms $CuO/ZnO/ZrO_2/Al_2O_3$ (CZZA) with HZSM-5, shows improvement stability with methanol production by reduction from 18.5% to 14.1% with more than 58.7% selectivity after 100 h of DME reaction [286]. The DME reaction by using $CuZn/Al_2O_3$ catalyst recorded optimum conditions at 250 °C and 40 bar, resulting in a methanol selectivity of 58% [287]. The optimum reaction condition for DME synthesis requires temperatures and pressures ranging from 200 °C to 300 °C and from 20 bar to 50 bar, respectively [288–290].

The direct production of DME in a one-step process involves the simultaneous completion of two stages of reactions, i.e., methanol generation (via CO_2 hydrogenation) and methanol dehydration to DME, in the same reactor by using hybrid/bifunctional catalysts in a closed system, avoiding the need for intermediate purification steps and transportation units to minimize the cost of operation [273,291,292]. The hybrid/bifunctional catalysts needed for direct DME production require the combination of metal sites with redox function properties for the selective CO_2 hydrogenation to methanol and acidic function for the transformation of methanol dehydration to produce DME. Based on the Le Chatelier principle, the high water content limits the production of methanol that occurs in the hydrogenation of CO_2. The dehydration reaction contributes to the production of water. If the reaction area is divided through the core-shell structure, the presence of water on metallic sites can be significantly limited [291,293,294]. Water molecules tend to be ad-

sorbed on the surface of catalysts which deactivation of catalyst function by metal oxidation of the catalytic phase and constructs a faster metal sintering and destroys the structure of the acid catalysts blocking the production of methanol on the hydrogenation sites. Hence, an investigation is conducted to increase the stability of the catalyst implemented in the hydrogenation reaction. A remarkable improvement in catalytic stabilities has been recorded in In_2O_3/ZrO_2 [295], interlinkage of CuO–ZnO–ZrO_2 on the surface of the zeolite [296], zirconium-modified CZA [286], gallium nitride [297], Cu–Ho–Ga/γ-Al_2O_3 [298], Cu/ZnO/ZrO_2//H-FER 20 [299], and PdZn/TiO_2-ZSM-5 hybrid [300]. The introduction of membrane reactor technologies [292,301] and adsorbent material [288,289,302] has been proposed to limit the effectiveness of water in DME production. Additionally, stable acid sites are needed in DME production due to the presence of water because strong acidic sites catalyze secondary dehydration reactions that deposit carbon and form hydrocarbon [273,276].

The Cu-MOR@SiO_2 core−shell microcapsules catalyst in tandem with the ternary oxide CZA catalyst recorded the catalytic activity of DME conversion at 83.8% and ethanol selectivity at 48.7% over 50 h at 220 °C of reaction [303]. On the reaction of CZ@Cu-MOR microcapsule catalyst for 50 h at 400 °C, DME carbonylation converted to methyl acetate on the active sites of the zeolite subsequently hydrogenated the syngas to DME conversion, and ethanol selectivity of about 26.8% and 45.8%, respectively, was achievable [304]. In the optimal reaction condition of 24 h at 220 °C, the proximity effect in the two components of NMOR zeolite and CZA tandem catalysts exposed to syngas achieved a DME conversion of 66% along with ethanol selectivity of 43.4% [305]. The most challenging aspect of the direct production of DME from CO_2 by utilizing hybrid/bifunctional catalysts is ensuring the correct ratio with regulated metal and acid interaction that is required for methanol production and dehydration. The detriment of utilizing DME as an alternative fuel to diesel is due to its low viscosity, which causes a leak and component damage. Furthermore, DME has low heating point than diesel. Therefore, despite its higher energy performance, DME still requires fuel insertion every cycle of the reaction. DME also has low combustion enthalpy, low modulus of elasticity, and fuel tanks with low energy content. These disadvantages counteract the features of DME's low boiling point, and a pressured system must be used to keep the fuel in a liquid condition.

3.3. Ethanol Synthesis Based on RWGS

One of the most promising methods for CO_2 consumption as a renewable system delivering feedstock for nonfossil fuel synthesis and important chemical processes is the RWGS procedure [306–309]. The hydrogenation of CO_2 is converted into hydrocarbons via the RWGS reaction, which is catalyzed in tandem and subsequently modified by the Fischer–Tropsch synthesis (FTS) mechanism, where the intermediate product of the reaction is CO before hydrocarbons or alcohols are formed [310,311].

CO_2 hydrogenation:

$$nCO_2 + (3n+1)H_2 \rightarrow C_nH_{2n+2} + 2nH_2O \rightarrow \Delta_RH_{573K} = -128\ kJ{\cdot}mol^{-1} \quad (10)$$

RWGS:

$$CO_2 + H_2 \rightarrow CO + H_2O \rightarrow \Delta_RH_{573K} = 38\ kJ{\cdot}mol^{-1} \quad (11)$$

FTS:

$$nCO + (2n+1)H_2 \rightarrow C_nH_{2n+2} + nH_2O \rightarrow \Delta_RH_{573K} = -166\ kJ{\cdot}mol^{-1} \quad (12)$$

This process is also known as the CO_2-FTS mechanism, where the CO produced from the RWGS reaction is inserted into the $*CH_3$ or $*CH_3(CH_2)_n$ generated from the CO-FTS mechanism to form methanol, ethanol, or other higher alcohol synthesis [312,313]. The RWGS reaction is an endothermic process favored at high temperatures, resulting in a high equilibrium conversion of CO_2 and performed at relatively low contact times [307,314].

The hydrogenation of the CO_2 reaction path is an inherent drawback because the FTS mechanism is an exothermic process that favors low temperatures [311,315]. Active sites for dissociating hydrogen and adsorbing CO_2 should be present in RWGS catalysts. The excellent performance of the precious metal-based catalyst in RWGS reactions has been recorded in a few studies due to their ability to dissociate hydrogen at low-temperature catalytic activities [316–318]. However, these catalysts are not suitable for industrial-scale promotion and application due to limitations of high prices and rare resources. In the RWGS reaction, Ni and Cu-based catalysts have demonstrated good activity and selectivity but are prone to sintering deactivation at high temperatures [318–321]. Transition-metal carbides are also favorable in RWGS reactions due to their dual functionality for dissociating hydrogen and C=O bond cleavages [322,323]. In ethanol production, Fe-based catalysts with the right combination of promoters, organized additives, or assistance form the active area of reaction. Alkali metals particularly Na and K elements have been identified as the most effective promoters of the catalytic performance of Fe-based by producing highly active for the FTS mechanism in improving the selectivity and CO_2 conversion during ethanol production [324,325]. Carbon support substances are natural support materials for Fe-based catalysts and show outstanding catalytic achievement for ethanol generation by enhancing selectivity and expanding the active dispersion phase in the FTS mechanism [326].

The catalytic performance of carbon support materials is based on the surface area, pore size, distribution, and pore structure [327,328]. Unfortunately, the use of Fe-based catalysts for CO_2 hydrogenation reactions produces highly toxic precursors and needs a long time of carbonization [326]. Cu-based catalysts in RWGS reactions have been extensively investigated due to their high stability, low cost, high-performance atmospheric pressure at very low temperatures, and excellent selectivity for CO [283,316,329,330]. When a considerable quantity of CO_2 in the feed is adsorbed on the surface, the oxidation and reduction processes of Cu-based catalysts demonstrate strong activity with a minimal number of undesirable products [283,331,332]. In the RWGS reaction, the hydrogenation of the CO_2 mechanism happens by using a Cu-based catalyst, with CO as an intermediate product before forming hydroxyl species on the surface, thus constraining the operative area for alcohol synthesis when CO_2 decomposes into water molecules. This process is the redox mechanism with the Cu-based catalyst involving CO_2 reduction, the rate-determining step, and active sites in RWGS reactions. CO_2 oxidizes into Cu^0 to produce Cu^+, which improves the CO selectivity by 10%, whereas H_2 reduces the Cu^+ to form Cu^0 to generate H_2O [306,333]. The investigation of the morphological effect shows that Cu/CeO_2 nanorods exhibit the highest CO_2 conversion compared with Cu/CeO_2 nanocubes and favor the strong link of metal–support interaction in generating a high density of oxygen vacancies under reducing conditions [334,335]. The rod-like morphology of CuO/CeO_2 demonstrates the highest catalytic activity and stability and achieves the thermodynamic equilibrium conversion at 350 °C [336]. In the RWGS reaction, the oxygen vacancies on the spinel oxide surfaces are vital in the adsorption and activation of CO_2 [337]. Based on the activation method, the adsorption of CO_2 on oxygen vacancies is the initial step of RWGS, which involves C=O bond cleavages under a high-temperature energy-driven process [338]. A study on the role of copper as a promoter has shown an indirect effect on catalyst activity. The study reported that the addition of Cu to the Mo_2C catalyst enhances the selectivity of CO yield [333]. The presence of Cu in MoO_3/FAU zeolite catalysts influences the reduction step of MoO_3 to MoO_2, thus improving the CO yield [332]. However, the major drawback of the Cu-based catalyst, which undergoes deactivation during the RWGS reaction because of poor thermal stability due to the fractional oxidation of the Cu metal, leads to the reduction in the surface area of the active sites and copper particle agglomeration at high temperatures. The effective metal stage and/or coke deposition are hampered by material sintering, which lowers the CO_2 transformation degree by restricting catalyst activity.

Some thermodynamic limits in RWGS reactions are present. The CO_2 reactant has the potential to damage the CO hydrogenation catalyst, and the water that is inevitably retained in the end product, generally 20–45% of the whole product, decreases product selectivity and catalytic activity. The endothermic nature of the RWGS reaction uses sophisticated catalysts that are frequently necessary to customize the cascade reactions, and a high temperature, typically above 300 °C, is required to drive these processes. Although methanol is used as an intermediary to make liquid hydrocarbon from CO_2 hydrogenation at high temperatures on some occasions, the end product has remarkable CO byproducts. The low activity and unstable C–C coupling formation in the FTS mechanism is another challenge in the CO_2 hydrogenation process that usually produces light hydrocarbons, particularly methane. Catalyst deactivation has been identified in the FTS mechanism by poising the catalyst in the presence of sulfur and nitrogen compounds, inactive metal support compound, hydrothermal sintering, and the formation of inactive catalytic phases as oxides.

3.4. Ethanol Synthesis Based on Catalytic Hydrogenation

Catalytic hydrogenation is one of the promising approaches to overcoming the obstacle in the chemical reduction activation of CO_2 [316,339,340]. The hydrogenation of CO_2 yields useful alcohols, such as methanol, ethanol, and higher alcohol, that have impressive energy density with broad applications to value-added chemicals, such as neat fuels, fuel additives, and raw chemicals [16,17,297,341]. However, due to a shortage of effective catalysts with excellent stability, the effective cleavage of the C–O bond, excessive strength barrier of C–C coupling, and generation of water as a byproduct in the process can simply inactivate several catalysts for CO_2 transformation, and the direct synthesis of ethanol via CO_2 hydrogenation is substantially more difficult than methanol synthesis [16,342,343]. The most efficient catalytic technique for producing ethanol directly from CO_2 should encourage partial CO_2 reduction, hydroxylation, and C–C bond formation at the same time [232]. According to theoretical investigations, minor catalyst effects improve CO_2 hydrogenation catalytic performance. The link between the structure and catalytic performance is established by regulating the catalyst structure of active sites, and constructing optimum catalysts is the most effective technique in managing carbon chain expansion with controlled alcohol arrangement [341,344]. The calcination process to synthesize the catalyst has also been identified to affect the performance of the catalyst. The maximum product yield of the CO_2 hydrogenation reaction is obtained from nickel(II) oxide supported on alumina and calcined at 700 °C with rod-like morphology and tiny crystallite size of nickel(II) oxide nanoparticles (12.7 nm) at facet (111) [345].

The fabrication of efficient heterogeneous Rh-based catalysts on TiO_2 nanorods should be beneficial in boosting ethanol selectivity due to a synergetic combination of surface hydroxyls and widely dispersed Rh nanoparticles. The use of promoters particularly Li and Fe is generally effective in enhancing the activity and ethanol selectivity by increasing the strength of adsorption of bridged-bond CO species and influencing the electronic condition of Rh [346]. Therefore, the RhFeLi/TiO_2 nanorod catalysts in CO_2 hydrogenation exhibit 30% ethanol selectivity, 15% CO_2 conversion, and stable performance for 20 h of operation. The effect on promotion is associated with the prominent density of the hydroxyl group on TiO_2 nanorods and the excessive distribution of Rh elements. Hydroxyl groups have been demonstrated to equalize the protonation of methanol and formate compounds, which are efficiently detached to form $*CH_x$. The production of CO from the RWGS reaction is then introduced to construct CH_3CO*, which is hydrogenated to further produce ethanol [347]. Rh-based catalysts may catalyze CO dissociation and CO insertion over their atomically neighboring Rh^0–Rh^{n+} species, increasing the possibility of coupling between *CO and $*CH_3$ in the synthesis of C_{2+} oxygenates from syngas, such as ethanol, acetic acid, and acetaldehyde [348]. The strong interaction in Rh/TiO_2 catalysts demonstrates excellent steady-state activity with 40% ethanol conversion at 120 min of reaction. The transformation of TiO_2 nanotubes into the anatase structure due to the acceleration of Rh nanowires has

a remarkable impact on catalytic effects. The positive charge on Rh activates the CO_2 hydrogenation and promotes the further decomposition of formate intermediates [349]. Simulations through DFT reveal that the ionic liquid connects to the Rh species on TiO_2 with a binding energy from 0.69 eV to 1.19 eV. The turnover frequency (TOF) of the stabilized single atom Rh/TiO_2 is 800 h^{-1} in styrene hydroformylation and potentially recycled for five runs under harsh reaction conditions [350].

The quantity of vanadium oxide loaded and promoted on Rh-based catalysts enclosed in mesopore MCM-41 (Rh-0.3VO_x/MCM-41) has been demonstrated as extremely promising for ethanol synthesis, with CO_2 transformation and ethanol selectivity of 12% and 24%, respectively. This result is contributed by the equilibrium amount of CO dissociative adsorbed with nondissociative adsorbed affecting the yield and selectivity of ethanol synthesis. The electrical effect is thought to be responsible for the creation of Rh^+ species and the construction of interfacial VO_x–Rh active sites, which dissociate CO into *CH_x and aid in the synthesis of ethanol following CO introduction [351]. The 2K20Fe5Rh–SiO_2 catalyst in CO_2 hydrogenation has recorded 16% ethanol selectivity and 18% CO_2 conversion for 6 h of stability. The presence of K as a promoter in this experiment stabilizes the CO intermediate produced and C–H bond formation during CO_2 hydrogenation [346,352]. Rh10Se clusters supported on TiO_2 (Rh10Se/TiO_2) and treated in a fixed-bed reactor at 350 °C show optimized selectivity to ethanol synthesis at 83% and CO_2 conversion of 27%. The strong electrical interaction between Rh10 and Se is thought to hinder methane production and boost ethanol synthesis on Rh sites by encouraging C–C bond formation via CH_x and carbonyl coupling on the surface to produce acetate substances [353]. The scarcity and high cost of Rh-based catalysts restrict further development. Table 3 shows a summary of CO_2 hydrogenation over homogeneous and heterogeneous catalysts.

Pd-based catalysts have shown promise because they aid in C–C coupling, a crucial step in the formation of C_{2+} molecules, and precisely modify nanoparticle composition, nanoparticle structure, and support materials [354,355]. As a result, numerous Pd-based catalysts for direct ethanol synthesis from CO_2 hydrogenation with good selectivity in an autoclave reactor at a very high reaction temperature (>250 °C) and confined to standard disordered architectures have been created [313,347,356]. Ordered catalysts with considerable interaction with active sites have been proposed to increase charge transfer and regulate electronic effects. Other disordered catalysts may be outperformed by such a catalytic system [357,358]. Within 5 h of the experiment, the Pd_2/CeO_2 nanorod catalyst with a unique two-atom geometric feature arrangement enables the facile cleavage of the C–O bond and efficiently contributes to C–C coupling, yielding 99.2% ethanol selectivity, 9.2% CO_2 conversion, and TOF value of 211.7 h^{-1}. DFT results show that Pd dimers bind CO tightly, preventing CO desorption and forming the precursor of ethanol via connecting CO and CH_3 intermediates [343]. Similar to precious metal group materials, the Pd-based catalyst is scarce and expensive, thus hindering its large-scale application.

At 200 °C for 5 h, the Ir_1–N_2O_3 single-atom catalyst displays exceptional efficiency for CO_2 hydrogenation with 99% ethanol selectivity and a TOF value of 481 h^{-1}. The isolated monoatomic Ir atom interacts with the neighboring oxygen vacancy on In_2O_3 to create a Lewis acid-base pair. This phenomenon generates two independent catalytic centers that reduce CO_2 into active intermediate species of carbonyl (CO*) adsorbed on the Ir atom and subsequently contribute to the C–C coupling to ethanol production [344]. However, the scarcity and high cost of In-based catalysts render them unsuitable for practical application. Co-based catalysts may generate a high selectivity of alcohol products due to excellent CO insertion ability and catalyze C–C coupling. The synergistic impact of facets Co^0 and $Co^{\delta+}$ provides the remarkable achievement of the Co/La–Ga–O composite oxide catalyst in CO_2 hydrogenation, with 9.8% CO_2 conversion, 74.7% ethanol selectivity, and 88.1% ethanol [359]. The introduction of nickel into a Co-based catalyst exhibits high activity and selectivity in forming ethanol by CO_2 hydrogenation. The optimized $Co_{0.52}Ni_{0.48}AlO_x$ catalyst has recorded ethanol synthesis of 85.7% at 200 °C for 12 h on stream. This catalyst

also shows high stability by remaining unchanged metal nanoparticle size and composition five times, whereas the selectivity of ethanol is maintained [360].

The study of the catalytic achievement of Na–Co/SiO_2 catalyst at 250 °C, 5 Mpa, gas hourly space velocity (GHSV) of 4000 h^{-1} for 300 h of reaction recorded 62.8% ethanol selectivity and 18% CO_2 conversion. The CO generated in the Co_2C active phase is injected into CH_x intermediates, leading to the production of ethanol according to in situ DRIFTS data [313]. The interaction between Na and Co_2C produces ethanol efficiently with a CO_2 conversion of 53%. The electronic environment of Na–Co_2C active sites and the effects of CO activation are revealed using DFT calculations. The Bader charge analysis revealed that Na is a cation on the Co_2C surface with a Bader charge of 0.78 e, suggesting electron transfer from Na to Co_2C and the presence of contact between Na and Co_2C (Figure 4a). When CO_2 is adsorbed (Figure 4b), the most charge transferred and the stable adsorption structure on Na–Co_2C active sites reveal that the O–C–O bond of CO_2 is bent from linear in gaseous to 122.4, in which C and two O atoms contact with 2 Co atoms and 1 Na atom, showing that Na–Co_2C allows for easy adsorption and activation [361].

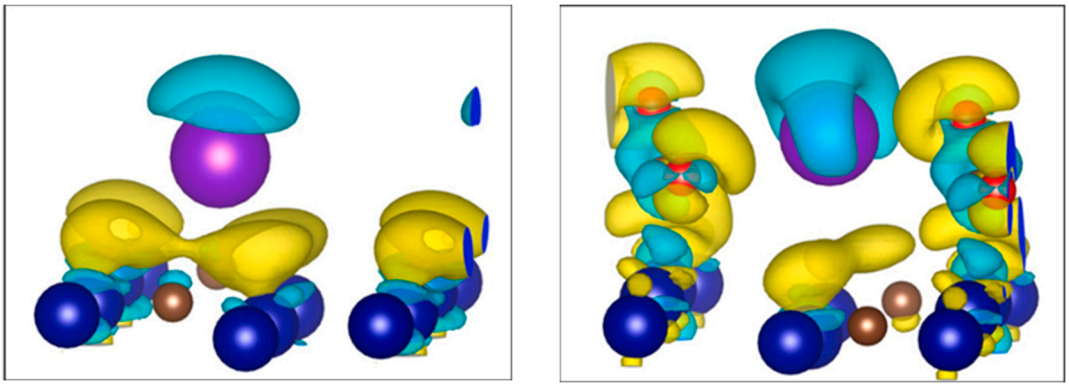

(**a**) (**b**)

Figure 4. (**a**) Charge density calculations of Na adsorbed on the Co_2C surface. (**b**) Charge density calculations of CO_2 adsorbed on Na–Co_2C surface (blue: Co atom; grey: C atom; purple: Na atom) Reprinted with permission from Ref. [361] 2021 Copyright Elsevier.

The energy barriers of transition states on the Na–Co_2C surface are higher than that on the Co_2C surface regardless of CO-direct or H-assisted dissociation. A large number of alkyl species (CH_x) formed on the Co_2C surface (formate species or CO hydrogenation) and the adsorption energies of CH_x species are constant on Na–Co_2C functional surface area. The increase in CO non-dissociative adsorption improves the CO/CH_x ratio, which is conductive and allows for easier CO activation and coupling on Na–Co sites into the adjacent CH_x on Co atoms to synthesize ethanol [361]. The use of $CoMoC_x$ catalyst prepared using the ionic liquid method as all-in-one precursors at 800 °C carbonized temperature results in the optimal catalytic performance of 97.4% ethanol selectivity for 6 h of the experiment. This catalyst also shows high stability performance in the seventh run without remarkable deactivation. This study also found that the most electron transfer and the largest shift towards the low binding energy occur at 180 °C and 2 Mpa and detected CO gas as a byproduct of the reaction. Water, a green solvent used in this reaction, is combined with CO_2 to form bicarbonate and accelerate CO_2 conversion [362]. However, the conventional Co_2C phase under H_2 above 220 °C usually suffers from the rate of deactivation in the long-term catalyst performance. The uncontrollable synergism between CO dissociative activation and CO insertion of metallic Co-based catalysts generates the high selectivity of methane in CO_2 hydrogenation.

Fe-based catalysts possess the ability of CO dissociation catalyzed by an operative composition, and the catalytic activity can be constructed in the formation of hydrocarbon products [363,364]. The improvement of the CO insertion procedure and match the alkyl species formed on Fe sites to make alcohol products, a Fe-based catalyst combined with a noble metal is required [347,356,365]. The catalytic activity of FeMnNa catalyst under experimental conditions of 340 °C, 2.0 Mpa, and $CO_2/H_2/Ar$ ratio of 24/72/4 has resulted in 35% CO_2 conversion and 31.7% ethanol selectivity. The temperature-programmed reduction analysis has also recorded excellent performance of the FeMnNa catalyst by promoting the formation of $MnCO_3$ from MnO in the presence of CO_2 and indicated that the Na component hinders the synergy between Fe and Mn in the reduction of FeMnNa catalyst for selective CO_2 hydrogenation to form ethanol [366]. The monometallic Fe-based catalyst co-modified with Na and S (FeNaS-0.6) achieves 16% ethanol selectivity, 32% CO_2 conversion, and high stability performance of over 100 h of the evaluation with no methanol formation [367]. In the CO_2 hydrogenation process, the sulfur present in the sulfate and its electron-withdrawing effects on Na-assisted Fe sites contribute to CO dissociation, nondissociative CO adsorption, boosting the hydrogenation barrier of $*CH_x$ compound and improving the production of ethanol [23,366].

The development of Mo-based catalysts has opened the door to a new strategy in the hydrogenation of CO_2, which promotes the C–C coupling in ethanol synthesis. The deposition reaction of atomic operative elements Rh and K successfully synthesizes the one-dimensional b-phase of Mo_2C nanowires with specified crystal facets (101). The modification of the $K_{0.2}Rh_{0.2}$/b-Mo_2C complex catalyst results in a prominent production of 33.7 $\mu mol \cdot g^{-1} \cdot h^{-1}$ ethanol and ethanol selectivity of 72.1% at 150 °C [368]. Cu-based catalysts have been extensively studied in the hydrogenation of CO_2 to form ethanol products from syngas although their activity and selectivity are highly dependent on the support and promoter. Through local arrangement and fine-tuning of the catalytic centers by alkali promoters, the Zr12-bpdc-CuCs catalyst demonstrates ethanol synthesis with 99% selectivity in a 10 h assessment. With the help of alkali–metal promoters, the Cu-based catalyst facilitates H_2 activation and promotes direct C–C coupling and formyl species to offer an electron-rich environment for Cu-based catalysts and boost the stability and activity of a formyl intermediate [369]. Alkali promoters (K, Rb, and Cs) influence the achievement of CO_2 hydrogenation reactions made of precipitated iron-based catalysts; 1.5 Cs boosted catalyst has the best steady-state conversion stability of all the catalysts. Results show that these promoters have a synergistic impact that may result in improved CO_2 hydrogenation catalysts if balanced [370].

Table 3. Summary of CO_2 hydrogenation over homogeneous and heterogeneous catalysts.

Catalysts	Reactor	Reaction Temperature (°C)	Pressure (MPa)	Mixed Gas Ratio	Time Reaction (h)	CO_2 Conversion (%)	Ethanol Selectivity (%)	Ethanol STY (mmol g^{-1} h^{-1})	Brief Description	Ref
Na/Co_2C	Fixed-bed	250	5	$CO_2/H_2/N_2$ = 24.6/72.4/3	5	23.8	17.5	0.72	The active sites of Na/Co_2C improve the CO_2 and CO non-dissociative adsorption, then regulated the surface CO/CH_x ratio to accelerate CO insertion in generating ethanol.	[361]
CoMoC	Fixed-bed	180	2	CO_2/H_2 = 1/3	6	n.d	97.4	0.53	The excellent stability of $CoMoC_x$ promotes the activation of H_2 and CO_2 and C-C coupling which is generated by the HCOO* and DMF species.	[362]
Pt/Co_3O_4	Fixed-bed	200	8	CO_2/H_2 = 1/3	15	n.d	82.5	0.42	Water protonates methanol followed by dissociation into CH_3*, OH*, and H* (or H_2O) species on the Pt/Co_3O_4 surface that promotes CH_3*−CO coupling to form ethanol.	[353]
Cs/CuFeZn	Fixed-bed	330	5	$CO_2/H_2/N_2$ = 24/72/4	3	36.6	20.7	1.47	The synergetic combination of Cu-Fe dual interfaces sites in the Cs/CuFeZn overrides methanol synthesis through a direct CO_2 hydrogenation route via HCOO* intermediates.	[356]
Ir/In_2O_3	Fixed-bed	200	6	CO_2/H_2 = 1/5	5	n.d	99.7	0.99	The Ir/In_2O_3 reduced a Lewis acid−base pair between Ir and adjacent oxygen vacancy to form a distinct catalytic center, which reduces CO_2 to active intermediates and facilitates the C−C coupling to form ethanol.	[344]

Table 3. *Cont.*

Catalysts	Reactor	Reaction Temperature (°C)	Pressure (MPa)	Mixed Gas Ratio	Time Reaction (h)	CO_2 Conversion (%)	Ethanol Selectivity (%)	Ethanol STY (mmol g^{-1} h^{-1})	Brief Description	Ref
Cu/Co_3O_4	Fixed-bed	200	30	CO_2/H_2 = 1/3	2	13.9	15.2	1.87	The adjacent oxygen vacancy on the surface of CoO promotes the CH_3O* intermediate dissociation is the rate-determining step for ethanol synthesis.	[371]
Co_3O_4	Fixed-bed	200	2	$CO_2/H_2/N_2$ = 22/66/12	2	28.9	19.2	1.60	The metallic Co reduced from Co_3O_4 was the main activity site for CO_2 hydrogenation by promoting the growth of the C−C coupling for the production of ethanol.	[372]
CoAlO	Fixed-bed	200	4	CO_2/H_2 = 1/3	15	n.d	92.1	0.44	The CoAlO is attributed to the formation of acetate from formate with the insertion of *CH_x which is an important intermediate to produce ethanol from CO_2 hydrogenation.	[373]
Pt/Co_3O_4	Fixed-bed	200	2	$CO_2/H_2/N_2$ = 22.5/67.5/10	2	44.5	26.7	0.69	The synergic effect of Pt, Co nanoparticles, and oxygen vacancies of Co_3O_4 improved the adsorption of H_2 and CO_2 with stable CO_2 conversion in the synthesis of ethanol.	[374]

However, remarkable drawbacks to CO_2 hydrogenation for alcohol syntheses, such as CO_2 activation problems, a high energy barrier for C–O bond scission, and the creation of C1 by-products, remain. As a result, designing effective heterogeneous catalysts for ethanol generation is critical. The morphology of catalysts, such as the particle size and dispersion of deposited metal particles, influences the optimization of the metal/oxide interface to improve CO_2 conversion and product selectivity. The collision theory explained by increasing the surface area of a reactant created by high dispersion increases the frequency of collisions and increases the reaction rate. Reducing metal particle sizes leads to a high fraction of low-coordinate surface atoms at locations, such as corners and edges, especially when the particle size is smaller than 2–3 nm [353,375–377]. The small particle size content high in the surface area that generates by high dispersion is available for particles to collide, leading to improved catalytic performance of the reaction. Appropriate reducible metal oxide supports, such as TiO_2 and ZrO_2, have been used extensively to tailor the particle size. The Au/TiO_2 catalyst has good selectivity for ethanol from CO_2 reduction in DMF solvent due to the abundance of oxygen vacancies. With the addition of water, the bimetallic Pd_2Cu/P25 catalyst produces a high yield of ethanol. Other studies indicated that by manipulating the particle size, the electronic state of Rh for alcohol production from CO_2 hydrogenation can be adjusted. In CO hydrogenation, a promotion strategy based on hydroxyl groups is an effective way to improve alcohol selectivity at a high conversion rate and a wide range of operating temperatures.

4. Future Direction and Perspective

Ethanol is a fundamental chemical product, an important solvent, an industrial building block, and a promising renewable fuel. The chemical equilibrium conversion of the hydration of ethylene decreases at high temperatures to increase the rate of reaction. The excessive amount of energy to heat gases generates high pressure and utilizes crude oil, which is a nonrenewable resource. Ethanol synthesis from biomass residue produces a huge amount of CO_2 with a high cost of operation because of expensive machinery and fuel. The ethanol production from total sugars in lignocellulosic materials is inhibited by the action of pentose sugars, which are not fermentable by the brewer's yeast, i.e., *S. cerevisiae*, during the hydrolysis of hemicellulose. Although the fermentation route has been commercially realized, the cost of operation for this process is expensive due to the energy-intensive distillation steps at high dilution rates, which allow for high productivities, and the incomplete utilization of substrate, resulting in low yields to meet the market demand. Creating highly operative and selective nanocatalysts for the electrochemical CO_2 reduction reaction remains a major issue in the electrochemical CO_2 reduction process. DME is not suitable as an alternative fuel to diesel due to its lower viscosity, which causes leaking and component damage. The RWGS reaction uses sophisticated catalysts that are frequently necessary to customize the cascade reactions and require a high temperature (typically above 300 °C) to drive the processes still experiencing difficulty; low activity and unstable C–C coupling formation in the FTS mechanism is another challenge in the CO_2 hydrogenation process that are usually producing light hydrocarbons, methane in particular. The heterogeneous catalytic CO_2 hydrogenation approach is one of the initiatives to reduce CO_2 emissions as the source of GHG, which prompts the climate change or global warming that currently shows an effect worldwide, into the numerous high economic value-added chemicals and easily marketable fuel additives that have made substantial progress to explore as new concepts and opportunities for industrial manufacture. The hydrogenation of CO_2 into C_{2+} products occurs via a methanol-mediated route or modified FTS mechanism that involves two steps of the reaction, and these routes are distinguished by the intermediate's product. In the methanol-mediated route, CO_2 is hydrogenated into methanol and then converted into hydrocarbons, whereas CO_2 is reduced to CO via RWGS followed by chain propagation via a modified FTS mechanism. A recent development showed that the direct catalytic hydrogenation of CO_2 into ethanol in a single reactor is one of the promising strategies based on economic potential and energy efficiency. The formation of $*CH_x$ is the

rate-determining step in this process because the *HCOO generation and coupling steps are known to be accelerated in the CO_2-to-ethanol transformation. The reaction mechanism is also closely associated with multiple catalytic active sites controlling every elementary reaction over catalysts. Thus, catalysts for optimum active sites should be designed and prepared to improve CO_2 conversion and ethanol selectivity. The formation rate of ethanol increases with increasing reaction temperature because thermodynamic equilibrium is still not reached. However, many challenges, e.g., the control of the ratio of multiple active sites, regulation of interface sites, and device of catalyst structures need to be explored in future research to improve the conversion and selectivity in ethanol production.

5. Conclusions

In this exploration, we discuss current research discoveries in the improvement of technologies and operation procedures in ethanol production. The catalytic hydrogenation of CO_2 promises development direction in the production of ethanol and reduces environmental pollution problems. The limitations of CO_2, i.e., a fully oxidized, chemically inert and thermodynamically stable molecule, should be considered in designing the research because its conversion into chemicals requires large amounts of energy and H_2. The production of ethanol reduces CO_2 emissions globally, but reducing the dependence on conventional gasoline shows a decreasing pattern of production every year because ethanol has been identified as an ecological fuel due to its nontoxicity, accumulation of high oxygen content to promote better combustion with reduced exhaust emissions, and high-octane rating to giving high resistance to engine knock. The outcomes of this review will play a crucial and interesting role in further research development in providing the latest proposed approach for effective CO_2 hydrogenation to promote C–C coupling in ethanol production.

Author Contributions: M.N.L.: Literature collection and manuscript writing; A.S.: Literature collection and analysis; W.N.M.: Literature collection; S.Z.H.: Content design; W.N.R.W.I. and Z.Y.: Content design, revision, project administration, and funding acquisition. All authors have read and agreed to the published version of the manuscript.

Funding: This work was financially supported by Universiti Kebangsaan Malaysia under research code DIP-2022-010 and GENIUSpintar-2022-022.

Acknowledgments: Authors would like to thank the Ministry of Higher Education of Malaysia under the research code Fundamental Research Grant Scheme (FRGS/1/2020/TK0/UKM/02/31), Universiti Kebangsaan Malaysia under research code DIP-2022-010 and GENIUSpintar-2022-022.

Conflicts of Interest: The authors declare no conflict of interest.

References

1. Berrill, P.; Gillingham, K.T.; Hertwich, E.G. Drivers of Change in U.S. Residential Energy Consumption and Greenhouse Gas Emissions, 1990–2015. *Environ. Res. Lett.* **2021**, *16*, 034045. [CrossRef]
2. Li, J.; Tian, Y.; Deng, Y.; Zhang, Y.; Xie, K. Improving the Estimation of Greenhouse Gas Emissions from the Chinese Coal-to-Electricity Chain by a Bottom-up Approach. *Resour. Conserv. Recycl.* **2021**, *167*, 105237. [CrossRef]
3. Karmaker, A.K.; Rahman, M.M.; Hossain, A.M.; Ahmed, R.M. Exploration and Corrective Measures of Greenhouse Gas Emission from Fossil Fuel Power Stations for Bangladesh. *Clean. Prod.* **2020**, *244*, 118645. [CrossRef]
4. Babatundea, K.A.; Saida, F.F.; Nor, N.G.M. Reducing Carbon Dioxide Emissions from Malaysian Power Sector: Current Issues and Future Directions. *Eng. J.* **2018**, *1*, 59–69. [CrossRef] [PubMed]
5. Tchanche, B. Dynamics of Greenhouse Gas (GHG) Emissions in the Transportation Sector of Senegal. *Earth* **2021**, *2*, 1–15. [CrossRef]
6. Umar, M.; Ji, X.; Kirikkaleli, D.; Alola, A.A. The Imperativeness of Environmental Quality in the United States Transportation Sector amidst Biomass-Fossil Energy Consumption and Growth. *Clean. Prod.* **2021**, *285*, 124863. [CrossRef]
7. Olivier, J.G.J.; Peters, J.A.H.W. *Trends in Global CO_2 and Total Greenhouse Gas Emissions: Report 2019*; PBL Netherlands Environmental Assessment Agency: The Hague, The Netherlands, 2020; Volume 2020, p. 70.
8. Javadi, P.; Yeganeh, B.; Abbasi, M.; Alipourmohajer, S. Energy Assessment and Greenhouse Gas Predictions in the Automotive Manufacturing Industry in Iran. *Sustain. Prod. Consum.* **2021**, *26*, 316–330. [CrossRef]

9. Udmale, P.; Pal, I.; Szabo, S.; Pramanik, M. International Cereal Trade of Bangladesh: Implications for Virtual Land, Water, and GHG Emissions from Agriculture. *Int. Energy J.* **2021**, *21*, 107–118.
10. Ntinyari, W.; Gweyi-onyango, J. *Greenhouse Gases Emissions in Agricultural Systems and Climate Change Effects in Sub-Saharan Africa*; Springer Nature: Berlin, Germany, 2020; pp. 1–25.
11. Panchasara, H.; Samrat, N.H.; Islam, N. Greenhouse Gas Emissions Trends and Mitigation Measures in Australian Agriculture Sector—A Review. *Agriculture* **2021**, *11*, 85. [CrossRef]
12. Zhang, X.; Li, X.; Chen, D.; Cui, H.; Ge, Q. Overestimated Climate Warming and Climate Variability Due to Spatially Homogeneous CO_2 in Climate Modeling over the Northern Hemisphere since the Mid-19th Century. *Sci. Rep.* **2019**, *9*, 17426. [CrossRef]
13. Nunes, L.J.R.; Meireles, C.I.R.; Gomes, C.J.P.; Ribeiro, N.M.C.A. Forest Contribution to Climate Change Mitigation: Management Oriented to Carbon Capture and Storage. *Climate* **2020**, *8*, 21. [CrossRef]
14. Panda, R.; Maity, M. Global Warming and Climate Change on Earth: Duties and Challenges of Human Beings. *Res. Eng. Sci. Manag.* **2021**, *4*, 122–125.
15. Friedlingstein, P.; Jones, M.; Sullivan, M.O.; Hauck, J. Global Carbon Budget 2021. *Earth Syst. Sci. Data* **2021**, *14*, 1917–2005. [CrossRef]
16. Zhou, W.; Cheng, K.; Kang, J.; Zhou, C.; Subramanian, V.; Zhang, Q.; Wang, Y. New Horizon in C1 Chemistry: Breaking the Selectivity Limitation in Transformation of Syngas and Hydrogenation of CO_2 into Hydrocarbon Chemicals and Fuels. *Chem. Soc. Rev.* **2019**, *48*, 3193–3228. [CrossRef] [PubMed]
17. Kumaravel, V.; Bartlett, J.; Pillai, S.C. Photoelectrochemical Conversion of Carbon Dioxide (CO_2) into Fuels and Value-Added Products. *ACS Energy Lett.* **2020**, *5*, 486–519. [CrossRef]
18. Tan, X.; Sun, X.; Han, B. Ionic Liquid-Based Electrolytes for CO_2 Electroreduction and CO_2 Electroorganic Transformation. *Natl. Sci. Rev.* **2021**, *9*, nwab022. [CrossRef]
19. Hasan, S.Z.; Ahmad, K.N.; Isahak, W.N.R.W.; Pudukudy, M.; Masdar, M.S.; Jahim, J.M. Synthesis, Characterisation and Catalytic Activity of NiO Supported Al_2O_3 for CO_2 Hydrogenation to Carboxylic Acids: Influence of Catalyst Structure. *IOP Conf. Ser. Earth Environ. Sci.* **2019**, *268*, 012079. [CrossRef]
20. Xu, Y.; Shi, C.; Liu, B.; Wang, T.; Zheng, J.; Li, W.; Liu, D.; Liu, X. Selective Production of Aromatics from CO_2. *Catal. Sci. Technol.* **2019**, *9*, 593–610. [CrossRef]
21. Guzmán, H.; Russo, N.; Hernandez, S. CO_2 Valorisation towards Alcohols by Cu-Based Electrocatalysts: Challenges and Perspectives. *Green Chem.* **2021**, *23*, 1897–1920. [CrossRef]
22. Yao, B.; Xiao, T.; Makgae, O.A.; Jie, X.; Gonzalez-Cortes, S.; Guan, S.; Kirkland, A.I.; Dilworth, J.R.; Al-Megren, H.A.; Alshihri, S.M.; et al. Transforming Carbon Dioxide into Jet Fuel Using an Organic Combustion-Synthesized Fe-Mn-K Catalyst. *Nat. Commun.* **2020**, *11*, 6395. [CrossRef]
23. Yang, Q.; Skrypnik, A.; Matvienko, A.; Lund, H.; Holena, M.; Kondratenko, E.V. Revealing Property-Performance Relationships for Efficient CO_2 Hydrogenation to Higher Hydrocarbons over Fe-Based Catalysts: Statistical Analysis of Literature Data and Its Experimental Validation. *Appl. Catal. B Environ.* **2021**, *282*, 119554. [CrossRef]
24. Xing, Y.; Ma, Z.; Su, W.; Wang, Q.; Wang, X.; Zhang, H. Analysis of Research Status of CO_2 Conversion. *Catalysts* **2020**, *10*, 370. [CrossRef]
25. Duyar, M.S.; Gallo, A.; Regli, S.K.; Snider, J.L.; Singh, J.A.; Valle, E.; Mcenaney, J.; Bent, S.F.; Rønning, M.; Jaramillo, T.F. Understanding Selectivity in CO_2 Hydrogenation to Methanol for MoP Nanoparticle Catalysts Using in Situ Techniques. *Catalysts* **2021**, *11*, 143. [CrossRef]
26. Xu, D.; Wang, Y.; Ding, M.; Hong, X.; Liu, G.; Tsang, S.C.E. Advances in Higher Alcohol Synthesis from CO_2 Hydrogenation. *Chem* **2020**, *7*, 849–881. [CrossRef]
27. Weilhard, A.; Argent, S.P.; Sans, V. Efficient Carbon Dioxide Hydrogenation to Formic Acid with Buffering Ionic Liquids. *Nat. Commun.* **2021**, *12*, 231. [CrossRef]
28. Pandey, P.H.; Pawar, H.S. Cu Dispersed TiO_2 Catalyst for Direct Hydrogenation of Carbon Dioxide into Formic Acid. *J. CO_2 Util.* **2020**, *41*, 101267. [CrossRef]
29. Singh, D.; Gupta, S.K.; Seriani, N.; Lukacevic, I.; Sonvane, Y.; Gajjar, P.N.; Ahuja, R. Mechanism of Formaldehyde and Formic Acid Formation on (101)-TiO_2@Cu_4 Systems through CO_2 Hydrogenation. *Sustain. Energy Fuels* **2021**, *5*, 564–574. [CrossRef]
30. Yang, W.; Chernyshov, I.Y.; van Schendel, R.K.A.; Weber, M.; Müller, C.; Filonenko, G.A.; Pidko, E.A. Robust and Efficient Hydrogenation of Carbonyl Compounds Catalysed by Mixed Donor Mn(I) Pincer Complexes. *Nat. Commun.* **2021**, *12*, 12. [CrossRef]
31. Damyanov, A.; Hofmann, P. Operation of a Diesel Engine with Intake Manifold Alcohol Injection. *Automot. Engine Technol.* **2019**, *4*, 17–28. [CrossRef]
32. Zhao, L.; Wang, D. Combined Effects of a Biobutanol/Ethanol-Gasoline (E10) Blend and Exhaust Gas Recirculation on Performance and Pollutant Emissions. *ACS Omega* **2020**, *5*, 3250–3257. [CrossRef]
33. Elfasakhany, A. State of Art of Using Biofuels in Spark Ignition Engines. *Energies* **2021**, *14*, 779. [CrossRef]
34. Pang, J.; Zheng, M.; Zhang, T. Synthesis of Ethanol and Its Catalytic Conversion. *Adv. Catal.* **2019**, *64*, 89–191. [CrossRef]
35. Mizik, T.; Gyarmati, G. Economic and Sustainability of Biodiesel Production—A Systematic Literature Review. *Clean Technol.* **2021**, *3*, 19–36. [CrossRef]

36. Zhang, Z.; Lis, M. Modeling Green Energy Development Based on Sustainable Economic Growth in China. *Sustainability* **2020**, *12*, 1368. [CrossRef]
37. Cooper, G.; McCaherty, J.; Huschitt, E.; Schwarck, R.; Wilson, C. 2021 Ethanol Industry Outlook. *Renew. Fuels Assoc.* **2021**, 1–40.
38. Alalwan, H.A.; Alminshid, A.H.; Aljaafari, H.A.S. Promising Evolution of Biofuel Generations. Subject Review. *Renew. Energy Focus* **2019**, *28*, 127–139. [CrossRef]
39. Jeswani, H.K.; Chilvers, A.; Azapagic, A. Environmental Sustainability of Biofuels: A Review. *Proc. R. Soc. A* **2020**, *476*, 20200351. [CrossRef] [PubMed]
40. Momose, H.; Kusumoto, K.; Izumi, Y.; Mizutani, Y. Vapor-Phase Direct Hydration of Ethylene over Zirconium Tungstate Catalyst. I. Catalytic Behavior and Kinetics at Atmospheric Pressure. *J. Catal.* **1982**, *77*, 23–31. [CrossRef]
41. Mohsenzadeh, A.; Zamani, A.; Taherzadeh, M.J. Bioethylene Production from Ethanol: A Review and Techno-Economical Evaluation. *ChemBioEng Rev.* **2017**, *4*, 75–91. [CrossRef]
42. Zimmermann, H.; Walzl, R. Ethylene. In *Ullmann's Encyclopedia of Industrial Chemistry*; Wiley-VCH Verlag GmbH & Co. KGaA: Weinheim, Germany, 2000.
43. Chu, W.; Echizen, T.; Kamiya, Y.; Okuhara, T. Gas-Phase Hydration of Ethene over Tungstena-Zirconia. *Appl. Catal. A Gen.* **2004**, *259*, 199–205. [CrossRef]
44. Katada, N.; Iseki, Y.; Shichi, A.; Fujita, N.; Ishino, I.; Osaki, K.; Torikai, T.; Niwa, M. Production of Ethanol by Vapor Phase Hydration of Ethene over Tungsta Monolayer Catalyst Loaded on Titania. *Appl. Catal. A Gen.* **2008**, *349*, 55–61. [CrossRef]
45. Isobe, A.; Yabuuchi, Y.; Iwasa, N.; Takezawa, N. Gas-Phase Hydration of Ethene over $Me(HPO_4)_2 \cdot NH_2O$ (Me = Ge, Zr, Ti, and Sn). *Appl. Catal. A Gen.* **2000**, *194*, 395–401. [CrossRef]
46. Gao, J.; Li, Z.; Dong, M.; Fan, W.; Wang, J. Thermodynamic Analysis of Ethanol Synthesis from Hydration of Ethylene Coupled with a Sequential Reaction. *Front. Chem. Sci. Eng.* **2020**, *14*, 847–856. [CrossRef]
47. Llano-Restrepo, M.; Muñoz-Muñoz, Y.M. Combined Chemical and Phase Equilibrium for the Hydration of Ethylene to Ethanol Calculated by Means of the Peng-Robinson-Stryjek-Vera Equation of State and the Wong-Sandler Mixing Rules. *Fluid Phase Equilib.* **2011**, *307*, 45–57. [CrossRef]
48. Roozbehani, B.; Mirdrikvand, M.; Imani, S.; Roshan, A.C.; Africa, S. Synthetic Ethanol Production in the Middle East: A Way to Make Environmentally Friendly Fuels. *Chem. Technol. Fuels Oils* **2013**, *49*, 115–124. [CrossRef]
49. Malico, I.; Nepomuceno, R.; Cristina, A.; Sousa, A.M.O. Current Status and Future Perspectives for Energy Production from Solid Biomass in the European Industry. *Renew. Sustain. Energy Rev.* **2019**, *112*, 960–977. [CrossRef]
50. Clauser, N.M.; González, G.; Mendieta, C.M.; Kruyeniski, J.; Area, M.C.; Vallejos, M.E. Biomass Waste as Sustainable Raw Material for Energy and Fuels. *Sustainability* **2021**, *13*, 794. [CrossRef]
51. Reid, W.V.; Ali, M.K.; Field, C.B. The Future of Bioenergy. *Glob. Chang. Biol.* **2020**, *26*, 274–286. [CrossRef]
52. Sudagar, S.; Adhisegar, C.; Bernadsha, P.; Balamurugan, R. A Comparative Study of Different Biomass Properties by Using Pyrolysis Process. *AIP Conf. Proc.* **2020**, *2225*, 040001. [CrossRef]
53. Lee, S.Y.; Sankaran, R.; Chew, K.W.; Tan, C.H.; Krishnamoorthy, R.; Chu, D.-T.; Show, P.-L. Waste to Bioenergy: A Review on the Recent Conversion Technologies. *BMC Energy* **2019**, *1*, 4. [CrossRef]
54. Debrah, J.K.; Vidal, D.G.; Dinis, M.A.P. Raising Awareness on Solid Waste Management through Formal Education for Sustainability: A Developing Countries. *Recycling* **2021**, *6*, 6. [CrossRef]
55. Haus, S.; Björnsson, L.; Börjesson, P. Lignocellulosic Ethanol in a Greenhouse Gas Emission Reduction Obligation System—A Case Study of Swedish Sawdust Based-Ethanol Production. *Energies* **2020**, *13*, 1048. [CrossRef]
56. Singh, K.; Kumar, R.; Chaudhary, V.; Sunil, V.; Arya, A.M.; Sharma, S. Sugarcane Bagasse: Foreseeable Biomass of Bio - Products and Biofuel: An Overview. *Pharmacogn. Phytochem.* **2019**, *8*, 2356–2360.
57. Formann, S.; Hahn, A.; Janke, L.; Stinner, W.; Sträuber, H.; Logroño, W.; Nikolausz, M. Beyond Sugar and Ethanol Production: Value Generation Opportunities through Sugarcane Residues. *Front. Energy Res.* **2020**, *8*, 579577. [CrossRef]
58. Ntimbani, R.N.; Farzad, S.; Görgens, J.F. Furfural Production from Sugarcane Bagasse along with Co-Production of Ethanol from Furfural Residues. *Biomass Convers. Biorefinery* **2021**, *12*, 5257–5267. [CrossRef]
59. Cotana, F.; Cavalaglio, G.; Gelosia, M.; Coccia, V.; Petrozzi, A.; Ingles, D.; Pompili, E. A Comparison between SHF and SSSF Processes from Cardoon for Ethanol Production. *Ind. Crop. Prod.* **2015**, *69*, 424–432. [CrossRef]
60. Ji, L.; Zheng, T.; Zhao, P.; Zhang, W.; Jiang, J. Ethanol Production from a Biomass Mixture of Furfural Residues with Green Liquor-Peroxide Saccarified Cassava Liquid. *BMC Biotechnol.* **2016**, *16*, 48. [CrossRef]
61. da Silva, F.L.; de Oliveira Campos, A.; dos Santos, D.A.; Batista Magalhães, E.R.; de Macedo, G.R.; dos Santos, E.S. Valorization of an Agroextractive Residue-Carnauba Straw-for the Production of Bioethanol by Simultaneous Saccharification and Fermentation (SSF). *Renew. Energy* **2018**, *127*, 661–669. [CrossRef]
62. Cho, E.J.; Park, C.S.; Bae, H.J. Transformation of Cheaper Mangosteen Pericarp Waste into Bioethanol and Chemicals. *J. Chem. Technol. Biotechnol.* **2020**, *95*, 348–355. [CrossRef]
63. Idris, M.; Novalia, U. Experimental Study of Bioethanol Production as Fuel from Salacca Zalacca Saste and Coconut Water Waste Combination. *IOP Conf. Ser. Mater. Sci. Eng.* **2019**, *506*, 012003. [CrossRef]
64. Rahman, Q.M.; Zhang, B.; Wang, L.; Joseph, G.; Shahbazi, A. A Combined Fermentation and Ethanol-Assisted Liquefaction Process to Produce Biofuel from *Nannochloropsis* sp. *Fuel* **2019**, *238*, 159–165. [CrossRef]

65. Chitranshi, R.; Kapoor, R. Utilization of over—Ripened Fruit (Waste Fruit) for the Eco - Friendly Production of Ethanol. *Vegetos* **2021**, *34*, 270–276. [CrossRef]
66. Al-Azkawi, A.; Elliston, A.; Al-bahry, S.; Sivakumar, N. Waste Paper to Bioethanol: Current and Future Prospective. *Biofuels Bioprod. Biorefining* **2019**, *13*, 1106–1118. [CrossRef]
67. Annamalai, N.; Al, H.; Nair, B.S.; Ahlam, A.; Azkawi, A.; Al, S. Enhanced Bioethanol Production from Waste Paper through Separate Hydrolysis and Fermentation. *Waste Biomass Valoriz.* **2020**, *11*, 121–131. [CrossRef]
68. Jha, P.; Singh, S.; Raghuram, M.; Nair, G.; Jobby, R.; Gupta, A.; Desai, N. Valorisation of Orange Peel: Supplement in Fermentation Media for Ethanol Production and Source of Limonene. *Environ. Sustain.* **2019**, *2*, 33–41. [CrossRef]
69. Jiménez-Castro, M.P.; Buller, L.S.; Sganzerla, W.G.; Forster-Carneiro, T. Bioenergy Production from Orange Industrial Waste: A Case Study. *Biofuels Bioprod. Biorefining* **2020**, *14*, 1239–1253. [CrossRef]
70. Mesa, L.; Martínez, Y.; Celia de Armas, A.; González, E. Ethanol Production from Sugarcane Straw Using Different Configurations of Fermentation and Techno-Economical Evaluation of the Best Schemes. *Renew. Energy* **2020**, *156*, 377–388. [CrossRef]
71. Salina, F.H.; Molina, F.B.; Gallego, A.G.; Palacios-Bereche, R. Fast Pyrolysis of Sugarcane Straw and Its Integration into the Conventional Ethanol Production Process through Pinch Analysis. *Energy* **2021**, *215*, 119066. [CrossRef]
72. Zhang, C.; Chen, H.; Pang, S.; Su, C.; Lv, M.; An, N.; Wang, K.; Cai, D.; Qin, P. Importance of Redefinition of Corn Stover Harvest Time to Enhancing Non-Food Bio-Ethanol Production. *Renew. Energy* **2020**, *146*, 1444–1450. [CrossRef]
73. Li, Q.; Qin, Y.; Liu, Y.; Liu, J.; Liu, Q.; Li, P.; Liu, L. Detoxification and Concentration of Corn Stover Hydrolysate and Its Fermentation for Ethanol Production. *Front. Chem. Sci. Eng.* **2019**, *13*, 140–151. [CrossRef]
74. da Siva Martins, L.H.; Komesu, A.; Neto, J.M.; de Oliveira, J.A.R.; Rabelo, S.C.; da Costa, A.C. Pretreatment of Sugarcane Bagasse by OX-B to Enhancing the Enzymatic Hydrolysis for Ethanol Fermentation. *J. Food Process Eng.* **2021**, *44*, 13579. [CrossRef]
75. Konde, K.S.; Nagarajan, S.; Kumar, V.; Patil, S.V.; Ranade, V.V. Sugarcane Bagasse Based Biorefineries in India: Potential and Challenges. *Sustain. Energy Fuels* **2021**, *5*, 52–78. [CrossRef]
76. Jin, X.; Song, J.; Liu, G. Bioethanol Production from Rice Straw through an Enzymatic Route Mediated by Enzymes Developed In-House from Aspergillus Fumigatus. *Energy* **2020**, *190*, 116395. [CrossRef]
77. Tajmirriahi, M.; Momayez, F.; Karimi, K. The Critical Impact of Rice Straw Extractives on Biogas and Bioethanol. *Bioresour. Technol.* **2021**, *319*, 124167. [CrossRef] [PubMed]
78. Zwirzitz, A.; Alteio, L.; Sulzenbacher, D.; Atanasoff, M.; Selg, M. Ethanol Production from Wheat Straw Hydrolysate by Issatchenkia Orientalis Isolated from Waste Cooking Oil. *J. Fungi* **2021**, *7*, 121. [CrossRef] [PubMed]
79. Hermosilla, E.; Schalchli, H.; Diez, M.C. Biodegradation Inducers to Enhance Wheat Straw Pretreatment by Gloeophyllum Trabeum to Second-Generation Ethanol Production. *Environ. Sci. Pollut. Res.* **2020**, *27*, 8467–8480. [CrossRef] [PubMed]
80. Fu, J.; Yan, X.; Jiang, D. Assessing the Sweet Sorghum—Based Ethanol Potential on Saline—Alkali Land with DSSAT Model and LCA Approach. *Biotechnol. Biofuels* **2021**, *14*, 44. [CrossRef] [PubMed]
81. Rakhmetova, S.O.; Vergun, O.M.; Blume, R.Y.; Bondarchuk, O.P.; Shymanska, O.V.; Tsygankov, S.P.; Yemets, A.I.; Blume, Y.B.; Rakhmetov, D.B. Ethanol Production Potential of Sweet Sorghum in North and Central Ukraine. *Open Agric. J.* **2020**, *14*, 321–338. [CrossRef]
82. Sukhang, S.; Choojit, S.; Reungpeerakul, T.; Sangwichien, C. Bioethanol Production from Oil Palm Empty Fruit Bunch with SSF and SHF Processes Using Kluyveromyces Marxianus Yeast. *Cellulose* **2020**, *27*, 301–314. [CrossRef]
83. Pangsang, N.; Rattanapan, U.; Thanapimmetha, A.; Srinopphakhun, P.; Liu, C.-G.; Zhao, X.-Q.; Bai, F.-W.; Sakdaronnarong, C. Chemical-Free Fractionation of Palm Empty Fruit Bunch and Palm Fiber by Hot-Compressed Water Technique for Ethanol Production. *Energy Rep.* **2019**, *5*, 337–348. [CrossRef]
84. Redondo-Gómez, C.; Quesada, M.R.; Astúa, S.V.; Zamora, J.P.M.; Lopretti, M.; Vega-Baudrit, J.R. Biorefinery of Biomass of Agro-Industrial Banana Waste to Obtain High-Value Biopolymers. *Molecules* **2020**, *25*, 3829. [CrossRef] [PubMed]
85. Utama, G.L.; Kurniawan, M.O.; Natiqoh, N.; Balia, R.L. Species Identification of Stress Resistance Yeasts Isolated from Banana Waste for Ethanol Production. *IOP Conf. Ser. Earth Environ. Sci.* **2019**, *306*, 12021. [CrossRef]
86. Karagoz, P.; Bill, R.M.; Ozkan, M. Lignocellulosic Ethanol Production: Evaluation of New Approaches, Cell Immobilization and Reactor Configurations. *Renew. Energy* **2019**, *143*, 741–752. [CrossRef]
87. Arora, A.; Nandal, P.; Singh, J.; Verma, M.L. Nanobiotechnological Advancements in Lignocellulosic Biomass Pretreatment. *Mater. Sci. Energy Technol.* **2020**, *3*, 308–318. [CrossRef]
88. Okolie, J.A.; Nanda, S.; Dalai, A.K.; Kozinski, J.A. Chemistry and Specialty Industrial Applications of Lignocellulosic Biomass. *Waste Biomass Valoriz.* **2020**, *12*, 2145–2169. [CrossRef]
89. Gopal, L.C.; Govindarajan, M.; Kavipriya, M.R.; Mahboob, S.; Al-ghanim, K.A.; Virik, P.; Ahmed, Z.; Al-mulhm, N.; Senthilkumaran, V.; Shankar, V. Science Optimization Strategies for Improved Biogas Production by Recycling of Waste through Response Surface Methodology and Artificial Neural Network: Sustainable Energy Perspective Research. *J. King Saud Univ.-Sci.* **2021**, *33*, 101241. [CrossRef]
90. Nishimura, H.; Kamiya, A.; Nagata, T.; Katahira, M.; Watanabe, T. Direct Evidence for α Ether Linkage between Lignin and Carbohydrates in Wood Cell Walls. *Sci. Rep.* **2018**, *8*, 6538. [CrossRef]
91. Santos, C.M.; Brito, P.L.; de Oliveira Santos, A.T.; de Araújo Pantoja, L.; da Costa, A.S.V.; dos Santos, A.S. Production of Lignocellulosic Ethanol from Waste Paper: Review on Production Technology. *Int. J. Dev. Res.* **2019**, *9*, 28383–28390.

92. Peinemann, J.C.; Pleissner, D. Continuous Pretreatment, Hydrolysis, and Fermentation of Organic Residues for the Production of Biochemicals. *Bioresour. Technol.* **2020**, *295*, 122256. [CrossRef]
93. Dey, P.; Pal, P.; Kevin, J.D.; Das, D.B. Lignocellulosic Bioethanol Production: Prospects of Emerging Membrane Technologies to Improve the Process—A Critical Review. *Rev. Chem. Eng.* **2020**, *36*, 333–367. [CrossRef]
94. Deng, L.; Li, J. Thread Rolling: An Efficient Mechanical Pretreatment for Corn Stover Saccharificatio. *Energies* **2021**, *14*, 542. [CrossRef]
95. Bhatia, L.; Garlapati, V.K.; Chandel, A.K. *Scalable Technologies for Lignocellulosic Biomass Processing into Cellulosic Ethanol*; Springer International Publishing: Cham, Swizerland, 2019; ISBN 9783030290696.
96. Cheah, W.Y.; Sankaran, R.; Show, P.L.; Ibrahim, T.N.B.T.; Chew, K.W.; Culaba, A.; Chang, J.S. Pretreatment Methods for Lignocellulosic Biofuels Production: Current Advances, Challenges and Future Prospects. *Biofuel Res. J.* **2020**, *7*, 1115–1127. [CrossRef]
97. Vasic, K.; Knez, Ž.; Leitgeb, M. Bioethanol Production by Enzymatic Hydrolysis from Different Lignocellulosic Sources. *Molecules* **2021**, *26*, 753. [CrossRef] [PubMed]
98. Aftab, M.N.; Iqbal, I.; Riaz, F.; Karadag, A.; Tabatabaei, M. Different Pretreatment Methods of Lignocellulosic Biomass for Use in Biofuel Production. In *Biomass for Bioenergy-Recent Trends and Future Challenges*; IntechOpen: London, UK, 2019; pp. 1–24. [CrossRef]
99. Shukla, A.; Kumar, D.; Girdhar, M.; Kumar, A.; Goyal, A.; Malik, T.; Mohan, A. Strategies of Pretreatment of Feedstocks for Optimized Bioethanol Production: Distinct and Integrated Approaches. *Biotechnol. Biofuels Bioprod.* **2023**, *16*, 44. [CrossRef]
100. Mustafa, A.H.; Rashid, S.S.; Rahim, M.H.A.; Roslan, R.; Musa, W.A.M.; Sikder, B.H.; Sasi, A.A. Enzymatic Pretreatment of Lignocellulosic Biomass: An Overview. *J. Chem. Eng. Ind. Biotechnol.* **2022**, *8*, 1–7. [CrossRef]
101. Sharma, S.; Tsai, M.-L.; Sharma, V.; Sun, P.-P.; Nargotra, P.; Bajaj, B.K.; Chen, C.-W.; Dong, C.-D. Environment Friendly Pretreatment Approaches for the Bioconversion of Lignocellulosic Biomass into Biofuels and Value-Added Products. *Environments* **2022**, *10*, 6. [CrossRef]
102. Klongklaew, A.; Unban, K.; Kalaimurugan, D.; Kanpiengjai, A.; Azaizeh, H.; Schroedter, L.; Venus, J.; Khanongnuch, C. Bioconversion of Dilute Acid Pretreated Corn Stover to L-Lactic Acid Using Co-Culture of Furfural Tolerant Enterococcus Mundtii WX1 and Lactobacillus Rhamnosus SCJ9. *Fermentation* **2023**, *9*, 112. [CrossRef]
103. Gong, J.-S.-Q.; Su, J.-E.; Cai, J.-Y.; Zou, L.; Chen, Y.; Jiang, Y.-L.; Hu, B.-B. Enhanced Enzymolysis and Bioethanol Yield from Tobacco Stem Waste Based on Mild Synergistic Pretreatment. *Front. Energy Res.* **2023**, *10*, 989393. [CrossRef]
104. Usino, D.O.; Sar, T.; Ylitervo, P.; Richards, T. Effect of Acid Pretreatment on the Primary Products of Biomass Fast Pyrolysis. *Energies* **2023**, *16*, 2377. [CrossRef]
105. Abdurrahman, A.; Richard, P.; Ibrahim Galadima, A.; Ubaida Muhammad, A.; Adamu, M. Dilute Sulphuric Acid Pre-Treatment for Efficient Production of Bioethanol from Sugarcane Bagasse Using Saccharomyces Cerevisiae. *J. Biotechnol.* **2022**, *1*, 56–65. [CrossRef]
106. Mazlan, N.A.; Samad, K.A.; Yussof, H.W.; Samah, R.A.; Jahim, J.M. Xylan Recovery from Dilute Nitric Acid Pretreated Oil Palm Frond Bagasse Using Fractional Factorial Design. *J. Oil Palm Res.* **2021**, *33*, 307–319. [CrossRef]
107. Woiciechowski, A.L.; Neto, C.J.D.; Vandenberghe, L.P.d.S.; Neto, D.P.d.C.; Sydney, A.C.N.; Letti, L.A.J.; Karp, S.G.; Torres, L.A.Z.; Soccol, C.R. Lignocellulosic Biomass: Acid and Alkaline Pretreatments and Their Effects on Biomass Recalcitrance—Conventional Processing and Recent Advances. *Bioresour. Technol.* **2020**, *304*, 122848. [CrossRef] [PubMed]
108. Eswari, A.P.; Ravi, Y.K.; Kavitha, S.; Banu, J.R. Recent Insight into Anaerobic Digestion of Lignocellulosic Biomass for Cost Effective Bioenergy Generation. *Adv. Electr. Eng. Electron. Energy* **2023**, *3*, 100119. [CrossRef]
109. Zhang, R.; Gao, H.; Wang, Y.; He, B.; Lu, J.; Zhu, W.; Peng, L.; Wang, Y. Challenges and Perspectives of Green-like Lignocellulose Pretreatments Selectable for Low-Cost Biofuels and High-Value Bioproduction. *Bioresour. Technol.* **2023**, *369*, 128315. [CrossRef]
110. Le Tan, N.T.; Dam, Q.P.; Mai, T.P.; Nguyen, Q.D. The Combination of Acidic and Alkaline Pretreatment for a Lignocellulose Material in Simultaneous Saccharification and Fermentation (SSF) Process. *Chem. Eng. Trans.* **2021**, *89*, 43–48. [CrossRef]
111. Siddique, M.; Mengal, A.N.; Khan, S.; Khan, L.A.; Kakar, E.K. Pretreatment of Lignocellulosic Biomass Conversion into Biofuel and Biochemical: A Comprehensive Review. *J. Biol. Med.* **2023**, *8*, 39–43. [CrossRef]
112. Li, P.; Yang, C.; Jiang, Z.; Jin, Y.; Wu, W. Lignocellulose Pretreatment by Deep Eutectic Solvents and Related Technologies: A Review. *J. Bioresour. Bioprod.* **2023**, *8*, 33–44. [CrossRef]
113. Tareen, A.K.; Punsuvon, V.; Parakulsuksatid, P. Investigation of Alkaline Hydrogen Peroxide Pretreatment to Enhance Enzymatic Hydrolysis and Phenolic Compounds of Oil Palm Trunk. *3 Biotech* **2020**, *10*, 179. [CrossRef]
114. Belay, J.B.; Habtu, N.G.; Ancha, V.R.; Hussen, A.S. Alkaline Hydrogen Peroxide Pretreatment of Cladodes of Cactus (Opuntia Ficus-Indica) for Biogas Production. *Heliyon* **2021**, *7*, e08002. [CrossRef]
115. Yang, L.; Ru, Y.; Xu, S.; Liu, T.; Tan, L. Features Correlated to Improved Enzymatic Digestibility of Corn Stover Subjected to Alkaline Hydrogen Peroxide Pretreatment. *Bioresour. Technol.* **2021**, *325*, 124688. [CrossRef]
116. Damaurai, J.; Preechakun, T.; Raita, M.; Champreda, V.; Laosiripojana, N. Investigation of Alkaline Hydrogen Peroxide in Aqueous Organic Solvent to Enhance Enzymatic Hydrolysis of Rice Straw. *BioEnergy Res.* **2021**, *14*, 122–134. [CrossRef]
117. Broda, M.; Yelle, D.J.; Serwanska, K. Bioethanol Production from Lignocellulosic Biomass—Challenges and Solutions. *Molecules* **2022**, *27*, 8717. [CrossRef]

118. Halim, F.N.B.A.; Taheri, A.; Yassin, Z.A.R.; Chia, K.F.; Goh, K.K.T.; Goh, S.M.; Du, J. Effects of Incorporating Alkaline Hydrogen Peroxide Treated Sugarcane Fibre on the Physical Properties and Glycemic Potency of White Bread. *Foods* **2023**, *12*, 1460. [CrossRef] [PubMed]
119. Chin, D.W.K.; Lim, S.; Pang, Y.L.; Lim, C.H.; Shuit, S.H.; Lee, K.M.; Chong, C.T. Effects of Organic Solvents on the Organosolv Pretreatment of Degraded Empty Fruit Bunch for Fractionation and Lignin Removal. *Sustainability* **2021**, *13*, 6757. [CrossRef]
120. Parchami, M.; Agnihotri, S.; Taherzadeh, M.J. Aqueous Ethanol Organosolv Process for the Valorization of Brewer's Spent Grain (BSG). *Bioresour. Technol.* **2022**, *362*, 127764. [CrossRef] [PubMed]
121. Adamcyk, J.; Beisl, S.; Friedl, A. High Temperature Lignin Separation for Improved Yields in Ethanol Organosolv Pre-Treatment. *Sustainability* **2023**, *15*, 3006. [CrossRef]
122. Chin, D.W.K.; Lim, S.; Pang, Y.L. Fundamental Review of Organosolv Pretreatment and Its Challenges in Emerging Consolidated Bioprocessing. *Biofuels Bioprod. Biorefining* **2020**, *14*, 808–829. [CrossRef]
123. Siacor, F.D.C.; Tabañag, I.D.F.; Lobarbio, C.F.Y.; Taboada, E.B. Effects of Aqueous Ethanol Concentration and Solid-to-Liquid Ratio in the Extraction of Organosolv Lignin from Mango (*Mangifera indica* L.) Seed Husk. *Sci. Technol. Asia* **2021**, *26*, 34–35. [CrossRef]
124. Ifeanyi-nze, F.O.; Omiyale, C.O. Insights into the Recent Advances in the Pretreatment of Biomass for Sustainable Bioenergy and Bio-Products Synthesis: Challenges and Future Directions. *Eur. J. Sustain. Dev. Res.* **2023**, *7*, em0209. [CrossRef]
125. Rabelo, S.C.; Nakasu, P.Y.S.; Scopel, E.; Araújo, M.F.; Cardoso, L.H.; da Costa, A.C. Organosolv Pretreatment for Biorefineries: Current Status, Perspectives, and Challenges. *Bioresour. Technol.* **2023**, *369*, 128331. [CrossRef]
126. Wang, R.; Yue, J.; Jiang, J.; Li, J.; Zhao, J.; Xia, H.; Wang, K.; Xu, J. Hydrothermal CO_2-Assisted Pretreatment of Wheat Straw for Hemicellulose Degradation Followed with Enzymatic Hydrolysis for Glucose Production. *Waste Biomass Valoriz.* **2020**, *12*, 1483–1492. [CrossRef]
127. Cano, M.E.; García-Martin, A.; Morales, P.C.; Wojtusik, M.; Santos, V.E.; Kovensky, J.; Ladero, M. Production of Oligosaccharides from Agrofood Wastes. *Fermentation* **2020**, *6*, 31. [CrossRef]
128. Nwachukwu, B.C.; Ayangbenro, A.S.; Babalola, O.O. Elucidating the Rhizosphere Associated Bacteria for Environmental Sustainability. *Agriculture* **2021**, *11*, 75. [CrossRef]
129. Parapouli, M.; Vasileiadis, A.; Afendra, A.S.; Hatziloukas, E. Saccharomyces Cerevisiae and Its Industrial Applications. *AIMS Microbiol.* **2020**, *6*, 1–31. [CrossRef]
130. Sharma, S.; Arora, A. Tracking Strategic Developments for Conferring Xylose Utilization / Fermentation by Saccharomyces Cerevisiae. *Ann. Microbiol.* **2020**, *70*, 50. [CrossRef]
131. Pacho, E.R.; Vaskan, P.; Gorgens, J.F.; Gnansounou, E. Process Design, Techno-Economic, and Life-Cycle Assessments of Selected Sugarcane-Based Biorefineries: A Case Study in the South African Context. In *Refining Biomass Residues for Sustainable Energy and Bioproducts*; Elsevier: Amsterdam, The Netherlands, 2020; pp. 567–597. [CrossRef]
132. Hernández, D.; Rebolledo-Leiva, R.; Fern, H.; Quinteros-Lama, H.; Cataldo, F.; Muñoz, E.; Tenreiro, C. Recovering Apple Agro-Industrial Waste for Bioethanol and Vinasse Joint Production: Screening the Potential of Chile. *Fermentation* **2021**, *7*, 203. [CrossRef]
133. Ma, S.; Dong, C.; Hu, X.; Xue, J.; Zhao, Y.; Wang, X. Techno-Economic Evaluation of a Combined Biomass Gasification-Solid Oxide Fuel Cell System for Ethanol Production via Syngas Fermentation. *Fuel* **2022**, *324*, 124395. [CrossRef]
134. Zentou, H.; Abidin, Z.Z.; Yunus, R.; Biak, D.R.A.; Korelskiy, D. Overview of Alternative Ethanol Removal Techniques for Enhancing Bioethanol Recovery from Fermentation Broth. *Processes* **2019**, *7*, 458. [CrossRef]
135. Do Thi, H.T.; Mizsey, P.; Toth, A.J. Separation of Alcohol-Water Mixtures by a Combination of Distillation, Hydrophilic and Organophilic Pervaporation Processes. *Membranes* **2020**, *10*, 345. [CrossRef]
136. Tareen, A.K.; Sultan, I.N.; Songprom, K.; Laemsak, N.; Sirisansaneeyakul, S.; Vanichsriratana, W.; Parakulsuksatid, P. Two-Step Pretreatment of Oil Palm Trunk for Ethanol Production by Thermotolerent Saccharomyces Cerevisiae SC90. *Bioresour. Technol.* **2021**, *320*, 124298. [CrossRef]
137. Morales, M.; Arvesen, A.; Cherubini, F. Integrated Process Simulation for Bioethanol Production: Effects of Varying Lignocellulosic Feedstocks on Technical Performance. *Bioresour. Technol.* **2021**, *328*, 124833. [CrossRef]
138. Cunha, J.T.; Romaní, A.; Inokuma, K.; Johansson, B.; Hasunuma, T.; Kondo, A.; Domingues, L. Consolidated Bioprocessing of Corn Cob - Derived Hemicellulose: Engineered Industrial Saccharomyces Cerevisiae as Efficient Whole Cell Biocatalysts. *Biotechnol. Biofuels* **2020**, *13*, 138. [CrossRef]
139. Baig, K.S. Interaction of Enzymes with Lignocellulosic Materials: Causes, Mechanism and Influencing Factors. *Bioresour. Bioprocess.* **2020**, *7*, 21. [CrossRef]
140. Marnoto, T.; Budiaman, I.G.S.; Hapsari, C.R.; Prakosa, R.A.Y.; Arifin, K. Dehydrating Ethanol Using a Ternary Solute and Extractive Batch Distillation. *Malays. J. Anal. Sci.* **2019**, *23*, 124–130. [CrossRef]
141. Nakamura, M.; Noguchi, K. Tolerant Mechanisms to O_2 Deficiency under Submergence Conditions in Plants. *J. Plant Res.* **2020**, *133*, 343–371. [CrossRef] [PubMed]
142. Galvanauskas, V.; Simutis, R.; Levišauskas, D.; Urniežius, R. Practical Solutions for Specific Growth Rate Control Systems in Industrial Bioreactors. *Processes* **2019**, *7*, 693. [CrossRef]
143. Gomes, D.; Cruz, M.; de Resende, M.; Ribeiro, E.; Teixeira, J.; Domingues, L. Very High Gravity Bioethanol Revisited: Main Challenges and Advances. *Fermentation* **2021**, *7*, 38. [CrossRef]

144. Veloso, I.I.K.; Rodrigues, K.C.S.; Sonego, J.L.S.; Cruz, A.J.G.; Badino, A.C. Fed-Batch Ethanol Fermentation at Low Temperature as a Way to Obtain Highly Concentrated Alcoholic Wines: Modeling and Optimization. *Biochem. Eng. J.* **2019**, *141*, 60–70. [CrossRef]
145. Knudsen, J.D.; Rønnow, B. Extended Fed-Batch Fermentation of a C5/C6 Optimised Yeast Strain on Wheat Straw Hydrolysate Using an Online Refractive Index Sensor to Measure the Relative Fermentation Rate. *Sci. Rep.* **2020**, *10*, 6705. [CrossRef]
146. Cruz, M.L.; de Resende, M.M.; Ribeiro, E.J. Improvement of Ethanol Production in Fed-Batch Fermentation Using a Mixture of Sugarcane Juice and Molasse under Very High-Gravity Conditions. *Bioprocess Biosyst. Eng.* **2021**, *44*, 617–625. [CrossRef]
147. Puligundla, P.; Smogrovicova, D.; Mok, C.; Obulam, V.S.R. A Review of Recent Advances in High Gravity Ethanol Fermentation. *Renew. Energy* **2019**, *133*, 1366–1379. [CrossRef]
148. Margono, M.; Kaavessina, M.; Mohd Zahari, M.A.K.; Hisyam, A. Continuous Bioethanol Production Using Uncontrolled Process in a Laboratory Scale of Integrated Aerobic-Anaerobic Baffled Reactor. *Period. Polytech. Chem. Eng.* **2020**, *64*, 172–178. [CrossRef]
149. Liu, Q.; Zhao, N.; Zou, Y.; Ying, H.; Liu, D.; Chen, Y. Feasibility Study on Long-Term Continuous Ethanol Production from Cassava Supernatant by Immobilized Yeast Cells in Packed Bed Reactor. *J. Microbiol. Biotechnol.* **2020**, *30*, 1227–1234. [CrossRef] [PubMed]
150. Degweker, G.; Lali, A. High Productivity Ethanol Fermentation of Glucose & Xylose Using Membrane Assisted Continuous Cell Recycle. *Sustain. Chem. Eng.* **2021**, *2*, 8–19. [CrossRef]
151. Benevenuti, C.; Branco, M.; Do Nascimento-Correa, M.; Botelho, A.; Ferreira, T.; Amaral, P. Residual Gas for Ethanol Production by Clostridium Carboxidivorans in a Dual Impeller Stirred Tank Bioreactor (STBR). *Fermentation* **2021**, *7*, 199. [CrossRef]
152. Pacheco, M.; Moura, P.; Silva, C. A Systematic Review of Syngas Bioconversion to Value-Added Products from 2012 to 2022. *Energies* **2023**, *16*, 3241. [CrossRef]
153. Rückel, A.; Hannemann, J.; Maierhofer, C.; Fuchs, A.; Weuster-Botz, D. Studies on Syngas Fermentation with Clostridium Carboxidivorans in Stirred-Tank Reactors with Defined Gas Impurities. *Front. Microbiol.* **2021**, *12*, 655390. [CrossRef]
154. Fernández-Blanco, C.; Robles-Iglesias, R.; Naveira-Pazos, C.; Veiga, M.C.; Kennes, C. Production of Biofuels from C1-Gases with Clostridium and Related Bacteria—Recent Advances. *Microb. Biotechnol.* **2023**, *16*, 726–741. [CrossRef]
155. Bäumler, M.; Schneider, M.; Ehrenreich, A.; Liebl, W.; Weuster-Botz, D. Synthetic Co-Culture of Autotrophic Clostridium Carboxidivorans and Chain Elongating Clostridium Kluyveri Monitored by Flow Cytometry. *Microb. Biotechnol.* **2022**, *15*, 1471–1485. [CrossRef]
156. Mann, M.; Effert, D.; Kottenhahn, P.; Hüser, A.; Philipps, G.; Jennewein, S.; Büchs, J. Impact of Different Trace Elements on Metabolic Routes during Heterotrophic Growth of C. Ljungdahlii Investigated through Online Measurement of the Carbon Dioxide Transfer Rate. *Biotechnol. Prog.* **2022**, *38*, e3263. [CrossRef]
157. Lakhssassi, N.; Baharlouei, A.; Meksem, J.; Hamilton-Brehm, S.D.; Lightfoot, D.A.; Meksem, K.; Liang, Y. EMS-Induced Mutagenesis of Clostridium Carboxidivorans for Increased Atmospheric CO_2 Reduction Efficiency and Solvent Production. *Microorganisms* **2020**, *8*, 1239. [CrossRef]
158. Pavan, M.; Reinmets, K.; Garg, S.; Mueller, A.P.; Marcellin, E.; Köpke, M.; Valgepea, K. Advances in Systems Metabolic Engineering of Autotrophic Carbon Oxide-Fixing Biocatalysts towards a Circular Economy. *Metab. Eng.* **2022**, *71*, 117–141. [CrossRef] [PubMed]
159. Vees, C.A.; Herwig, C.; Pflügl, S. Mixotrophic Co-Utilization of Glucose and Carbon Monoxide Boosts Ethanol and Butanol Productivity of Continuous Clostridium Carboxidivorans Cultures. *Bioresour. Technol.* **2022**, *353*, 127138. [CrossRef]
160. Liu, K.; Phillips, J.R.; Sun, X.; Mohammad, S.; Huhnke, R.L.; Atiyeh, H.K. Investigation and Modeling of Gas-Liquid Mass Transfer in a Sparged and Non-Sparged Continuous Stirred Tank Reactor with Potential Application in Syngas Fermentation. *Fermentation* **2019**, *5*, 75. [CrossRef]
161. Elisiário, M.P.; De Wever, H.; Van Hecke, W.; Noorman, H.; Straathof, A.J.J. Membrane Bioreactors for Syngas Permeation and Fermentation. *Crit. Rev. Biotechnol.* **2022**, *42*, 856–872. [CrossRef]
162. Puiman, L.; Abrahamson, B.; van der Lans, R.G.J.M.; Haringa, C.; Noorman, H.J.; Picioreanu, C. Alleviating Mass Transfer Limitations in Industrial External-Loop Syngas-to-Ethanol Fermentation. *Chem. Eng. Sci.* **2022**, *259*, 117770. [CrossRef]
163. Sajeev, E.; Shekher, S.; Ogbaga, C.C.; Desongu, K.S.; Gunes, B.; Okolie, J.A. Application of Nanoparticles in Bioreactors to Enhance Mass Transfer during Syngas Fermentation. *Encyclopedia* **2023**, *3*, 387–395. [CrossRef]
164. Sun, X.; Atiyeh, H.K.; Huhnke, R.L.; Tanner, R.S. Syngas Fermentation Process Development for Production of Biofuels and Chemicals: A Review. *Bioresour. Technol. Rep.* **2019**, *7*, 100279. [CrossRef]
165. Benevenuti, C.; Amaral, P.; Ferreira, T.; Seidl, P. Impacts of Syngas Composition on Anaerobic Fermentation. *Reactions* **2021**, *2*, 391–407. [CrossRef]
166. Prasoulas, G.; Gentikis, A.; Konti, A.; Kalantzi, S.; Kekos, D.; Mamma, D. Bioethanol Production from Food Waste Applying the Multienzyme System Produced On-Site by Fusarium Oxysporum F3 and Mixed Microbial Cultures. *Fermentation* **2020**, *6*, 39. [CrossRef]
167. Barahona, P.P.; Mayorga, B.B.; Martín-Gil, J.; Martín-Ramos, P.; Barriga, E.J.C. Cellulosic Ethanol: Improving Cost Efficiency by Coupling Semi-Continuous Fermentation and Simultaneous Saccharification Strategies. *Processes* **2020**, *8*, 1459. [CrossRef]
168. Hemansi; Kaushik, A.; Yadav, G.; Saini, J.K. Simultaneous Sacchari Fi Cation and Fermentation of Sequential Dilute Acid-Alkali Pretreated Cotton (*Gossypium hirsutum* L.) Stalk for Cellulosic Ethanol Production. *J. Chem. Technol. Biotechnol.* **2021**, *97*, 534–542. [CrossRef]

169. Yong, K.J.; Wu, T.Y. Second-Generation Bioenergy from Oilseed Crop Residues: Recent Technologies, Techno-Economic Assessments and Policies. *Energy Convers. Manag.* **2022**, *267*, 115869. [CrossRef]
170. David, A.N.; Sewsynker-Sukai, Y.; Sithole, B.; Kana, E.B.G. Development of a Green Liquor Dregs Pretreatment for Enhanced Glucose Recovery from Corn Cobs and Kinetic Assessment on Various Bioethanol Fermentation Types. *Fuel* **2020**, *274*, 117797. [CrossRef]
171. Tareen, A.K.; Punsuvon, V.; Sultan, I.N.; Khan, M.W.; Parakulsuksatid, P. Cellulase Addition and Pre-Hydrolysis Effect of High Solid Fed-Batch Simultaneous Saccharification and Ethanol Fermentation from a Combined Pretreated Oil Palm Trunk. *ACS Omega* **2021**, *6*, 26119–26129. [CrossRef]
172. Palacios, A.S.; Ilyina, A.; Ramos-gonzález, R.; Aguilar, C.N.; Martínez-hernández, J.L.; Segura-ceniceros, E.P.; Lizeth, M.; González, C.; Aguilar, M.; Ballesteros, M.; et al. Ethanol Production from Banana Peels at High Pretreated Substrate Loading: Comparison of Two Operational Strategies. *Biomass Convers. Biorefinery* **2019**, *11*, 1587–1596. [CrossRef]
173. Paschos, T.; Louloudi, A.; Papayannakos, N.; Kekos, D.; Mamma, D. Potential of Barley Straw for High Titer Bioethanol Production Applying Pre-Hydrolysis and Simultaneous Saccharification and Fermentation at High Solid Loading Pre-Hydrolysis and Simultaneous Saccharification and Fermentation at High. *Biofuels* **2020**, *13*, 467–473. [CrossRef]
174. Aparicio, E.; Rodríguez-Jasso, R.M.; Pinales-Marquez, C.D.; Loredo-Trevino, A.; Robledo-Olivo, A.; Aguilar, C.N.; Kostas, E.T.; Ruiz, H.A. High-Pressure Technology for Sargassum Spp Biomass Pretreatment and Fractionation in the Third Generation of Bioethanol Production. *Bioresour. Technol.* **2021**, *329*, 124935. [CrossRef]
175. Rodríguez-Martínez, B.; Coelho, E.; Gullon, B.; Yanez, R.; Domingues, L. Potato Peels Waste as a Sustainable Source for Biotechnological Production of Biofuels: Process Optimization. *Waste Manag.* **2023**, *155*, 320–328. [CrossRef]
176. Zhu, J.Q.; Zong, Q.J.; Li, W.C.; Chai, M.Z.; Xu, T.; Liu, H.; Fan, H.; Li, B.Z.; Yuan, Y.J. Temperature Profiled Simultaneous Saccharification and Co-Fermentation of Corn Stover Increases Ethanol Production at High Solid Loading. *Energy Convers. Manag.* **2020**, *205*, 112344. [CrossRef]
177. Tu, W.-L.; Ma, T.-Y.; Ou, C.-M.; Guo, G.-L.; Chao, Y. Simultaneous Saccharification and Co-Fermentation with a Thermotolerant Saccharomyces Cerevisiae to Produce Ethanol from Sugarcane Bagasse under High Temperature Conditions. *BioResources* **2021**, *16*, 1358–1372. [CrossRef]
178. Pinheiro, T.; Ying, K.; Lip, F.; Ríos, E.G.; Querol, A.; Teixeira, J. Differential Proteomic Analysis by SWATH - MS Unravels the Most Dominant Mechanisms Underlying Yeast Adaptation to Non-Optimal Temperatures under Anaerobic Conditions. *Sci. Rep.* **2020**, *10*, 22329. [CrossRef] [PubMed]
179. Fernandes, F.d.S.; de Souza, E.S.; Carneiro, L.M.; Silva, J.P.A.; de Souza, J.V.B.; Batista, J.d.S. Current Ethanol Production Requirements for the Yeast Saccharomyces Cerevisiae. *Int. J. Microbiol.* **2022**, *2022*, 7878830.
180. Phong, H.X.; Klanrit, P.; Thi, N.; Dung, P.; Thanonkeo, S. High-Temperature Ethanol Fermentation from Pineapple Waste Hydrolysate and Gene Expression Analysis of Thermotolerant Yeast Saccharomyces Cerevisiae. *Sci. Rep.* **2022**, *12*, 13965. [CrossRef]
181. Yang, P.; Wu, W.; Chen, J.; Jiang, S.; Zheng, Z.; Deng, Y.; Lu, J.; Wang, H.; Zhou, Y.; Geng, Y.; et al. Thermotolerance Improvement of Engineered Saccharomyces Cerevisiae ERG5 Delta ERG4 Delta ERG3 Delta, Molecular Mechanism, and Its Application in Corn Ethanol Production. *Biotechnol. Biofuels Bioprod.* **2023**, *16*, 66. [CrossRef]
182. Rahmadhani, N.; Astuti, R.I.; Meryandini, A. Ethanol Productivity of Ethanol-Tolerant Mutant Strain Pichia Kudriavzevii R-T3 in Monoculture and Co-Culture Fermentation with Saccharomyces Cerevisiae. *J. Biosci.* **2022**, *29*, 435–444. [CrossRef]
183. Van Nguyen, P.; Nguyen, K.H.V.; Nguyen, N.L.; Ho, X.T.T.; Truong, P.H.; Nguyen, K.C.T. Lychee-Derived, Thermotolerant Yeasts for Second-Generation Bioethanol Production. *Fermentation* **2022**, *8*, 515. [CrossRef]
184. Nuanpeng, S.; Thanonkeo, S.; Klanrit, P.; Yamada, M.; Thanonkeo, P. Optimization Conditions for Ethanol Production from Sweet Sorghum Juice by Thermotolerant Yeast Saccharomyces Cerevisiae: Using a Statistical Experimental Design. *Fermentation* **2023**, *9*, 450. [CrossRef]
185. Iyyappan, J.; Pravin, R.; Al-Ghanim, K.A.; Govindarajan, M.; Marcello, N.; Baskar, G. Dual Strategy for Bioconversion of Elephant Grass Biomass into Fermentable Sugars Using Trichoderma Reesei towards Bioethanol Production. *Bioresour. Technol.* **2023**, *374*, 128804. [CrossRef]
186. Oh, E.J.; Jin, Y. Engineering of Saccharomyces Cerevisiae for Efficient Fermentation of Cellulose. *FEMS Yeast Res.* **2020**, *20*, foz089. [CrossRef]
187. Singhania, R.R.; Patel, A.K.; Singh, A.; Haldar, D.; Soam, S.; Chen, C.-W.; Tsai, M.-L.; Dong, C.-D. Consolidated Bioprocessing of Lignocellulosic Biomass: Technological Advances and Challenges. *Bioresour. Technol.* **2022**, *354*, 127153. [CrossRef]
188. Banner, A.; Toogood, H.S.; Scrutton, N.S. Consolidated Bioprocessing: Synthetic Biology Routes to Fuels and Fine Chemicals. *Microorganisms* **2021**, *9*, 1079. [CrossRef]
189. Malherbe, S.J.M.; Cripwell, R.A.; Favaro, L.; Van Zyl, W.H.; Viljoen-bloom, M. Triticale and Sorghum as Feedstock for Bioethanol Production via Consolidated Bioprocessing. *Renew. Energy* **2023**, *206*, 498–505. [CrossRef]
190. Re, A.; Mazzoli, R. Current Progress on Engineering Microbial Strains and Consortia for Production of Cellulosic Butanol through Consolidated Bioprocessing. *Microb. Biotechnol.* **2023**, *16*, 238–261. [CrossRef]
191. Kavitha, S.; Gajendran, T.; Saranya, K.; Selvakumar, P.; Manivasagan, V. Study on Consolidated Bioprocessing of Pre-Treated Nannochloropsis Gaditana Biomass into Ethanol under Optimal Strategy. *Renew. Energy* **2021**, *172*, 440–452. [CrossRef]

192. Ghazali, M.F.S.M.; Mustafa, M.; Zainudin, N.A.I.M.; Aziz, N.A.A. Consolidated Bioethanol Production Using Trichoderma Asperellum B1581. *Jordan J. Biol. Sci.* **2022**, *15*, 621–627.
193. Lao, M.; Alfafara, C.; de Leon, R. Screening of Fusarium Moniliforme as Potential Fungus for Integrated Biodelignification and Consolidated Bioprocessing of Napier Grass for Bioethanol Production. *Catalysts* **2022**, *12*, 1204. [CrossRef]
194. Kavitha, S.; Gajendran, T.; Saranya, K.; Manivasagan, V. Bioconversion of Sargassum Wightii to Ethanol via Consolidated Bioprocessing Using Lachnoclostridium Phytofermentans KSM 1203. *Fuel* **2023**, *347*, 128465. [CrossRef]
195. Joshi, J.; Dhungana, P.; Prajapati, B.; Maharjan, R.; Poudyal, P.; Yadav, M.; Mainali, M.; Yadav, A.P.; Bhattarai, T.; Sreerama, L. Enhancement of Ethanol Production in Electrochemical Cell by Saccharomyces Cerevisiae (CDBT2) and Wickerhamomyces Anomalus (CDBT7). *Front. Energy Res.* **2019**, *7*, 1–11. [CrossRef]
196. Ruchala, J.; Kurylenko, O.O.; Dmytruk, K.V.; Sibirny, A.A. Construction of Advanced Producers of First- and Second-Generation Ethanol in Saccharomyces Cerevisiae and Selected Species of Non-Conventional Yeasts (Scheffersomyces Stipitis, Ogataea Polymorpha). *Ind. Microbiol. Biotechnol.* **2020**, *47*, 109–132. [CrossRef]
197. Kim, J.H.; Ryu, J.; Huh, I.Y.; Hong, S.K.; Kang, H.A.; Chang, Y.K. Ethanol Production from Galactose by a Newly Isolated Saccharomyces Cerevisiae KL17. *Bioprocess Biosyst. Eng.* **2014**, *37*, 1871–1878. [CrossRef]
198. Nachaiwieng, W.; Lumyong, S.; Yoshioka, K.; Watanabe, T.; Khanongnuch, C. Bioethanol Production from Rice Husk under Elevated Temperature Simultaneous Saccharification and Fermentation Using Kluyveromyces Marxianus CK8. *Biocatal. Agric. Biotechnol.* **2015**, *4*, 543–549. [CrossRef]
199. Saad, M.M.E.; Amani, F.A.H.; Keong, L.C. Optimization of Bioethanol Production Process Using Oil Palm Frond Juice as Substrate. *Malays. J. Microbiol.* **2016**, *12*, 308–314.
200. Li, Y.J.; Lu, Y.Y.; Zhang, Z.J.; Mei, S.; Tan, T.W.; Fan, L.H. Co-Fermentation of Cellulose and Sucrose/Xylose by Engineered Yeasts for Bioethanol Production. *Energy Fuels* **2017**, *31*, 4061–4067. [CrossRef]
201. Abdulla, R.; Derman, E.; Ravintaran, P.T.; Jambo, S.A. Fuel Ethanol Production from Papaya Waste Using Immobilized Saccharomyces Cerevisiae. *ASM Sci. J.* **2018**, *11*, 112–123.
202. Choojit, S.; Ruengpeerakul, T.; Sangwichien, C. Optimization of Acid Hydrolysis of Pineapple Leaf Residue and Bioconversion to Ethanol by Saccharomyces Cerevisiae. *Cell. Chem. Technol.* **2018**, *52*, 247–257.
203. Demiray, E.; Karatay, S.E.; Dönmez, G. Evaluation of Pomegranate Peel in Ethanol Production by Saccharomyces Cerevisiae and Pichia Stipitis. *Energy* **2018**, *159*, 988–994. [CrossRef]
204. Nuanpeng, S.; Thanonkeo, S.; Klanrit, P.; Thanonkeo, P. Ethanol Production from Sweet Sorghum by Saccharomyces Cerevisiae DBKKUY-53 Immobilized on Alginate-Loofah Matrices. *Braz. J. Microbiol.* **2018**, *49*, 140–150. [CrossRef]
205. Pandey, A.K.; Kumar, M.; Kumari, S.; Kumari, P.; Yusuf, F.; Jakeer, S.; Naz, S.; Chandna, P.; Bhatnagar, I.; Gaur, N.A. Evaluation of Divergent Yeast Genera for Fermentation-Associated Stresses and Identification of a Robust Sugarcane Distillery Waste Isolate Saccharomyces Cerevisiae NGY10 for Lignocellulosic Ethanol Production in SHF and SSF. *Biotechnol. Biofuels* **2019**, *12*, 40. [CrossRef]
206. Cripwell, R.A.; Rose, S.H.; Favaro, L.; Van Zyl, W.H. Construction of Industrial Saccharomyces Cerevisiae Strains for the Efficient Consolidated Bioprocessing of Raw Starch. *Biotechnol. Biofuels* **2019**, *12*, 201. [CrossRef]
207. Anu; Singh, B.; Kumar, A. Process Development for Sodium Carbonate Pretreatment and Enzymatic Saccharification of Rice Straw for Bioethanol Production. *Biomass Bioenergy* **2020**, *138*, 105574. [CrossRef]
208. Wu, R.; Chen, D.; Cao, S.; Lu, Z.; Huang, J.; Lu, Q.; Chen, Y.; Chen, X.; Guan, N.; Wei, Y.; et al. Enhanced Ethanol Production from Sugarcane Molasses by Industrially Engineered: Saccharomyces Cerevisiae via Replacement of the PHO4 Gene. *RSC Adv.* **2020**, *10*, 2267–2276. [CrossRef]
209. Aderibigbe, F.A.; Amosa, M.K.; Adejumo, A.L.; Mohammed, I.A.; Mustapha, S.I.; Saka, H.B.; Tijani, I.A.; Olufowora, F.O.; Bello, B.T.; Owolabi, R.U.; et al. Optimized Production of Bioethanol by Fermentation of Acid Hydrolyzed-Corn Stover Employing Saccharomyces Cerevisiae Yeast Strain. *J. Eng. Technol.* **2021**, *15*, 93–98.
210. Dhandayuthapani, K.; Sarumathi, V.; Selvakumar, P.; Temesgen, T.; Asaithambi, P.; Sivashanmugam, P. Study on the Ethanol Production from Hydrolysate Derived by Ultrasonic Pretreated Defatted Biomass of Chlorella Sorokiniana NITTS3. *Chem. Data Collect.* **2021**, *31*, 100641. [CrossRef]
211. Beigbeder, J.-B.; de Medeiros Dantas, J.M.; Lavoie, J.-M. Optimization of Yeast, Sugar and Nutrient Concentrations for High Ethanol Production Rate Using Industrial Sugar Beet Molasses and Response Surface Methodology. *Fermentation* **2021**, *7*, 86. [CrossRef]
212. Krajang, M.; Malairuang, K.; Sukna, J.; Rattanapradit, K.; Chamsart, S. Single-Step Ethanol Production from Raw Cassava Starch Using a Combination of Raw Starch Hydrolysis and Fermentation, Scale-up from 5-L Laboratory and 200-L Pilot Plant to 3000-L Industrial Fermenters. *Biotechnol. Biofuels* **2021**, *14*, 68. [CrossRef] [PubMed]
213. Hargono, H.; Jos, B.; Purwanto, P.; Sumardiono, S.; Zakaria, M. Bioethanol Purification from Fermentation of Suweg Starch Using Two Stage Distillation Method. *IOP Conf. Ser. Mater. Sci. Eng.* **2021**, *1053*, 012114. [CrossRef]
214. Kooprasertying, P.; Vanichsriratana, W.; Sirisansaneeyakul, S.; Laemsak, N.; Tareen, A.K.; Ullah, Z.; Parakulsuksatid, P.; Sultan, I.N. Ethanol Production through Optimized Alkaline Pretreated Elaeis Guineensis Frond Waste from Krabi Province, Thailand. *Fermentation* **2022**, *8*, 648. [CrossRef]

215. Tran, P.H.N.; Ko, J.K.; Gong, G.; Um, Y.; Lee, S.M. Improved Simultaneous Co-Fermentation of Glucose and Xylose by Saccharomyces Cerevisiae for Efficient Lignocellulosic Biorefinery. *Biotechnol. Biofuels* **2020**, *13*, 12. [CrossRef]
216. Lopez, P.C.; Abeykoon Udugama, I.; Thomsen, S.T.; Bayer, C.; Junicke, H.; Gernaey, K.V. Promoting the Co-Utilisation of Glucose and Xylose in Lignocellulosic Ethanol Fermentations Using a Data-Driven Feed-Back Controller. *Biotechnol. Biofuels* **2020**, *13*, 190. [CrossRef]
217. Sjulander, N.; Kikas, T. Origin, Impact and Control of Lignocellulosic Inhibitors in Bioethanol Production—A Review. *Energies* **2020**, *13*, 4751. [CrossRef]
218. Oktaviani, M.; Hermiati, E.; Thontowi, A.; Laksana, R.P.B.; Kholida, L.N.; Andriani, A.; Yopi; Mangunwardoyo, W. Production of Xylose, Glucose, and Other Products from Tropical Lignocellulose Biomass by Using Maleic Acid Pretreatment. *IOP Conf. Ser. Earth Environ. Sci.* **2019**, *251*, 012013. [CrossRef]
219. Galan-Mascaros, J.R. Photoelectrochemical Solar Fuels from Carbon Dioxide, Water and Sunlight. *Catal. Sci. Technol.* **2020**, *10*, 1967–1974. [CrossRef]
220. González-Garay, A.; Mac Dowell, N.; Shah, N. A Carbon Neutral Chemical Industry Powered by the Sun. *Discov. Chem. Eng.* **2021**, *1*, 2. [CrossRef]
221. Han, H.; Noh, Y.; Kim, Y.; Park, S.; Yoon, W.; Jang, D.; Choi, S.M.; Kim, W.B. Selective Electrochemical CO_2 Conversion to Multicarbon Alcohols on Highly Efficient N-Doped Porous Carbon-Supported Cu Catalysts. *Green Chem.* **2020**, *22*, 71–84. [CrossRef]
222. Yuan, C.Z.; Li, H.B.; Jiang, Y.F.; Liang, K.; Zhao, S.J.; Fang, X.X.; Ma, L.B.; Zhao, T.; Lin, C.; Xu, A.W. Tuning the Activity of N-Doped Carbon for CO_2 Reduction: Via in Situ Encapsulation of Nickel Nanoparticles into Nano-Hybrid Carbon Substrates. *Mater. Chem. A* **2019**, *7*, 6894–6900. [CrossRef]
223. Kou, W.; Zhang, Y.; Dong, J.; Mu, C.; Xu, L. Nickel-Nitrogen-Doped Three-Dimensional Ordered Macro-/Mesoporous Carbon as an Efficient Electrocatalyst for CO_2 Reduction to CO. *ACS Appl. Energy Mater.* **2020**, *3*, 1875–1882. [CrossRef]
224. Ramírez-Valencia, L.D.; Bailón-García, E.; Carrasco-Marín, F.; Pérez-Cadenas, A.F. From CO_2 to Value-Added Products: A Review about Carbon-Based Materials for Electro-Chemical CO_2 Conversion. *Catalysts* **2021**, *11*, 351. [CrossRef]
225. Liu, K.; Wang, J.; Shi, M.; Yan, J.; Jiang, Q. Simultaneous Achieving of High Faradaic Efficiency and CO Partial Current Density for CO_2 Reduction via Robust, Noble-Metal-Free Zn Nanosheets with Favorable Adsorption Energy. *Adv. Energy Mater.* **2019**, *9*, 1900276. [CrossRef]
226. Xu, H.; Rebollar, D.; He, H.; Chong, L.; Liu, Y.; Liu, C.; Sun, C.J.; Li, T.; Muntean, J.V.; Winans, R.E.; et al. Highly Selective Electrocatalytic CO_2 Reduction to Ethanol by Metallic Clusters Dynamically Formed from Atomically Dispersed Copper. *Nat. Energy* **2020**, *5*, 623–632. [CrossRef]
227. Park, S.; Wijaya, D.T.; Na, J.; Lee, C.W. Towards the Large-Scale Electrochemical Reduction of Carbon Dioxide. *Catalysts* **2021**, *11*, 253. [CrossRef]
228. Ramdin, M.; Morrison, A.R.T.; De Groen, M.; Van Haperen, R.; De Kler, R.; Van Den Broeke, L.J.P.; Martin Trusler, J.P.; De Jong, W.; Vlugt, T.J.H. High Pressure Electrochemical Reduction of CO_2 to Formic Acid/Formate: A Comparison between Bipolar Membranes and Cation Exchange Membranes. *Ind. Eng. Chem. Res.* **2019**, *58*, 1834–1847. [CrossRef] [PubMed]
229. Garg, S.; Li, M.; Weber, A.Z.; Ge, L.; Li, L.; Rudolph, V.; Wang, G.; Rufford, T.E. Advances and Challenges in Electrochemical CO_2 Reduction Processes: An Engineering and Design Perspective Looking beyond New Catalyst Materials. *J. Mater. Chem. A* **2020**, *8*, 1511–1544. [CrossRef]
230. Senocrate, A.; Battaglia, C. Electrochemical CO_2 Reduction at Room Temperature: Status and Perspectives. *J. Energy Storage* **2021**, *36*, 102373. [CrossRef]
231. Liu, X.; Schlexer, P.; Xiao, J.; Ji, Y.; Wang, L.; Sandberg, R.B.; Tang, M.; Brown, K.S.; Peng, H.; Ringe, S.; et al. PH Effects on the Electrochemical Reduction of CO_2 towards C_2 Products on Stepped Copper. *Nat. Commun.* **2019**, *10*, 32. [CrossRef] [PubMed]
232. Fan, L.; Xia, C.; Yang, F.; Wang, J.; Wang, H.; Lu, Y. Strategies in Catalysts and Electrolyzer Design for Electrochemical CO_2 Reduction toward C2+ Products. *Sci. Adv.* **2020**, *6*, eaay3111. [CrossRef] [PubMed]
233. Li, J.; Chang, X.; Zhang, H.; Malkani, A.S.; Cheng, M.J.; Xu, B.; Lu, Q. Electrokinetic and in Situ Spectroscopic Investigations of CO Electrochemical Reduction on Copper. *Nat. Commun.* **2021**, *12*, 3264. [CrossRef]
234. Shao, J.; Wang, C.; Shen, Y.; Shi, J.; Ding, D. Electrochemical Sensors and Biosensors for the Analysis of Tea Components: A Bibliometric Review. *Front. Chem.* **2022**, *9*, 818461. [CrossRef]
235. Li, Y.; Yuan, H.; Chen, Y.; Wei, X.; Sui, K.; Tan, Y. Application and Exploration of Nanofibrous Strategy in Electrode Design. *J. Mater. Sci. Technol.* **2021**, *74*, 189–202. [CrossRef]
236. Gao, D.; Arán-Ais, R.M.; Jeon, H.S.; Roldan Cuenya, B. Rational Catalyst and Electrolyte Design for CO_2 Electroreduction towards Multicarbon Products. *Nat. Catal.* **2019**, *2*, 198–210. [CrossRef]
237. Song, Y.; Chen, W.; Wei, W.; Sun, Y. Advances in Clean Fuel Ethanol Production from Electro-, Photo-and Photoelectro-Catalytic CO_2 Reduction. *Catalysts* **2020**, *10*, 1287. [CrossRef]
238. Sun, Y.; Dai, S. High-Entropy Materials for Catalysis: A New Frontier. *Sci. Adv.* **2021**, *7*, eabg1600. [CrossRef]
239. Nitopi, S.; Bertheussen, E.; Scott, S.B.; Liu, X.; Engstfeld, A.K.; Horch, S.; Seger, B.; Stephens, I.E.L.; Chan, K.; Hahn, C.; et al. Progress and Perspectives of Electrochemical CO_2 Reduction on Copper in Aqueous Electrolyte. *Chem. Rev.* **2019**, *119*, 7610–7672. [CrossRef] [PubMed]

240. Pei, Y.; Zhong, H.; Jin, F. A Brief Review of Electrocatalytic Reduction of CO_2—Materials, Reaction Conditions, and Devices. *Energy Sci. Eng.* **2021**, *9*, 1012–1032. [CrossRef]
241. Mustafa, A.; Lougou, B.G.; Shuai, Y.; Wang, Z.; Razzaq, S.; Zhao, J.; Tan, H. Theoretical Insights into the Factors Affecting the Electrochemical Reduction of CO_2. *Sustain. Energy Fuels* **2020**, *4*, 4352–4369. [CrossRef]
242. Liu, J.; Ma, J.; Zhang, Z.; Qin, Y.; Wang, Y.; Wang, Y.; Tan, R.; Duan, X.; Tian, T.Z.; Zhang, C.H.; et al. 2021 Roadmap: Electrocatalysts for Green Catalytic Processes. *J. Phys. Mater.* **2021**, *4*, 022004. [CrossRef]
243. Zhu, W.; Zhao, K.; Liu, S.; Liu, M.; Peng, F.; An, P.; Qin, B.; Zhou, H.; Li, H.; He, Z. Low-Overpotential Selective Reduction of CO_2 to Ethanol on Electrodeposited CuxAuy Nanowire Arrays. *Energy Chem.* **2019**, *37*, 176–182. [CrossRef]
244. Zhou, Y.; Yeo, B.S. Formation of C-C Bonds during Electrocatalytic CO_2 Reduction on Non-Copper Electrodes. *J. Mater. Chem. A* **2020**, *8*, 23162–23186. [CrossRef]
245. Chen, P.; Zhang, Y.; Zhou, Y.; Dong, F. Photoelectrocatalytic Carbon Dioxide Reduction: Fundamental, Advances and Challenges. *Nano Mater. Sci.* **2021**, *3*, 344–367. [CrossRef]
246. Zhang, X.; Guo, S.X.; Gandionco, K.A.; Bond, A.M.; Zhang, J. Electrocatalytic Carbon Dioxide Reduction: From Fundamental Principles to Catalyst Design. *Mater. Today Adv.* **2020**, *7*, 100074. [CrossRef]
247. da Gregorio, G.L.; Burdyny, T.; Loiudice, A.; Iyengar, P.; Smith, W.A.; Buonsanti, R. Facet-Dependent Selectivity of Cu Catalysts in Electrochemical CO_2 Reduction at Commercially Viable Current Densities. *ACS Catal.* **2020**, *10*, 4854–4862. [CrossRef] [PubMed]
248. Jung, H.; Lee, S.Y.; Lee, C.W.; Cho, M.K.; Won, D.H.; Kim, C.; Oh, H.S.; Min, B.K.; Hwang, Y.J. Electrochemical Fragmentation of Cu_2O Nanoparticles Enhancing Selective C-C Coupling from CO_2 Reduction Reaction. *J. Am. Chem. Soc.* **2019**, *141*, 4624–4633. [CrossRef] [PubMed]
249. Zhu, Q.; Sun, X.; Yang, D.; Ma, J.; Kang, X.; Zheng, L.; Zhang, J.; Wu, Z.; Han, B. Carbon Dioxide Electroreduction to C2 Products over Copper-Cuprous Oxide Derived from Electrosynthesized Copper Complex. *Nat. Commun.* **2019**, *10*, 3851. [CrossRef] [PubMed]
250. Ajmal, S.; Yang, Y.; Tahir, M.A.; Li, K.; Bacha, A.U.R.; Nabi, I.; Liu, Y.; Wang, T.; Zhang, L. Boosting C2 Products in Electrochemical CO_2 Reduction over Highly Dense Copper Nanoplates. *Catal. Sci. Technol.* **2020**, *10*, 4562–4570. [CrossRef]
251. Liu, G.; Lee, M.; Kwon, S.; Zeng, G.; Eichhorn, J.; Buckley, A.K.; Toste, F.D.; Goddard, W.A.; Toma, F.M. CO_2 Reduction on Pure Cu Produces Only H_2 after Subsurface O Is Depleted: Theory and Experiment. *Proc. Natl. Acad. Sci. USA* **2021**, *118*, 23. [CrossRef]
252. Bai, S.; Shao, Q.; Wang, P.; Dai, Q.; Wang, X.; Huang, X. Highly Active and Selective Hydrogenation of CO_2 to Ethanol by Ordered Pd-Cu Nanoparticles. *J. Am. Chem. Soc.* **2017**, *139*, 6827–6830. [CrossRef]
253. Jiwanti, P.K.; Natsui, K.; Nakata, K.; Einaga, Y. The Electrochemical Production of C2/C3 Species from Carbon Dioxide on Copper-Modified Boron-Doped Diamond Electrodes. *Electrochim. Acta* **2018**, *266*, 414–419. [CrossRef]
254. Li, F.; Li, Y.C.; Wang, Z.; Li, J.; Nam, D.H.; Lum, Y.; Luo, M.; Wang, X.; Ozden, A.; Hung, S.F.; et al. Cooperative CO_2-to-Ethanol Conversion via Enriched Intermediates at Molecule–Metal Catalyst Interfaces. *Nat. Catal.* **2020**, *3*, 75–82. [CrossRef]
255. Ting, L.R.L.; Piqué, O.; Lim, S.Y.; Tanhaei, M.; Calle-Vallejo, F.; Yeo, B.S. Enhancing CO_2 Electroreduction to Ethanol on Copper-Silver Composites by Opening an Alternative Catalytic Pathway. *ACS Catal.* **2020**, *10*, 4059–4069. [CrossRef]
256. Niu, D.; Wei, C.; Lu, Z.; Fang, Y.; Liu, B.; Sun, D.; Hao, X.; Pan, H.; Wang, G. Cu_2O-Ag Tandem Catalysts for Selective Electrochemical Reduction of CO_2 to C2 Products. *Molecules* **2021**, *26*, 2175. [CrossRef]
257. Ma, S.; Sadakiyo, M.; Luo, R.; Heima, M.; Yamauchi, M.; Kenis, P.J.A. One-Step Electrosynthesis of Ethylene and Ethanol from CO_2 in an Alkaline Electrolyzer. *J. Power Sources* **2016**, *301*, 219–228. [CrossRef]
258. Schmid, B.; Reller, C.; Neubauer, S.S.; Fleischer, M.; Dorta, R.; Schmid, G. Reactivity of Copper Electrodes towards Functional Groups and Small Molecules in the Context of CO_2 Electro-Reductions. *Catalysts* **2017**, *7*, 161. [CrossRef]
259. Zhuang, T.T.; Liang, Z.Q.; Seifitokaldani, A.; Li, Y.; De Luna, P.; Burdyny, T.; Che, F.; Meng, F.; Min, Y.; Quintero-Bermudez, R.; et al. Steering Post-C-C Coupling Selectivity Enables High Efficiency Electroreduction of Carbon Dioxide to Multi-Carbon Alcohols. *Nat. Catal.* **2018**, *1*, 421–428. [CrossRef]
260. Hoang, T.T.H.; Verma, S.; Ma, S.; Fister, T.T.; Timoshenko, J.; Frenkel, A.I.; Kenis, P.J.A.; Gewirth, A.A. Nanoporous Copper-Silver Alloys by Additive-Controlled Electrodeposition for the Selective Electroreduction of CO_2 to Ethylene and Ethanol. *J. Am. Chem. Soc.* **2018**, *140*, 5791–5797. [CrossRef]
261. Luo, M.; Wang, Z.; Li, Y.C.; Li, J.; Li, F.; Lum, Y.; Nam, D.H.; Chen, B.; Wicks, J.; Xu, A.; et al. Hydroxide Promotes Carbon Dioxide Electroreduction to Ethanol on Copper via Tuning of Adsorbed Hydrogen. *Nat. Commun.* **2019**, *10*, 5814. [CrossRef]
262. Zhang, J.; Luo, W.; Züttel, A. Self-Supported Copper-Based Gas Diffusion Electrodes for CO_2 Electrochemical Reduction. *J. Mater. Chem. A* **2019**, *7*, 26285–26292. [CrossRef]
263. Li, Y.C.; Wang, Z.; Yuan, T.; Nam, D.H.; Luo, M.; Wicks, J.; Chen, B.; Li, J.; Li, F.; De Arquer, F.P.G.; et al. Binding Site Diversity Promotes CO_2 Electroreduction to Ethanol. *J. Am. Chem. Soc.* **2019**, *141*, 8584–8591. [CrossRef] [PubMed]
264. Romero Cuellar, N.S.; Wiesner-Fleischer, K.; Fleischer, M.; Rucki, A.; Hinrichsen, O. Advantages of CO over CO_2 as Reactant for Electrochemical Reduction to Ethylene, Ethanol and n-Propanol on Gas Diffusion Electrodes at High Current Densities. *Electrochim. Acta* **2019**, *307*, 164–175. [CrossRef]
265. Wang, Y.; Wang, Z.; Dinh, C.T.; Li, J.; Ozden, A.; Golam Kibria, M.; Seifitokaldani, A.; Tan, C.S.; Gabardo, C.M.; Luo, M.; et al. Catalyst Synthesis under CO_2 Electroreduction Favours Faceting and Promotes Renewable Fuels Electrosynthesis. *Nat. Catal.* **2020**, *3*, 98–106. [CrossRef]

266. Wang, X.; Wang, Z.; García de Arquer, F.P.; Dinh, C.T.; Ozden, A.; Li, Y.C.; Nam, D.H.; Li, J.; Liu, Y.S.; Wicks, J.; et al. Efficient Electrically Powered CO_2-to-Ethanol via Suppression of Deoxygenation. *Nat. Energy* **2020**, *5*, 478–486. [CrossRef]
267. She, X.; Zhang, T.; Li, Z.; Li, H.; Xu, H.; Wu, J. Tandem Electrodes for Carbon Dioxide Reduction into C_{2+} Products at Simultaneously High Production Efficiency and Rate. *Cell Rep. Phys. Sci.* **2020**, *1*, 100051. [CrossRef]
268. Tan, Y.C.; Lee, K.B.; Song, H.; Oh, J. Modulating Local CO_2 Concentration as a General Strategy for Enhancing C-C Coupling in CO_2 Electroreduction. *Joule* **2020**, *4*, 1104–1120. [CrossRef]
269. Yang, Q.; Liu, X.; Peng, W.; Zhao, Y.; Liu, Z.; Peng, M.; Lu, Y.R.; Chan, T.S.; Xu, X.; Tan, Y. Vanadium Oxide Integrated on Hierarchically Nanoporous Copper for Efficient Electroreduction of CO_2 to Ethanol. *J. Mater. Chem. A* **2021**, *9*, 3044–3051. [CrossRef]
270. Zhu, S.; Ren, X.; Li, X.; Niu, X.; Wang, M.; Xu, S.; Wang, Z.; Han, Y.; Wang, Q. Core-shell ZnO@Cu_2O as Catalyst to Enhance the Electrochemical Reduction of Carbon Dioxide to C2 Products. *Catalysts* **2021**, *11*, 535. [CrossRef]
271. Puring, K.J.; Siegmund, D.; Timm, J.; Möllenbruck, F.; Schemme, S.; Marschall, R.; Apfel, U. Electrochemical CO_2 Reduction: Tailoring Catalyst Layers in Gas Diffusion Electrodes. *Av. Sustain. Syst.* **2021**, *5*, 2000088. [CrossRef]
272. Xing, Z.; Hu, L.; Ripatti, D.S.; Hu, X.; Feng, X. Enhancing Carbon Dioxide Gas-Diffusion Electrolysis by Creating a Hydrophobic Catalyst Microenvironment. *Nat. Commun.* **2021**, *12*, 136. [CrossRef]
273. Mota, N.; Ordoñez, E.M.; Pawelec, B.; Fierro, J.L.G.; Navarro, R.M. Direct Synthesis of Dimethyl Ether from CO_2: Recent Advances in Bifunctional/Hybrid Catalytic Systems. *Catalysts* **2021**, *11*, 411. [CrossRef]
274. Dieterich, V.; Buttler, A.; Hanel, A.; Spliethof, H.; Fendt, S. Power-to-Liquid via Synthesis of Methanol, DME or Fischer–Tropsch-Fuels: A Review. *Energy Environ. Sci.* **2020**, *13*, 3207–3252. [CrossRef]
275. Makos, P.; Słupek, E.; Sobczak, J.; Zabrocki, D.; Hupka, J.; Rogala, A. Dimethyl Ether (DME) as Potential Environmental Friendly Fuel. *E3S Web Conf.* **2019**, *116*, 00048. [CrossRef]
276. Catizzone, E.; Freda, C.; Braccio, G.; Frusteri, F.; Bonura, G. Dimethyl Ether as Circular Hydrogen Carrier: Catalytic Aspects of Hydrogenation/Dehydrogenation Steps. *J. Energy Chem.* **2021**, *58*, 55–77. [CrossRef]
277. Bahari, N.A.; Wan Isahak, W.N.R.; Masdar, M.S.; Yaakob, Z. Clean Hydrogen Generation and Storage Strategies via CO_2 Utilization into Chemicals and Fuels: A Review. *Int. J. Energy Res.* **2019**, *43*, 5128–5150. [CrossRef]
278. Bao, J.; Yang, G.; Yoneyama, Y.; Tsubaki, N. Significant Advances in C1 Catalysis: Highly Efficient Catalysts and Catalytic Reactions. *ACS Catal.* **2019**, *9*, 3026–3053. [CrossRef]
279. Du, C.; Lu, P.; Tsubaki, N. Efficient and New Production Methods of Chemicals and Liquid Fuels by Carbon, Monoxide Hydrogenation. *ACS Omega* **2020**, *5*, 49–56. [CrossRef]
280. Zhang, X.; Zhang, G.; Song, C.; Guo, X. Catalytic Conversion of Carbon Dioxide to Methanol: Current Status and Future Perspective. *Front. Energy Res.* **2021**, *8*, 621119. [CrossRef]
281. Han, T.; Xu, H.; Liu, J.; Zhou, L.; Li, X.; Dong, J.; Ge, H. One-pass Conversion of Benzene and Syngas to Alkylbenzenes by Cu-ZnO-Al_2O_3 and ZSM-5 Relay. *Catal. Lett.* **2021**, *152*, 467–479. [CrossRef]
282. Yerga, R.M.N. Catalysts for Production and Conversion of Syngas. *Catalysts* **2021**, *11*, 752. [CrossRef]
283. Kamsuwan, T.; Krutpijit, C.; Praserthdam, S.; Phatanasri, S.; Jongsomjit, B.; Praserthdam, P. Comparative Study on the Effect of Different Copper Loading on Catalytic Behaviors and Activity of Cu/ZnO/Al_2O_3 Catalysts toward CO and CO_2 Hydrogenation. *Heliyon* **2021**, *7*, e07682. [CrossRef] [PubMed]
284. Zhong, J.; Yang, X.; Wu, Z. State of the Art and Perspectives in Heterogeneous Catalysis of CO_2 Hydrogenation. *Chem. Soc. Rev.* **2020**, *49*, 1385–1413. [CrossRef]
285. Liang, B.; Ma, J.; Su, X.; Yang, C.; Duan, H.; Zhou, H.; Deng, S.; Li, L.; Huang, Y. Investigation on Deactivation of Cu/ZnO/Al_2O_3 Catalyst for CO_2 Hydrogenation to Methanol. *Ind. Eng. Chem. Res.* **2019**, *58*, 9030–9037. [CrossRef]
286. Ren, S.; Fan, X.; Shang, Z.; Shoemaker, W.R.; Ma, L.; Wu, T.; Li, S.; Klinghoffer, N.B.; Yu, M.; Liang, X. Enhanced Catalytic Performance of Zr Modified CuO/ZnO/Al_2O_3 Catalyst for Methanol and DME Synthesis via CO_2 Hydrogenation. *J. CO_2 Util.* **2020**, *36*, 82–95. [CrossRef]
287. Divins, N.J.; Kordus, D.; Timoshenko, J.; Sinev, I.; Zegkinoglou, I.; Bergmann, A.; Chee, S.W.; Widrinna, S.; Karslıoğlu, O.; Mistry, H.; et al. Operando High-Pressure Investigation of Size-Controlled CuZn Catalysts for the Methanol Synthesis Reaction. *Nat. Commun.* **2021**, *12*, 1435. [CrossRef] [PubMed]
288. van Kampen, J.; Boon, J.; Vente, J.; van Sint Annaland, M. Sorption Enhanced Dimethyl Ether Synthesis under Industrially Relevant Conditions: Experimental Validation of Pressure Swing Regeneration. *React. Chem. Eng.* **2021**, *6*, 244–257. [CrossRef]
289. Peinado, C.; Liuzzi, D.; Retuerto, M.; Boon, J.; Peña, M.A.; Rojas, S. Study of Catalyst Bed Composition for the Direct Synthesis of Dimethyl Ether from CO_2-Rich Syngas. *Chem. Eng. J. Adv.* **2020**, *4*, 100039. [CrossRef]
290. de Oliveira Campos, B.L.; Delgado, K.H.; Wild, S.; Studt, F.; Pitter, S.; Sauer, J. Surface Reaction Kinetics of the Methanol Synthesis and the Water Gas Shift Reaction on Cu/ZnO/Al_2O_3. *React. Chem. Eng.* **2021**, *6*, 868–887. [CrossRef]
291. Styring, P.; Dowson, G.R.M.; Tozer, I.O. Synthetic Fuels Based on Dimethyl Ether as a Future Non-Fossil Fuel for Road Transport from Sustainable Feedstocks. *Front. Energy Res.* **2021**, *9*, 663331. [CrossRef]
292. Brunetti, A.; Migliori, M.; Cozza, D.; Catizzone, E.; Giordano, G.; Barbieri, G. Methanol Conversion to Dimethyl Ether in Catalytic Zeolite Membrane Reactors. *ACS Sustain. Chem. Eng.* **2020**, *8*, 10471–10479. [CrossRef]
293. Bizon, K.; Skrzypek-Markiewicz, K.; Continillo, G. Enhancement of the Direct Synthesis of Dimethyl Ether (DME) from Synthesis Gas by Macro-and Microstructuring of the Catalytic Bed. *Catalysts* **2020**, *10*, 852. [CrossRef]

294. Guffanti, S.; Visconti, C.G.; Groppi, G. Model Analysis of the Role of Kinetics, Adsorption Capacity, and Heat and Mass Transfer Effects in Sorption Enhanced Dimethyl Ether Synthesis. *Ind. Eng. Chem. Res.* **2021**, *60*, 6767–6783. [CrossRef]
295. Chen, T.Y.; Cao, C.; Chen, T.B.; Ding, X.; Huang, H.; Shen, L.; Cao, X.; Zhu, M.; Xu, J.; Gao, J.; et al. Unraveling Highly Tunable Selectivity in CO_2 Hydrogenation over Bimetallic In-Zr Oxide Catalysts. *ACS Catal.* **2019**, *9*, 8785–8797. [CrossRef]
296. Bonura, G.; Cannilla, C.; Frusteri, L.; Catizzone, E.; Todaro, S.; Migliori, M.; Giordano, G.; Frusteri, F. Interaction Effects between CuO-ZnO-ZrO_2 Methanol Phase and Zeolite Surface Affecting Stability of Hybrid Systems during One-Step CO_2 Hydrogenation to DME. *Catal. Today* **2020**, *345*, 175–182. [CrossRef]
297. Liu, C.; Kang, J.; Huang, Z.Q.; Song, Y.H.; Xiao, Y.S.; Song, J.; He, J.X.; Chang, C.R.; Ge, H.Q.; Wang, Y.; et al. Gallium Nitride Catalyzed the Direct Hydrogenation of Carbon Dioxide to Dimethyl Ether as Primary Product. *Nat. Commun.* **2021**, *12*, 2305. [CrossRef]
298. Tuygun, C.; Ipek, B. CO_2 Hydrogenation to Methanol and Dimethyl Ether at Atmospheric Pressure Using Cu-Ho-Ga/γ-Al_2O_3 and Cu-Ho-Ga/ZSM-5: Experimental Study and Thermodynamic Analysis. *Turk. J. Chem.* **2021**, *45*, 231–247. [CrossRef] [PubMed]
299. Wild, S.; Polierer, S.; Zevaco, T.A.; Guse, D.; Kind, M.; Pitter, S.; Delgado, K.H.; Sauer, J. Direct DME Synthesis on CZZ/H-FER from Variable CO_2/CO Syngas Feeds. *RSC Adv.* **2021**, *11*, 2556–2564. [CrossRef] [PubMed]
300. Esquius, J.R.; Bahruji, H.; Bowker, M.; Hutchings, G.J. Identification of C2-C5 Products from CO_2 Hydrogenation over PdZn/TiO_2-ZSM-5 Hybrid Catalysts. *Faraday Discuss.* **2021**, *230*, 52–67. [CrossRef]
301. Rodriguez-Vega, P.; Ateka, A.; Kumakiri, I.; Vicente, H.; Ereña, J.; Aguayo, A.T.; Bilbao, J. Experimental Implementation of a Catalytic Membrane Reactor for the Direct Synthesis of DME from H_2+CO/CO_2. *Chem. Eng. Sci.* **2021**, *234*, 116396. [CrossRef]
302. Liuzzi, D.; Peinado, C.; Peña, M.A.; Van Kampen, J.; Boon, J.; Rojas, S. Increasing Dimethyl Ether Production from Biomass-Derived Syngas: Via Sorption Enhanced Dimethyl Ether Synthesis. *Sustain. Energy Fuels* **2020**, *4*, 5674–5681. [CrossRef]
303. Du, C.; Hondo, E.; Chizema, L.G.; Wang, C.; Tong, M.; Xing, C.; Yang, R.; Lu, P.; Tsubaki, N. Developing Cu-MOR@SiO_2 Core—Shell Catalyst Microcapsules for Two-Stage Ethanol Direct Synthesis from DME and Syngas. *Ind. Eng. Chem. Res.* **2020**, *59*, 3293–3300. [CrossRef]
304. Du, C.; Hondo, E.; Gapu, L.; Hassan, R.; Chang, X.; Dai, L.; Ma, Q.; Lu, P.; Tsubaki, N. An Efficient Microcapsule Catalyst for One-Step Ethanol Synthesis from Dimethyl Ether and Syngas. *Fuel* **2021**, *283*, 118971. [CrossRef]
305. Feng, X.-B.; He, Z.-M.; Zhang, L.-Y.; Zhao, X.-Y.; Cao, J.-P. Facile Designing a Nanosheet HMOR Zeolite for Enhancing the Efficiency of Ethanol Synthesis from Dimethyl Ether and Syngas. *Int. J. Hydrogen Energy* **2022**, *47*, 9273–9282. [CrossRef]
306. Chen, X.; Chen, Y.; Song, C.; Ji, P.; Wang, N.; Wang, W.; Cui, L. Recent Advances in Supported Metal Catalysts and Oxide Catalysts for the Reverse Water Gas Shift Reaction. *Front. Chem.* **2020**, *8*, 709. [CrossRef]
307. González-Castaño, M.; Dorneanu, B.; Arellano-García, H. The Reverse Water Gas Shift Reaction: A Process Systems Engineering Perspective. *React. Chem. Eng.* **2021**, *6*, 954–976. [CrossRef]
308. Pearson, R.; Coe, A.; Paterson, J. Innovation in Fischer-Tropsch: A Sustainable Approach to Fuels Production. *Johnson Matthey Technol. Rev.* **2021**, *65*, 395–403. [CrossRef]
309. Aziz, M.A.A.; Setiabudi, H.D.; Teh, L.P.; Annuar, N.H.R.; Jalil, A.A. A Review of Heterogeneous Catalysts for Syngas Production via Dry Reforming. *J. Taiwan Inst. Chem. Eng.* **2019**, *101*, 139–158. [CrossRef]
310. Tan, K.B.; Zhan, G.; Sun, D.; Huang, J.; Li, Q. The Development of Bifunctional Catalysts for Carbon Dioxide Hydrogenation to Hydrocarbons via the Methanol Route: From Single Component to Integrated Components. *J. Mater. Chem. A* **2021**, *9*, 5197–5231. [CrossRef]
311. He, Z.; Cui, M.; Qian, Q.; Zhang, J.; Liu, H.; Han, B. Synthesis of Liquid Fuel via Direct Hydrogenation of CO_2. *Proc. Natl. Acad. Sci. USA* **2019**, *116*, 12654–12659. [CrossRef]
312. Gao, P.; Zhang, L.; Li, S.; Zhou, Z.; Sun, Y. Novel Heterogeneous Catalysts for CO_2 Hydrogenation to Liquid Fuels. *ACS Cent. Sci.* **2020**, *6*, 1657–1670. [CrossRef]
313. Zhang, S.; Liu, X.; Shao, Z.; Wang, H.; Sun, Y. Direct CO_2 Hydrogenation to Ethanol over Supported Co_2C Catalysts: Studies on Support Effects and Mechanism. *J. Catal.* **2020**, *382*, 86–96. [CrossRef]
314. Liu, H.; Wang, L. Highly Dispersed and Stable Ni/SBA-15 Catalyst for Reverse Water Gas Shift Reaction. *Crystals* **2021**, *11*, 790. [CrossRef]
315. Pauletto, G.; Galli, F.; Gaillardet, A.; Mocellin, P.; Patience, G.S. Techno Economic Analysis of a Micro Gas-to-Liquid Unit for Associated Natural Gas Conversion. *Renew. Sustain. Energy Rev.* **2021**, *150*, 111457. [CrossRef]
316. Vu, T.T.N.; Desgagnés, A.; Iliuta, M.C. Efficient Approaches to Overcome Challenges in Material Development for Conventional and Intensified CO_2 Catalytic Hydrogenation to CO, Methanol, and DME. *Appl. Catal. A Gen.* **2021**, *617*, 118119. [CrossRef]
317. Lv, C.; Xu, L.; Chen, M.; Cui, Y.; Wen, X.; Li, Y.; Wu, C.E.; Yang, B.; Miao, Z.; Hu, X.; et al. Recent Progresses in Constructing the Highly Efficient Ni Based Catalysts with Advanced Low-Temperature Activity toward CO_2 Methanation. *Front. Chem.* **2020**, *8*, 269. [CrossRef] [PubMed]
318. Xing, Y.; Ouyang, M.; Zhang, L.; Yang, M.; Wu, X.; Ran, R.; Weng, D.; Kang, F.; Si, Z. Single Atomic Pt on $SrTiO_3$ Catalyst in Reverse Water Gas Shift Reactions. *Catalysts* **2021**, *11*, 738. [CrossRef]
319. Azancot, L.; Bobadilla, L.F.; Centeno, M.A.; Odriozola, J.A. IR Spectroscopic Insights into the Coking-Resistance Effect of Potassium on Nickel-Based Catalyst during Dry Reforming of Methane. *Appl. Catal. B Environ.* **2021**, *285*, 119822. [CrossRef]
320. Cui, S.; Wang, X.; Wang, L.; Zheng, X. Enhanced Selectivity of the CO_2 Reverse Water-Gas Reaction over a Ni_2P/CeO_2 Catalyst. *Dalt. Trans.* **2021**, *50*, 5978–5987. [CrossRef]

321. Chou, C.Y.; Loiland, J.A.; Lobo, R.F. Reverse Water-Gas Shift Iron Catalyst Derived from Magnetite. *Catalysts* **2019**, *9*, 773. [CrossRef]
322. Zhang, Q.; Pastor-Pérez, L.; Gu, S.; Reina, T.R. Transition Metal Carbides (TMCS) Catalysts for Gas Phase CO_2 Upgrading Reactions: A Comprehensive Overview. *Catalysts* **2020**, *10*, 955. [CrossRef]
323. Pajares, A.; Prats, H.; Romero, A.; Viñes, F.; de la Piscina, P.R.; Sayós, R.; Homs, N.; Illas, F. Critical Effect of Carbon Vacancies on the Reverse Water Gas Shift Reaction over Vanadium Carbide Catalysts. *Appl. Catal. B Environ.* **2020**, *267*, 118719. [CrossRef]
324. Kuang, H.-Y.; Lin, Y.-X.; Li, X.-H.; Chen, J.-S. Chemical Fixation of CO_2 on Nanocarbons and Hybrids. *J. Mater. Chem. A* **2021**, *9*, 20857–20873. [CrossRef]
325. Chen, Y.; Wei, J.; Duyar, M.S.; Ordomsky, V.V.; Khodakov, A.Y.; Liu, J. Carbon-Based Catalysts for Fischer-Tropsch Synthesis. *Chem. Soc. Rev.* **2021**, *50*, 2337–2366. [CrossRef]
326. Zhang, P.; Han, F.; Yan, J.; Qiao, X.; Guan, Q.; Li, W. N-Doped Ordered Mesoporous Carbon (N-OMC) Confined Fe_3O_4-FeC_x Heterojunction for Efficient Conversion of CO_2 to Light Olefins. *Appl. Catal. B Environ.* **2021**, *299*, 120639. [CrossRef]
327. Li, Y.; Liang, G.; Wang, C.; Fang, Y.; Duan, H. Effect of Precipitated Precursor on the Catalytic Performance of Mesoporous Carbon Supported CuO-ZnO Catalysts. *Crystals* **2021**, *11*, 582. [CrossRef]
328. Valero-Romero, M.J.; Rodríguez-Cano, M.Á.; Palomo, J.; Rodríguez-Mirasol, J.; Cordero, T. Carbon-Based Materials as Catalyst Supports for Fischer–Tropsch Synthesis: A Review. *Front. Mater.* **2021**, *7*, 617432. [CrossRef]
329. González-Arias, J.; González-Castaño, M.; Sánchez, M.E.; Cara-Jiménez, J.; Arellano-García, H. Valorization of Biomass-Derived CO_2 Residues with Cu-MnOx Catalysts for RWGS Reaction. *Renew. Energy* **2022**, *182*, 443–451. [CrossRef]
330. Bahmanpour, A.M.; Signorile, M.; Kröcher, O. Recent Progress in Syngas Production via Catalytic CO_2 Hydrogenation Reaction. *Appl. Catal. B Environ.* **2021**, *295*, 120319. [CrossRef]
331. Elsernagawy, O.Y.H.; Hoadley, A.; Patel, J.; Bhatelia, T.; Lim, S.; Haque, N. Thermo-Economic Analysis of Reverse Water-Gas Shift Process with Different Temperatures for Green Methanol Production as a Hydrogen Carrier. *J. CO_2 Util.* **2020**, *41*, 101280. [CrossRef]
332. Okemoto, A.; Harada, M.R.; Ishizaka, T.; Hiyoshi, N.; Sato, K. Catalytic Performance of MoO_3/FAU Zeolite Catalysts Modified by Cu for Reverse Water Gas Shift Reaction. *Appl. Catal. A Gen.* **2020**, *592*, 117415. [CrossRef]
333. Zhang, Q.; Pastor-Pérez, L.; Jin, W.; Gu, S.; Reina, T.R. Understanding the Promoter Effect of Cu and Cs over Highly Effective B-Mo_2C Catalysts for the Reverse Water-Gas Shift Reaction. *Appl. Catal. B Environ.* **2019**, *244*, 889–898. [CrossRef]
334. Konsolakis, M.; Lykaki, M.; Stefa, S.; Carabineiro, S.A.C.; Varvoutis, G.; Papista, E.; Marnellos, G.E. CO_2 Hydrogenation over Nanoceria-Supported Transition Metal Catalysts: Role of Ceria Morphology (Nanorods versus Nanocubes) and Active Phase Nature (Co versus Cu). *Nanomaterials* **2019**, *9*, 1739. [CrossRef]
335. Zhang, Y.; Liang, L.; Chen, Z.; Wen, J.; Zhong, W.; Zou, S.; Fu, M.; Chen, L.; Ye, D. Highly Efficient Cu/CeO_2-Hollow Nanospheres Catalyst for the Reverse Water-Gas Shift Reaction: Investigation on the Role of Oxygen Vacancies through in Situ UV-Raman and DRIFTS. *Appl. Surf. Sci.* **2020**, *516*, 146035. [CrossRef]
336. Lykaki, M.; Stefa, S.; Carabineiro, S.A.C.; Soria, M.A.; Madeira, L.M.; Konsolakis, M. Shape Effects of Ceria Nanoparticles on the Water-Gas Shift Performance of CuOx/CeO_2 Catalysts. *Catalysts* **2021**, *11*, 753. [CrossRef]
337. Bahmanpour, A.M.; Héroguel, F.; Kılıç, M.; Baranowski, C.J.; Schouwink, P.; Röthlisberger, U.; Luterbacher, J.S.; Kröcher, O. Essential Role of Oxygen Vacancies of Cu-Al and Co-Al Spinel Oxides in Their Catalytic Activity for the Reverse Water Gas Shift Reaction. *Appl. Catal. B Environ.* **2020**, *266*, 118669. [CrossRef]
338. Su, X.; Yang, X.F.; Huang, Y.; Liu, B.; Zhang, T. Single-Atom Catalysis toward Efficient CO_2 Conversion to CO and Formate Products. *Acc. Chem. Res.* **2019**, *52*, 656–664. [CrossRef]
339. Liu, M.; Yi, Y.; Wang, L.; Guo, H.; Bogaerts, A. Hydrogenation of Carbon Dioxide to Value-Added Chemicals by Heterogeneous Catalysis and Plasma Catalysis. *Catalysts* **2019**, *9*, 275. [CrossRef]
340. Wang, L.; Guan, E.; Wang, Y.; Wang, L.; Gong, Z.; Cui, Y.; Meng, X.; Gates, B.C.; Xiao, F.S. Silica Accelerates the Selective Hydrogenation of CO_2 to Methanol on Cobalt Catalysts. *Nat. Commun.* **2020**, *11*, 1033. [CrossRef]
341. Ke, J.; Wang, Y.D.; Wang, C.M. First-Principles Microkinetic Simulations Revealing the Scaling Relations and Structure Sensitivity of CO_2 Hydrogenation to C1 & C2 Oxygenates on Pd Surfaces. *Catal. Sci. Technol.* **2021**, *11*, 4866–4881. [CrossRef]
342. Kang, J.; He, S.; Zhou, W.; Shen, Z.; Li, Y.; Chen, M.; Zhang, Q.; Wang, Y. Single-Pass Transformation of Syngas into Ethanol with High Selectivity by Triple Tandem Catalysis. *Nat. Commun.* **2020**, *11*, 827. [CrossRef] [PubMed]
343. Lou, Y.; Jiang, F.; Zhu, W.; Wang, L.; Yao, T.; Wang, S.; Yang, B.; Yang, B.; Zhu, Y.; Liu, X. CeO_2 Supported Pd Dimers Boosting CO_2 Hydrogenation to Ethanol. *Appl. Catal. B Environ.* **2021**, *291*, 120122. [CrossRef]
344. Ye, X.; Yang, C.; Pan, X.; Ma, J.; Zhang, Y.; Ren, Y.; Liu, X.; Li, L.; Huang, Y. Highly Selective Hydrogenation of CO_2 to Ethanol via Designed Bifunctional Ir1-In_2O_3 Single-Atom Catalyst. *J. Am. Chem. Soc.* **2020**, *142*, 19001–19005. [CrossRef] [PubMed]
345. Hasan, S.Z.; Ahmad, K.N.; Isahak, W.N.R.W.; Masdar, M.S.; Jahim, J.M. Synthesis of Low-Cost Catalyst NiO(111) for CO_2 Hydrogenation into Short-Chain Carboxylic Acids. *Int. J. Hydrogen Energy* **2020**, *45*, 22281–22290. [CrossRef]
346. Goryachev, A.; Pustovarenko, A.; Shterk, G.; Alhajri, N.S.; Jamal, A.; Albuali, M.; van Koppen, L.; Khan, I.S.; Russkikh, A.; Ramirez, A.; et al. A Multi-Parametric Catalyst Screening for CO_2 Hydrogenation to Ethanol. *ChemCatChem* **2021**, *13*, 3324–3332. [CrossRef]
347. Yang, C.; Mu, R.; Wang, G.; Song, J.; Tian, H.; Zhao, Z.J.; Gong, J. Hydroxyl-Mediated Ethanol Selectivity of CO_2 Hydrogenation. *Chem. Sci.* **2019**, *10*, 3161–3167. [CrossRef] [PubMed]

348. Wang, C.; Zhang, J.; Qin, G.; Wang, L.; Zuidema, E.; Yang, Q.; Dang, S.; Yang, C.; Xiao, J.; Meng, X.; et al. Direct Conversion of Syngas to Ethanol within Zeolite Crystals. *Chem* **2020**, *6*, 646–657. [CrossRef]
349. Kiss, J.; Sápi, A.; Tóth, M.; Kukovecz, Á.; Kónya, Z. Rh-Induced Support Transformation and Rh Incorporation in Titanate Structures and Their Influence on Catalytic Activity. *Catalysts* **2020**, *10*, 212. [CrossRef]
350. Ding, S.; Hülsey, M.J.; An, H.; He, Q.; Asakura, H.; Gao, M.; Hasegawa, J.; Tanaka, T.; Yan, N. Ionic Liquid-Stabilized Single-Atom Rh Catalyst against Leaching. *CCS Chem.* **2021**, *3*, 1814–1822. [CrossRef]
351. Wang, G.; Luo, R.; Yang, C.; Song, J.; Xiong, C.; Tian, H. Active Sites in CO_2 Hydrogenation over Confined VO_x-Rh Catalysts. *Sci. China Chem.* **2019**, *62*, 1710–1719. [CrossRef]
352. Ramirez, A.; Ould-Chikh, S.; Gevers, L.; Chowdhury, A.D.; Abou-Hamad, E.; Aguilar-Tapia, A.; Hazemann, J.L.; Wehbe, N.; Al Abdulghani, A.J.; Kozlov, S.M.; et al. Tandem Conversion of CO_2 to Valuable Hydrocarbons in Highly Concentrated Potassium Iron Catalysts. *ChemCatChem* **2019**, *11*, 2879–2886. [CrossRef]
353. Zeng, F.; Mebrahtu, C.; Xi, X.; Liao, L.; Ren, J.; Xie, J.; Heeres, H.J.; Palkovits, R. Catalysts Design for Higher Alcohols Synthesis by CO_2 Hydrogenation: Trends and Future Perspectives. *Appl. Catal. B Environ.* **2021**, *291*, 120073. [CrossRef]
354. Ojelade, O.A.; Zaman, S.F. A Review on Pd Based Catalysts for CO_2 Hydrogenation to Methanol: In-Depth Activity and DRIFTS Mechanistic Study. *Catal. Surv. Asia* **2020**, *24*, 11–37. [CrossRef]
355. Manrique, R.; Rodríguez-Pereira, J.; Rincón-Ortiz, S.A.; Bravo-Suárez, J.J.; Baldovino-Medrano, V.G.; Jiménez, R.; Karelovic, A. The Nature of the Active Sites of Pd-Ga Catalysts in the Hydrogenation of CO_2 to Methanol. *Catal. Sci. Technol.* **2020**, *10*, 6644–6658. [CrossRef]
356. Xu, D.; Ding, M.; Hong, X.; Liu, G.; Tsang, S.C.E. Selective C_{2+} Alcohol Synthesis from Direct CO_2 Hydrogenation over a Cs-Promoted Cu-Fe-Zn Catalyst. *ACS Catal.* **2020**, *10*, 5250–5260. [CrossRef]
357. Modak, A.; Bhanja, P.; Dutta, S.; Chowdhury, B.; Bhaumik, A. Catalytic Reduction of CO_2 into Fuels and Fine Chemicals. *Green Chem.* **2020**, *22*, 4002–4033. [CrossRef]
358. Mao, Z.; Gu, H.; Lin, X. Recent Advances of Pd/C-Catalyzed Reactions. *Catalysts* **2021**, *11*, 1078. [CrossRef]
359. Zheng, J.N.; An, K.; Wang, J.M.; Li, J.; Liu, Y. Direct Synthesis of Ethanol via CO_2 Hydrogenation over the Co/La-Ga-O Composite Oxide Catalyst. *Ranliao Huaxue Xuebao/J. Fuel Chem. Technol.* **2019**, *47*, 697–708. [CrossRef]
360. Wang, L.; He, S.; Wang, L.; Lei, Y.; Meng, X.; Xiao, F.S. Cobalt-Nickel Catalysts for Selective Hydrogenation of Carbon Ioxide into Ethanol. *ACS Catal.* **2019**, *9*, 11335–11340. [CrossRef]
361. Zhang, S.; Wu, Z.; Liu, X.; Shao, Z.; Xia, L.; Zhong, L.; Wang, H.; Sun, Y. Tuning the Interaction between Na and Co_2C to Promote Selective CO_2 Hydrogenation to Ethanol. *Appl. Catal. B Environ.* **2021**, *293*, 120207. [CrossRef]
362. Zhang, H.; Han, H.; Xiao, L.; Wu, W. Highly Selective Synthesis of Ethanol via CO_2 Hydrogenation over $CoMoC_x$ Catalysts. *ChemCatChem* **2021**, *13*, 3333–3339. [CrossRef]
363. Jiang, J.; Wen, C.; Tian, Z.; Wang, Y.; Zhai, Y.; Chen, L.; Li, Y.; Liu, Q.; Wang, C.; Ma, L. Manganese-Promoted Fe_3O_4 Microsphere for Efficient Conversion of CO_2 to Light Olefins. *Ind. Eng. Chem. Res.* **2020**, *59*, 2155–2162. [CrossRef]
364. Aitbekova, A.; Goodman, E.D.; Wu, L.; Boubnov, A.; Hoffman, A.S.; Genc, A.; Cheng, H.; Casalena, L.; Bare, S.R.; Cargnello, M. Engineering of Ruthenium–Iron Oxide Colloidal Heterostructures: Improved Yields in CO_2 Hydrogenation to Hydrocarbons. *Angew. Chem.-Int. Ed.* **2019**, *58*, 17451–17457. [CrossRef]
365. Li, Y.; Gao, W.; Peng, M.; Zhang, J.; Sun, J.; Xu, Y.; Hong, S.; Liu, X.; Liu, X.; Wei, M.; et al. Interfacial Fe_5C_2-Cu Catalysts toward Low-Pressure Syngas Conversion to Long-Chain Alcohols. *Nat. Commun.* **2020**, *11*, 61. [CrossRef]
366. Xu, Y.; Zhai, P.; Deng, Y.; Xie, J.; Liu, X.; Wang, S.; Ma, D. Highly Selective Olefin Production from CO_2 Hydrogenation on Iron Catalysts: A Subtle Synergy between Manganese and Sodium Additives. *Angew. Chem.-Int. Ed.* **2020**, *59*, 21736–21744. [CrossRef]
367. Yao, R.; Wei, J.; Ge, Q.; Xu, J.; Han, Y.; Ma, Q.; Xu, H.; Sun, J. Monometallic Iron Catalysts with Synergistic Na and S for Higher Alcohols Synthesis via CO_2 Hydrogenation. *Appl. Catal. B Environ.* **2021**, *298*, 120556. [CrossRef]
368. Ye, X.; Ma, J.; Yu, W.; Pan, X.; Yang, C.; Wang, C.; Liu, Q.; Huang, Y. Construction of Bifunctional Single-Atom Catalysts on the Optimized β-Mo_2C Surface for Highly Selective Hydrogenation of CO_2 into Ethanol. *J. Energy Chem.* **2022**, *67*, 184–192. [CrossRef]
369. An, B.; Li, Z.; Song, Y.; Zhang, J.; Zeng, L.; Wang, C.; Lin, W. Cooperative Copper Centres in a Metal-Organic Framework for Selective Conversion of CO_2 to Ethanol. *Nat. Catal.* **2019**, *2*, 709–717. [CrossRef]
370. Shafer, W.D.; Jacobs, G.; Graham, U.M.; Hamdeh, H.H.; Davis, B.H. Increased CO_2 Hydrogenation to Liquid Products Using Promoted Iron Catalysts. *J. Catal.* **2019**, *369*, 239–248. [CrossRef]
371. Yang, C.; Liu, S.; Wang, Y.; Song, J.; Wang, G.; Wang, S.; Zhao, Z.J.; Mu, R.; Gong, J. The Interplay between Structure and Product Selectivity of CO_2 Hydrogenation. *Angew. Chem.-Int. Ed.* **2019**, *58*, 11242–11247. [CrossRef]
372. Liu, B.; Ouyang, B.; Zhang, Y.; Lv, K.; Li, Q.; Ding, Y.; Li, J. Effects of Mesoporous Structure and Pt Promoter on the Activity of Co-Based Catalysts in Low-Temperature CO_2 Hydrogenation for Higher Alcohol Synthesis. *J. Catal.* **2018**, *366*, 91–97. [CrossRef]
373. Wang, L.; Wang, L.; Zhang, J.; Liu, X.; Wang, H.; Zhang, W.; Yang, Q.; Ma, J.; Dong, X.; Yoo, S.J.; et al. Selective Hydrogenation of CO_2 to Ethanol over Cobalt Catalysts. *Angew. Chem.-Int. Ed.* **2018**, *57*, 6104–6108. [CrossRef]
374. Ouyang, B.; Xiong, S.; Zhang, Y.; Liu, B.; Li, J. The Study of Morphology Effect of Pt/Co_3O_4 Catalysts for Higher Alcohol Synthesis from CO_2 Hydrogenation. *Appl. Catal. A Gen.* **2017**, *543*, 189–195. [CrossRef]
375. Li, Z.; Ji, S.; Liu, Y.; Cao, X.; Tian, S.; Chen, Y.; Niu, Z.; Li, Y. Well-Defined Materials for Heterogeneous Catalysis: From Nanoparticles to Isolated Single-Atom Sites. *Chem. Rev.* **2020**, *120*, 623–682. [CrossRef]

376. Häusler, J.; Pasel, J.; Woltmann, F.; Everwand, A.; Meledina, M.; Valencia, H.; Lipińska-Chwałek, M.; Mayer, J.; Peters, R. Elucidating the Influence of the D-Band Center on the Synthesis of Isobutanol. *Catalysts* **2021**, *11*, 406. [CrossRef]
377. Tang, C.W.; Liu, C.H.; Wang, C.C.; Wang, C. Bin Electro-Oxidation of Methanol, Ethanol and Ethylene Glycol over Pt/TiO_2-C and PtSn/TiO_2-C Anodic Catalysts. *Int. J. Electrochem. Sci.* **2021**, *16*, 211045. [CrossRef]

Disclaimer/Publisher's Note: The statements, opinions and data contained in all publications are solely those of the individual author(s) and contributor(s) and not of MDPI and/or the editor(s). MDPI and/or the editor(s) disclaim responsibility for any injury to people or property resulting from any ideas, methods, instructions or products referred to in the content.